
Electronic Thesis and Dissertation Repository

6-21-2017 12:00 AM

NUAK1 Has Tumor Suppressive Activity in Epithelial Ovarian Cancer

Parima Saxena, *The University of Western Ontario*

Supervisor: Dr. Trevor Shepherd, *The University of Western Ontario*

A thesis submitted in partial fulfillment of the requirements for the Master of Science degree in Anatomy and Cell Biology

© Parima Saxena 2017

Follow this and additional works at: <https://ir.lib.uwo.ca/etd>



Part of the [Cancer Biology Commons](#), and the [Cell Biology Commons](#)

Recommended Citation

Saxena, Parima, "NUAK1 Has Tumor Suppressive Activity in Epithelial Ovarian Cancer" (2017). *Electronic Thesis and Dissertation Repository*. 4598.

<https://ir.lib.uwo.ca/etd/4598>

This Dissertation/Thesis is brought to you for free and open access by Scholarship@Western. It has been accepted for inclusion in Electronic Thesis and Dissertation Repository by an authorized administrator of Scholarship@Western. For more information, please contact wlsadmin@uwo.ca.

Abstract

NUAK1, a downstream substrate of the stress metabolism regulator Liver kinase B1 (LKB1), has been implicated as an oncogene and tumor suppressor, with distinct roles in cell cycle, senescence and cell adhesion. Epithelial ovarian cancer (EOC) spheroids remain dormant during intraperitoneal metastasis with reduced proliferation and metabolism to survive metabolically harsh conditions, possibly implicating a role of NUAK1 in EOC spheroid biology. I hypothesize that NUAK1 is regulated by LKB1 to promote dormancy in EOC. I demonstrate that NUAK1 expression and phosphorylation is regulated by LKB1 in EOC cell lines. NUAK1 is largely under-expressed in many established and new ascites-derived EOC cell lines; in fact, further *NUAK1* knockdown increases spheroid cell viability, size, and reattachment capability. Pharmacologic NUAK1/2 inhibition increased EOC cell growth and clonogenicity. Collectively, my data supports NUAK1 as having tumour suppressive activity downstream of LKB1 in EOC.

Keywords

Liver Kinase B1, AMPK-related kinase, NUAK1, spheroid, tumor suppressor, epithelial ovarian cancer, metastasis

Co-Authorship Statement

OVCAR8 *STK11*KO cells were established by Dr. Trevor Shepherd using CRISPR-Cas9 technology to lack LKB1 expression.

iOvCa series, ascites-derived cell lines, were established by Dr. Gabriel DiMattia.

siARK screen was performed by Yudith Ramos-Valdes.

qPCR for ARK mRNA levels was conducted by Elizabeth Kobylecky.

Tritiated thymidine incorporation assay was performed in collaboration with Piru Perampalam and Dr. Fred Dick

Acknowledgments

I would like to acknowledge my supervisor, Dr. Trevor Shepherd, for allowing me to take on this interesting and engaging project and for his support throughout the course of my project. I would also like to thank my committee members for all of their insightful guidance which they have provided me, which has been critical for driving this project forward. I would also like to thank Dr. Gabriel DiMattia for all of his contributions towards my project, valuable insight into my work, and for generously allowing me to use the repository of ascites-derived cell lines. Furthermore, I would like to thank my past and present lab mates, Yudith, Adrian, Olga, Jessica and Samah, for not only helping me learn scientific techniques but for also providing an excellent work environment.

Table of Contents

Abstract	
Co-Authorship Statement.....	i
Acknowledgments.....	ii
Table of Contents	iii
List of Tables	vi
List of Figures	vii
List of Abbreviations	ix
Chapter 1	1
1 Introduction	1
1.1 Epidemiology, Clinical Presentation and Treatment of Epithelial Ovarian Cancer	1
1.2 Origin and Subtypes of EOC	3
1.3 EOC Metastasis and Experimental Model Systems.....	6
1.4 LKB1-AMPK in EOC Metastasis.....	9
1.5 AMPK-Related Kinases and Their Potential Importance in EOC Metastasis	12
1.6 NUA1 Regulation and Function	14
1.7 Research Goal, Hypothesis and Experimental Objectives.....	17
Chapter 2.....	18
2 Materials and Methods.....	18
2.1 Cell Culture.....	18
2.2 Western Blot	20
2.3 Phostag™ Western Blot.....	22
2.4 siRNA-mediated knockdown.....	22
2.5 Reattachment Assays	23
2.6 Clonogenic Assays.....	23

2.7 CellTiter-Glo® Viability Assay.....	23
2.8 CyQUANT Viability Assay	24
2.9 Trypan Blue Exclusion Viability Assay	24
2.10 IC50 Determination	25
2.11 Incucyte ZOOM Growth Curves	26
2.12 Quantitative Real-time PCR	26
2.13 Tritiated Thymidine Incorporation Assay.....	29
2.14 Spheroid size determination.....	29
2.15 Graphing and Statistical Analysis.....	29
Chapter 3.....	30
3 Results	30
3.1 NUAK1 has limited profile in EOC.....	30
3.2 NUAK1 expression decreases in spheroid culture.....	33
3.3 NUAK1 is regulated by LKB1	33
3.4 NUAK1 knockdown increases EOC spheroid cell viability.....	36
3.5 NUAK1 and NUAK2 are unable to functionally compensate for each other.....	38
3.6 NUAK1 inhibition increases EOC cell growth and clonogenicity	44
3.7 Specific NUAK1 inhibition increases EOC cell growth.....	45
3.8 NUAK1 inhibition is insufficient to induce platinum sensitivity	51
3.9 NUAK1 inhibition does not affect thymidine incorporation	55
Chapter 4.....	59
4 Discussion	59
4.1 Summary of findings.....	59
4.2 Potential growth suppressive of NUAK1 in EOC	60
4.3 Therapeutic implications of results.....	63
4.4 NUAK1 and LKB1	63

4.5	Limitations of current study.....	64
4.6	Future Work.....	65
4.7	Overall Conclusion.....	68
Chapter 5	70
5	Appendices.....	70
5.1	Appendix A: ARK mutations and mRNA expression.....	70
5.2	siARK Screen.....	73
5.3	MARK3 studies in EOC.....	76
References	81
Curriculum Vitae	90

List of Tables

Table 2.1. Summary of low-passage, ascites-derived cell lines.	19
Table 2.2. qPCR primer sequences	28
Table 3.1. Doubling times for WZ4003 treatment.....	48
Table 3.2. Doubling times for HTH01-015 treatment.	53

List of Figures

Figure 1.1. Mechanisms of EOC metastasis <i>in vitro</i> and <i>in vivo</i>	8
Figure 1.2. Summary of LKB1 signaling.....	10
Figure 1.3. NUAK1 regulation and function.	15
Figure 3.1.NUAK1 expression in EOC.	31
Figure 3.2. Quantification of NUAK1 expression across 38 cell lines.....	32
Figure 3.3. NUAK1 expression decreases in spheroid culture of some well-established cell lines.	34
Figure 3.4. NUAK1 is regulated by LKB1	35
Figure 3.5. NUAK1 knockdown increases spheroid viability and reattachment.....	37
Figure 3.6.NUAK1 knockdown increases viable cell number in spheroids	39
Figure 3.7. Validation of knockdown from single and double NUAK knockdown experiments	41
Figure 3.8. Assessment of single and double NUAK knockdown on EOC spheroids	42
Figure 3.9. Viability from single and double NUAK knockdowns	43
Figure 3.10. Dose-response curves using WZ4003 NUAK inhibitor.....	46
Figure 3.11.Treatment with WZ4003 influences growth kinetics of EOC cell lines.....	47
Figure 3.12. Treatment with WZ4003 produces a dose-dependent increase in clonogenicity.	49
Figure 3.13. WZ4003 clonogenic assay colony quantification.....	50
Figure 3.14. Dose response of HTH-01-015 on EOC cell growth.....	52

Figure 3.15. Treatment with HTH-01-015 has no effect on clonogenicity	54
Figure 3.16. Carboplatin dose-response curves in spheroids.....	56
Figure 3.17. WZ4003 does not further sensitize EOC cells to carboplatin	57
Figure 3.18. NUA1 inhibition does not affect thymidine incorporation.....	58
Supplementary Figure 5.1. Copy number and mutational status of ARK genes in serous ovarian cancer	71
Supplementary Figure 5.2. NUA1 and NUA2 mRNA expression from 47 EOC cell lines	72
Supplementary Figure 5.3. Affimetrix microarray analysis of ARK expression levels	74
Supplementary Figure 5.4. siRNA screen of all ARKs in 11 EOC cell lines.	75
Supplementary Figure 5.5. MARK3 is expressed in EOC cell lines	77
Supplementary Figure 5.6. p-MARK expression in EOC and regulation by LKB1	78
Supplementary Figure 5.7. MARK3 does not affect spheroid viability or reattachment potential.....	79

List of Abbreviations

Abbreviation	Term
AMPK	AMP-activated protein kinase
ARK	AMPK related kinase
BRSK	Brain specific serine-threonine kinase
CDK	Cyclin dependent kinase
DTT	Dithiothreitol
DMSO	Dimethyl sulfoxide
dNTP	Deoxyribose nucleoside triphosphate
EDTA	Ethylenediaminetetraacetic acid
EGFR	Epidermal growth factor receptor
EGTA	Ethylene glycol-bis(β -aminoethylether)- N,N,N',N'-tetraacetic acid
EOC	Epithelial ovarian cancer
EMT	Epithelial-to-mesenchymal transition
HGSOC	High-grade serous ovarian cancer
IC50	Half maximal inhibitory concentration
LGSOC	Low-grade serous ovarian cancer
LKB1	Liver kinase B1
MARK	Microtubule affinity regulatory kinase
MEF	Mouse embryonic fibroblast
MET	Mesenchymal-to-epithelial transition
ML	Monolayer culture
MLC2	Myosin light chain 2
MMP	Matrix metalloproteinase
MYPT1	Myosin phosphatase targeting subunit 1
NUAK	Nua kinase
OSE	Ovarian surface epithelium
PBS	Phosphate-buffered saline
PLK1	Polo-like kinase 1
PMSF	Phenylmethane sulfonyl fluoride

PP1	Protein phosphatase 1
PJS	Peutz-Jeghers syndrome
PVDF	Polyvinylidene fluoride
RIPA	Radioimmunoprecipitation assay
STIC	Serous tubal intraepithelial carcinoma
SIK	Salt inducible kinase
SNRK	Sucrose nonfermenting 1 (SNF-1) related kinase
SDS	Sodium dodecyl sulfate
TBST	Tris-buffered saline tween
TCA	Trichloroacetic acid
Sph	Spheroid culture
ULA	Ultra-low attachment

Chapter 1

1 Introduction

1.1 Epidemiology, Clinical Presentation and Treatment of Epithelial Ovarian Cancer

Epithelial ovarian cancer (EOC) is rare with respect to other malignancies affecting Canadian women, with approximately 2500 new cases each year. Despite its rarity, EOC is very aggressive in nature, causing approximately 1750 deaths each year (Canadian Cancer Society Statistics, 2015). The high death-to-incidence ratio associated with EOC is due to limited progress made with diagnosis and treatment. In most cases EOC is diagnosed when the disease has metastasized distantly in stages III or IV. As such, there continues to be a strong push for the research community to identify early detection methods and late stage therapies to reduce both morbidity and mortality associated with this group of diseases.

EOC has a low frequency in the general population, and it is believed that 1 in 70 women will develop ovarian cancer in their lifetimes (Han and Coleman, 2007). Oral contraceptive use and pregnancy are known to be protective against ovarian cancer, in support of the incessant ovulation hypothesis (Boscetti et al, 2002). According to this hypothesis, inflammation and damage to the fallopian tube and ovarian epithelium during the menstrual cycle increases the likelihood of mutation. Interrupting the cycle through pregnancy or oral contraceptive use is therefore thought to decrease the onset of cancer causing mutations (Fathalla, 1971). Likewise, risk factors for ovarian cancer include age, fertility treatment, hormone replacement therapies, and family history. Age is the leading risk factor, as the risk of developing ovarian cancer increases with age and most commonly occurs in post-menopausal women (Quirk and Nataraja, 2005). Ovulation stimulating drugs such as clomiphene citrate, used for the treatment of infertility, are known to increase the risk of ovarian cancer (Rossing et al, 1994). Clomiphene citrate in particular is known to increase cell proliferation in the ovarian and fallopian tube epithelium (Tomao et al, 2014). Hormone and estrogen replacement therapies increase

the risk of ovarian cancer by 60% in post-menopausal women (Lacey et al, 2002). Lastly, family history and hereditary mutations are known to cause between 10-15% of ovarian cancers (American Cancer Society, 2016). Germline mutations in the DNA repair genes, *BRCA1* and *BRCA2*, are the most common for risk of ovarian cancer. For this reason, genetic screening for *BRCA1* and *BRCA2* has become increasingly common and it is recommended that women bearing these mutations have their ovaries and fallopian tubes resected after child-bearing.

EOC is diagnosed in late stages because disease presentation is often vague and seemingly insignificant. Symptoms of ovarian cancer include abdominal pain, bloating, feeling full, weight change, gas, and nausea (Karst and Drapkin, 2010). These vague symptoms are often mistaken for conditions such as dyspepsia, menstruation and menopause. Staging for EOC is divided into 4 groups, and treatment efficacy decreases as the disease advances. Stage I is usually localized to one or both of the ovaries and does not involve the formation of ascites until stage IC. Treatment for stage I disease is often successful and surgery is sufficient to treat these patients, without the need for chemotherapy. Stage II involves locally metastatic disease, with extension to the pelvis. Stage III involves spread to the upper abdomen. Lastly, stage IV involves more distant metastasis to the liver, spleen and pleural parenchyma (Forstner et al, 2010).

Since most EOC patients are diagnosed during late-stage disease, treatment usually involves extensive disease management. Cytoreductive surgery is the most effective treatment to-date for EOC patients. This surgery involves removal of tumors within the peritoneal cavity, metastatic lesions, and locally affected organs such as the uterus and colon. "Optimal debulking," is considered complete once residual disease is less than 1cm in diameter (Schorge et al, 2010). Ovarian cancer management follows two arms of treatment: adjuvant and neoadjuvant. Adjuvant therapy is used for healthy patients, with no pre-existing conditions, and involves performing cytoreductive surgery prior to administering chemotherapeutics to reduce residual disease. Neoadjuvant therapy is used for patients with pre-existing conditions, who are not ideal surgical candidates, and involves shrinking the tumor with chemotherapy prior to cytoreductive surgery (Naora and Montell, 2005). While cytoreductive surgery is critical for reducing macroscopic

disease, therapeutic options for treatment of microscopic ovarian cancer are limited. Current chemotherapeutics involve the use of a combination of carboplatin and paclitaxel as standard of care. Carboplatin is a DNA damaging agent, containing platinum that is able to coordinately bind to DNA and prevent DNA replication (Naora and Montell, 2005). Paclitaxel is a microtubule stabilizing agent that causes mitotic catastrophe in rapidly dividing cells (Naora and Montell, 2005). It is common for patients to develop resistance to carboplatin upon recurrence, making treatment options limited. Furthermore, these chemotherapeutics are only able to target rapidly proliferating cells, letting dormant disease go untouched. Recent innovation has introduced the PARP inhibitor, Olaparib, into clinical trials for ovarian cancer treatment. Olaparib functions by taking advantage of the principle of synthetic lethality in BRCA deficient patients. By targeting the second arm of DNA repair, Olaparib is able to effectively kill ovarian cancer cells (Bixel and Hays, 2015). While Olaparib offers excellent innovation for BRCA deficient patients, there is still much progress to be made in terms of treatment options.

1.2 Origin and Subtypes of EOC

Historically it was believed that EOC arose from a structure lining the surface of the ovary, known as the ovarian surface epithelium (OSE). The OSE is composed of a single layer of cuboidal epithelium which lines the surface of the ovary. The OSE origin theory suggests that during repetitive ovulations and follicular ruptures, there may be invaginations of the OSE into the underlying stroma, leading to the formation of cortical inclusion cysts. It is thought that the influence of factors within the ovarian environment promotes metastatic transformation of these cysts (Auersperg et al, 1984). Evidence for this theory is supported by *in vitro* experiments using mouse and rat OSE in culture. Godwin et al. (1992) and Roby et al. (2000) demonstrated that repeated culture of mouse and rat OSE results in spontaneous transformation of tissue into a malignant phenotype. However, these studies were conducted on mouse and rat OSE which unlike human OSE, do not undergo senescence in culture, and therefore may not be representative of human EOC pathogenesis (Vanderhyden et al, 2003). Further evidence against this hypothesis may come from the fact that ovarian carcinomas resemble epithelial cells from extra-ovarian origins, such as the fallopian tube, rather than the OSE (Dubeau, 2008). It has

also been noted that women who have undergone resection of the ovaries can still develop ovarian cancer, suggesting an origin which is independent of the OSE (Dubeau, 2008). For these reasons, it is unlikely that the OSE is the true origin of epithelial ovarian cancers.

It is now widely accepted that Müllerian derived tissues are likely the origin of epithelial ovarian cancers, notably the fallopian tube in the case of high-grade serous ovarian cancer. To provide evidence for this, Marquez et al (2005) suggested that the gene expression profile of high grade serous ovarian cancer is more similar to the fallopian tube than the OSE. Additionally, the fallopian tube originates from the Müllerian duct during embryonic development, whereas the ovaries are derived from multiple embryonic structures such as the coelomic epithelium, subcoelomic epithelium, and primordial germ cells. PAX8 is a common marker of Müllerian derived tissues, such as the fallopian tube, uterus and vagina. It has been demonstrated that high-grade serous ovarian carcinomas express PAX8, suggesting a tubal origin of EOC (Kurman and Shih, 2010). Some more convincing evidence for the Müllerian origin of EOC came from Piek et al (2001) through analysis of tubal segments from women undergoing preventative bilateral salpingo oophorectomies. The authors found that in women with BRCA mutations and a strong genetic predisposition for EOC, 6 out of the 12 samples had cellular dysplasia at the fimbriated end of the fallopian tube which morphologically resembled high-grade serous EOC samples. For these reasons, it is likely that EOC subtypes that resemble Müllerian epithelium, such as the mucinous, serous and endometrioid subtypes, are likely derived from regions descended from the Müllerian duct rather than the OSE.

There are five histological subtypes of EOC, which are entirely distinct diseases at the molecular and cellular levels: low and high-grade serous ovarian cancers, endometrioid ovarian cancer, clear cell carcinomas and mucinous ovarian cancers. Serous ovarian cancers are recognized by enlarged nuclei and stromal invasion, and consist of two types: low-grade serous ovarian cancer and high-grade serous ovarian cancer (HGSOC). Low-grade serous ovarian cancers have been thought to originate from adenofibromas or borderline tumors (Vang et al, 2010). Low-grade tumors can be characterized by mutations in *KRAS*, *BRAF* and *ERRB2*, and it is estimated that two thirds of all low-grade

tumors have mutations in one of these genes (Vang et al, 2010). These 3 genes are upstream regulators of the MAPK pathway, therefore mutation results in uncontrolled proliferation (Vang et al, 2010). Surprisingly, low-grade tumors are typically more slow growing than high-grade tumors, and are characterized as type I EOC tumors (Vang et al, 2010). HGSOC is the most common form and has been identified as the most genomically unstable subtype of EOC, with 95% of tumors involving mutations in *TP53* (Karst and Drapkin, 2010). In addition to mutations in *TP53*, HGSOC tumors present with highly unstable genomes containing a significant number of chromosomal deletions and amplifications (Kuo et al, 2009). HGSOC is thought to arise from the fimbriated end of the fallopian tube epithelium, particularly from a lesion known as the serous tubal intraepithelial carcinoma (STIC) (Carlson et al., 2008). STIC lesions present with *TP53* mutations, similar to HGSOC tumors, and are thought to seed into the ovary to allow for the formation of HGSOC. HGSOC is the most common and possibly the most aggressive form of EOC, and is therefore the most well-studied disease site within ovarian cancer. Endometrioid ovarian tumors resemble the stratified columnar epithelium of the endometrium, and like HGSOC are derived from Müllerian epithelium. Endometrioid ovarian cancers are believed to be linked to endometriosis, and it is thought that endometriosis lesions may be a precursor to this subtype (Karst and Drapkin, 2010). Some endometrioid tumors are known to bear mutations in *PTEN*. Mucinous ovarian cancers represent less than 5% of all EOC tumors, and are more common in younger women aged 20-40 (Frumovitz et al, 2010). Histologically, these cells resemble intestinal epithelium. Mutationally, a significant proportion of mucinous tumors have alterations in *KRAS* and *HER2*, with recent innovation offering patients Herceptin as a treatment option (Brown and Frumovitz, 2014). Mucinous tumors are more epithelial in nature and have higher expression of E-cadherin compared to serous tumors (Brown and Frumovitz, 2014). Lastly, clear cell carcinomas of the ovary are so termed because they contain large glycogen filled granules which cause them to appear clear upon staining with hematoxylin and eosin. Clear cell carcinoma can be linked to endometriosis, with 25% of cases arising from patients with known endometriosis (Karst and Drapkin, 2010). These tumors have also been known to bear mutations in *ARID1A*, which regulates heterochromatin remodeling, and *PIK3CA*, which mediates cytokine production.

Unfortunately, current therapies have not widely exploited mutational or gene expression signatures of these histotypes of EOC. Therefore, it is important to understand the disease mechanisms behind each of these histotypes to better create targeted therapies which can respond to heterogeneity in EOC.

1.3 EOC Metastasis and Experimental Model Systems

EOC is distinct from other cancers, and has a unique metastatic mechanism that is usually contained within the abdominal cavity. A critical feature which is both a contributing factor and result of metastasis is ascites formation. Ovarian cancer patients typically present with ascites fluid, which collects in the abdomen. Ascites forms from a combination of vascular leakage and lymphatic blockage by the primary tumor. It is drained from a patient's abdomen during paracentesis or surgery (Naora and Montell, 2005). Ascites contributes to a complex tumor microenvironment because it contains a variety of cells in suspension, such as: cells disseminated from the primary tumor, fibroblasts, mesothelial cells, macrophages and leukocytes (Lengyel, 2010). This evident symptom of EOC is usually indicative of later stage disease progression and is an important feature of EOC metastasis.

EOC metastasis differs from that of other cancers, which metastasize via the vasculature and lymphatics. Instead, EOC has a unique metastatic mechanism that is usually limited to the peritoneal cavity (Kuwabara et al., 2008; Lengyel, 2010). The first step involves formation of the primary tumor in either the ovaries or fallopian tubes. In the case of HGSOC, cancer arises in the fallopian tubes upon loss of function mutations in *TP53*, causing further genomic instability and uncontrolled proliferation. Following primary tumor formation, single cells will disseminate from the primary tumor, and undergo epithelial-to-mesenchymal transition (EMT) becoming mesenchymal in nature; where these cells are exposed to the nutrient-deprived ascites environment. Exposed to detachment stress, these single cells are subject to cell death through anoikis. To evade cell death and respond to the nutrient-deprived environment, these detached cells aggregate together and form spheroids, and are frequently observed in native ascites samples from patients (Lengyel, 2010). EOC spheroids enter a state of dormancy due to a nutrient-poor environment (Lengyel, 2010; Correa et al., 2012). Dormancy in spheroids is

characterized by reduced proliferation, reduced metabolism and increased autophagy (Correa et al., 2012; Condello et al., 2015). This adaptation permits ovarian tumor cell survival during nutrient deprivation. Secondary tumor formation occurs when spheroids undergo a dormant-to-proliferative switch to initiate reattachment on to various peritoneal surfaces (Lengyel, 2010; Correa et al., 2012). The dormant-to-proliferative switch is characterized by an increase in proliferation, motility and invasion (Correa et al., 2012). This process is continually occurring within the peritoneal cavity to cause the development of multiple tumor nodules (Fig. 1.1A).

This unique metastatic model can be studied *in vitro*, using both cell lines and primary cells from EOC patients. In the case of primary cells, ascites fluid can be drained from a patient's abdomen during surgery or paracentesis. Ascites fluid often contains endogenous spheroids, which have likely metastasized from the primary tumor. These spheroids can be plated on regular tissue culture plastic, allowing the spheroid to disperse and form an adherent monolayer of cells. These adherent cells can be taken and plated on ultra-low attachment (ULA) dishes, which are hydrophilic and neutrally charged. This allows for aggregation of cells and causes the formation of spheroids *in vitro*; permitting the study of spheroid biology. Subsequently, these spheroids can be taken out of ULA culture and reattached onto regular tissue culture plastic to mimic the process of spheroid reattachment on to peritoneal surfaces (Fig. 1.1B) (Shepherd et al, 2006).

Spheroids are a unique aspect of EOC metastasis that have interesting survival mechanisms in response to nutrient deprivation. Firstly, spheroids are held within the nutrient-poor microenvironment found within ascites fluid. To adapt to this nutrient-poor microenvironment, spheroids enter a state of dormancy which is characterized by reduced proliferation, decreased metabolism, and increased autophagy (Correa et al., 2012; Condello et al., 2015). The dormant and anti-proliferative state of spheroids make them less sensitive to both platinum and taxol based chemotherapies (Sutherland et al., 1976). L'Esperance and colleagues (2008) performed gene expression profiling of EOC spheroids following treatment with chemotherapeutics and noted differential gene expression of genes implicated in proliferation, growth, cell assembly, cell death and cell cycle. They found that genes associated with DNA repair and cell cycle arrest were

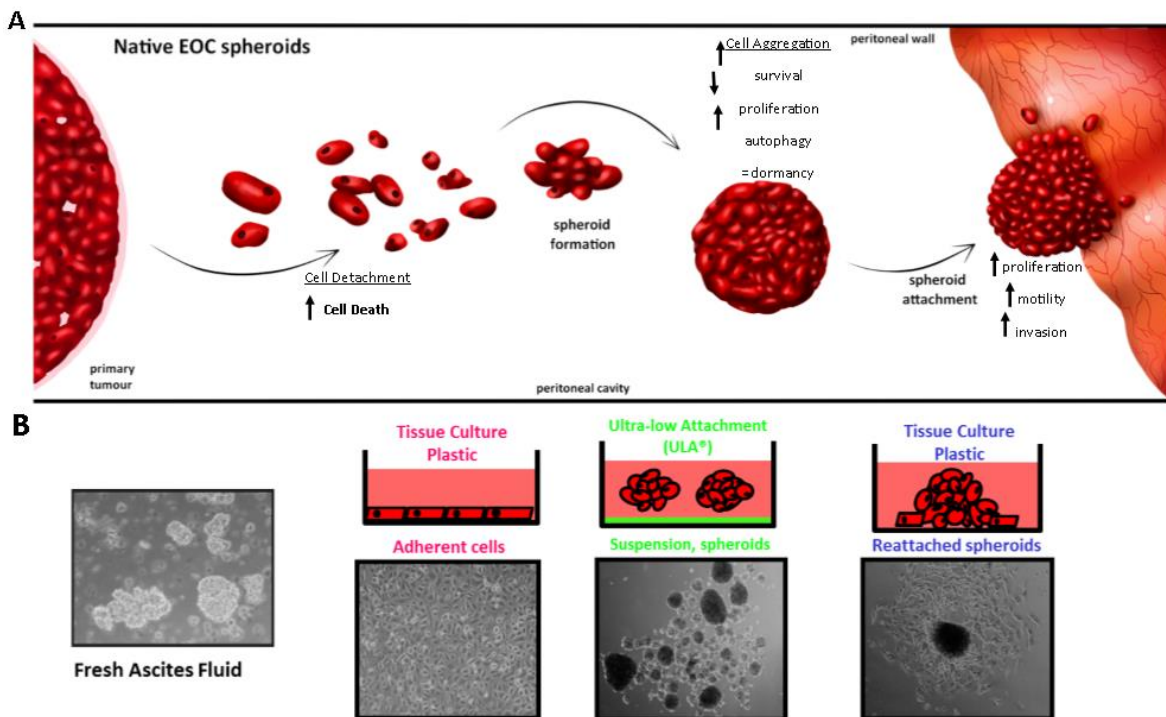


Figure 1.1. Mechanisms of EOC metastasis *in vitro* and *in vivo*. **(A)** EOC metastasis within the peritoneal cavity. EOC begins with the primary tumor in either the ovaries or fallopian tubes. Cells de-attach from the primary tumor, at which point there is an increase in cell death by anoikis. To evade anoikis, cells aggregate together and form dormant spheroids, where they conserve energy by decreasing proliferation. Spheroids can trigger secondary tumor development by reattaching to the wall of the peritoneal cavity, at which point there is a dormant to proliferative switch. **(B)** Modelling metastasis *in vitro*. Ascites samples, extracted from patients during surgery, contain spheroids in suspension. Spheroids from ascites can be plated on tissue culture plastic to produce an adherent monolayer of cells. Adherent cells can then be plated on ultra-low attachment plates to induce spheroid formation. Secondary tumor development can be mimicked using a reattachment assay, where spheroids are re-plated onto tissue culture plastic.

significantly upregulated in spheroids, while genes implicated in metabolism and inflammatory response were significantly downregulated; relative to adherent culture. To that end, Correa and colleagues (2012) found that spheroids exhibit reduced proliferation through decreased Akt activity; and despite displaying a phenotype that is similar to quiescence, spheroids can rapidly reinitiate proliferation and Akt activity upon reattachment. It is therefore critical to study EOC spheroids and understand the mechanistic behavior of spheroids. Therapies targeting EOC spheroids may allow for blockade of metastatic disease within the peritoneal cavity.

1.4 LKB1-AMPK in EOC Metastasis

A key limitation of all cells is that they must guarantee nutrient availability prior to proliferation. Nutrient availability is recognized by a variety of stress response factors, one of which is Liver Kinase B1 (LKB1). The LKB1-AMPK signaling pathway has been well documented as a fast-acting responder to nutrient starvation and metabolic stress (Mihaylova and Shaw, 2011). Under stress conditions (cell deattachment, hypoxia, glutamine/glucose deprivation, etc), LKB1 has been observed to phosphorylate AMPK to initiate a dormancy-like state and alter metabolic homeostasis in a wide-variety of cellular contexts.

Under nutrient starvation or cell stress conditions, phosphorylated LKB1 complexes with the pseudokinases STRAD and MO25 (Alexander and Walker, 2011), causing phosphorylation of the α subunit of AMPK at Thr172. The AMPK $\alpha\beta$ subunits can then complex with the γ subunit, initiating downstream signaling to reduce glucose and lipid metabolism, decrease protein translation, trigger cell cycle arrest and increase autophagy (van Veelen et al., 2011; Shaw et al., 2004; Yang et al., 2010) (Fig. 1.2). The responses elicited by the LKB1-AMPK pathway are critical in helping cells respond to stress conditions.

LKB1, encoded by the *STK11* gene on chromosome 19p13, was originally identified as a tumor suppressor gene due to its association with an inherited cancer disorder known as Peutz-Jeghers Syndrome (PJS). Patients with PJS have heterozygous mutations in *STK11*, with one allele lacking a functional protein product. PJS families have a strong cancer

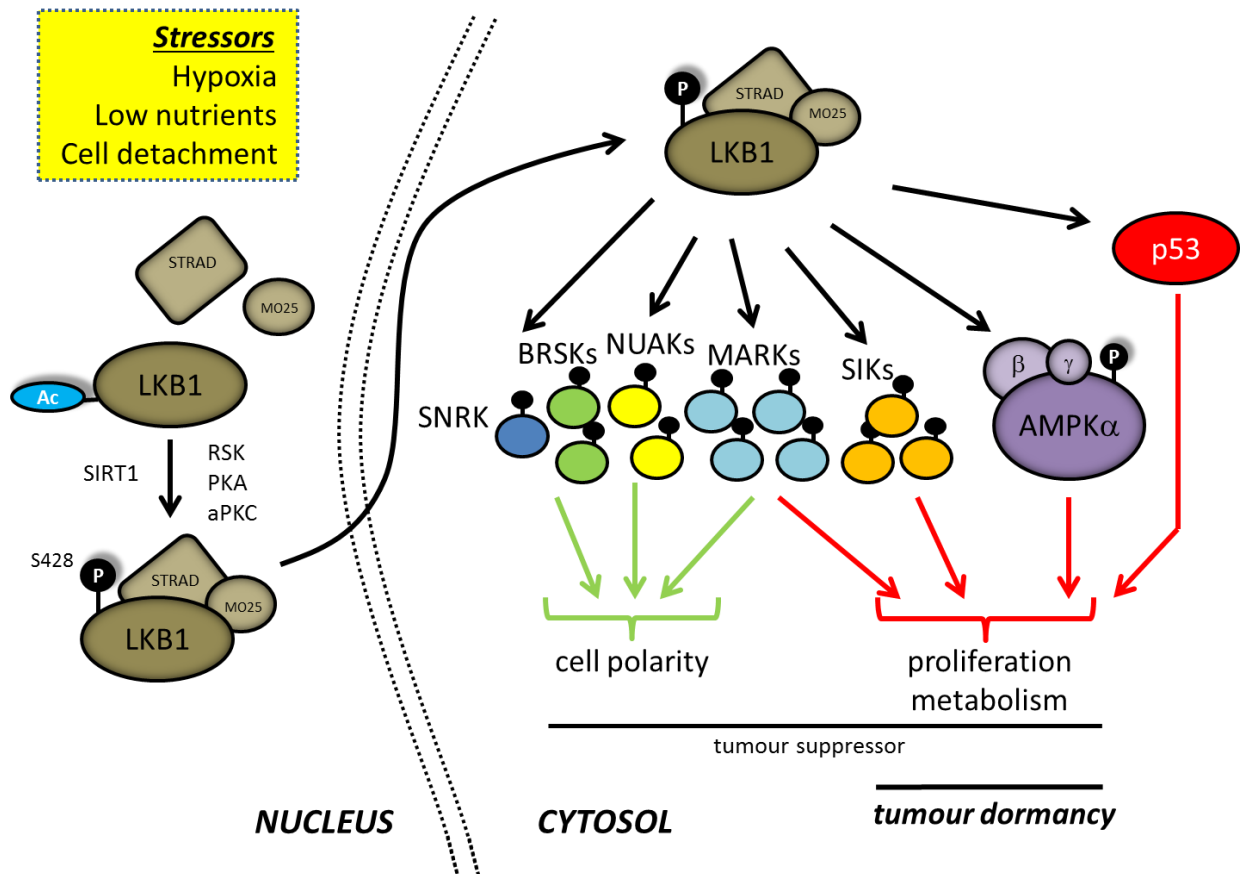


Figure 1.2. Summary of LKB1 signaling. During conditions of cell stress (cell detachment, hypoxia, low nutrients) LKB1 complexes with the pseudokinases STRAD and MO25 to initiate downstream signaling through p53, AMPK and the AMPK related kinases (ARKs). This downstream signaling acts to reduce proliferation and metabolism (red arrows), while positively regulating cell polarity (green arrows). These downstream signals are important to tumor suppression because they restrict normal cells from displaying neoplastic behaviour. These functions could also be important to tumor dormancy after tumor formation, allowing tumors to survive metabolically challenging conditions. LKB1 can be post-translationally modified by SIRT1, RSK, PKA and aPKC. *Figure generated by Dr. Trevor Shepherd.*

history, and are at risk of developing gastrointestinal cancers, pancreatic cancer, cervical cancer, ovarian cancer and breast cancer (Whittle et al., 2011). It is also common for patients to develop benign polyps in the stomach and intestinal tract (Whittle et al., 2011). In addition to PJS, *STK11* is commonly mutated in non-small cell lung cancer (NSCLC), with 15-35% of tumors bearing mutations in *STK11* (Shackleford and Shaw, 2009). Furthermore, *STK11* is mutated in 20% of cervical carcinomas (Shackleford and Shaw, 2009). In mice, heterozygous deletion of LKB1 causes the development of gastrointestinal polyps, similar to PJS patients (Miyoshi et al., 2002). Likewise, site specific deletion of LKB1 in various epithelial tissues leads to tumor formation. For instance, LKB1 deletion in the endometrial epithelium of female mice has been shown to lead to invasive adenocarcinoma (Contareas et al., 2008). Additionally, loss of LKB1 in the skin of mice promotes squamous cell carcinoma development (Gurumurthy et al., 2008). The notion of LKB1 being a tumor suppressor can be supported by its role in stress response and nutrient deprivation. Under cell stress conditions, LKB1 acts to stimulate p53 activity, decrease proliferation, and decrease cellular metabolism (Tiainen et al., 2002). All of these outcomes would in theory be counterproductive for cancer initiation and tumor progression, hence, loss of LKB1 drives tumor formation in many cancer models.

Recent evidence has brought to light the possible pro-metastatic function of LKB1, suggesting that the role of LKB1 in tumor formation or tumor suppression may be context dependent. Peart and colleagues (2015) uncovered an oncogenic role of LKB1, suggesting its importance in tumor progression in ovarian cancer. They screened 7 ascites derived ovarian cancer patient samples and found that LKB1 and its direct downstream substrate, AMPK, were phosphorylated and activated, suggesting that the LKB1-AMPK pathway is active, rather than suppressed, in metastatic ovarian cancer cells (Peart et al., 2015). Furthermore, using 3 cell lines and 3 ascites derived patient samples, they discovered that LKB1-AMPK signaling is activated specifically in dormant ovarian cancer spheroids. This suggests that LKB1 mediated signaling is important to maintain dormancy or promote survival in spheroids during the unique metastatic process of this disease.

Although the authors noted that LKB1-AMPK signaling is likely important to spheroids, it appears that this may not be the only pathway involved. Using siRNA against *STK11* and *PRKAA1*, encoding for AMPK α 1, they found that knockdown of LKB1 but not AMPK α decreased cell viability in the presence or absence of carboplatin (Peart et al., 2015). This indicates that there may be other downstream targets of LKB1, independent of AMPK, which promote cell viability, chemoresistance and dormancy in EOC spheroids.

1.5 AMPK-Related Kinases and Their Potential Importance in EOC Metastasis

The AMPK Related Kinases (ARKs) are a group of 12 kinases that are known to be phosphorylated by LKB1 at threonine residues similar to that on AMPK (Lizcano et al., 2004). These 12 kinases consist of the nua kinases (NUAKs), Microtubule affinity regulatory kinases (MARKs), Salt inducible kinases (SIKs), Brain specific serine-threonine kinases (BRSKs) and Sucrose non-fermenting 1 (SNF) related kinase (SNRK). Some of these kinases have been documented as stress responders downstream of LKB1, independent of AMPK.

The NUAKs consist of two family members, and have been implicated in processes such as cell senescence (Humbert et al., 2010), suppression of cell death during glucose starvation (Suzuki et. al, 2003), inhibition of protein synthesis and mitochondrial respiration (Liu et al., 2012), and tumor invasion through stimulation of metalloproteinase (MMP) secretion (Suzuki et al., 2004). In cancer, NUAK family functions have been regarded as both tumor suppressive and oncogenic (Chen et al., 2013; Lu et al., 2013, Namiki et al., 2011; Ye et al., 2014; Tsuchihara et al., 2008; Sun et al., 2013). Downstream of LKB1, NUAKs have been observed to promote cell detachment and trigger cell cycle arrest through p53 activation (Hou et al., 2011). In a single study involving NUAK1 cell signaling in ovarian cancer by Zhang et, al. (2015), NUAK1 was seen to trigger epithelial-to-mesenchymal transition (EMT) through suppression of microRNAs which promote mesenchymal-to-epithelial transition (MET). Similarly, a recently published study by Phippen et. al (2016) suggested that increased NUAK1 expression at the RNA level was associated with poor prognosis in HGSOE

patients. However, these studies did not interrogate NUA1 signalling in the context of ovarian cancer models such as EOC spheroids and dormancy maintenance.

The MARKs consist of four family members and in many cases can act to phosphorylate downstream targets, making them docking sites for the 14-3-3 protein, a mediator of subcellular localization (Lizcano et al., 2004). MARK signaling has been implicated in processes such as cell cycle arrest (Bachmann et al., 2004), epithelial cell polarity (Lewandowski et al., 2014), and activation of Wnt signaling (Spicer et al., 2003). Downstream of LKB1, MARKs have been implicated in cell adhesion in melanoma (Chan et al., 2014), inhibition of EMT (Goodwin et al., 2014), and localization of histone deacetylases (Lizcano et al., 2004). Many of these functions may be important in the context of ovarian cancer spheroids and have yet to be studied.

The SIKs consist of three family members and have been observed in processes including inhibition of NF κ B signaling (Yong Kim et al., 2013), autophagy (Yang et al., 2014), and cell cycle transition (Chen et al., 2014). Downstream of LKB1, SIKs have been implicated in nucleocytoplasmic transport of histone deacetylases (Walkinshaw et al., 2013), intracellular junction stability in epithelial cells (Eneling et al., 2012), and p53-dependent anoikis (Cheng et al., 2009). In ovarian cancer, SIK2 has been seen to trigger mitotic initiation through recruitment of the centrosome linker protein, C-nap1 (Ahmed et al., 2010). Likewise, SIK3 is involved with G1 \rightarrow S transition in ovarian cancer, and overexpression has been observed to promote tumor progression in mice (Charoenfuprasert et al., 2011).

The BRSKs consist of two family members and are predominantly expressed in the mammalian brain, and have been implicated mainly in neuronal polarity (Bright et al., 2008). These kinases have not been well documented in cancer, or in the context of cancer dormancy, and thus remain to be investigated in the context of EOC spheroids.

Lastly SNRK, or sucrose nonfermenting 1 (SNF-1) related kinase, has been largely described as a plant kinase. However, one study has looked at the effects of SNRK in colon cancer. Rines et al. (2012) found that SNRK antagonizes β -catenin signaling to reduce proliferation in colon cancer cells. This model may be relevant in the context of

ovarian cancer dormancy, potentially downstream of LKB1, but remains to be investigated.

Many of the ARKs have been documented in the literature to have roles related to metabolic stress response and dormancy, but few have been investigated in ovarian cancer and remain largely understudied in the context of EOC dormancy.

Through the course of my project, I have gathered evidence to suggest that NUA1 plays an important role in EOC cell and spheroid viability, downstream of LKB1, and have thus focused my project exclusively on the role of NUA1 in EOC metastasis.

1.6 NUA1 Regulation and Function

NUA1, also known as ARK5, is encoded on chromosome 12 on cytogenetic band q23.3 (Scherer et al., 2006). The NUA1 gene is encoded as 2 isoforms, with isoform 1 being the canonical sequence (Scherer et al., 2006). It is highly expressed in the brain, spinal cord and heart, with lower expression in skeletal muscle, ovaries, fallopian tube, placenta, lung and liver (Kusaki et al., 2004). It is predominantly localized cytoplasmically within the cell (Hou et al., 2011).

NUA1 is regulated by LKB1 at Thr211 to initiate kinase activity. There is also evidence to suggest that NUA1 is positively regulated by AKT at Ser600 to mediate downstream signalling (Suzuki et al., 2013). NUA1 is negatively regulated by PLK1 and CDKs at Ser476, Ser480 and Ser445 (Banerjee et al., 2014). Upon phosphorylation by these negative regulators, NUA1 is tagged for ubiquitination and subsequent degradation (Fig. 1.3).

Functionally, NUA1 kinase activity has been implicated in cell cycle arrest during the G1→S phase of cell cycle through phosphorylation of Ser15 and Ser392 on p53, which in turn mediates p21 transcription to promote cell cycle arrest (Hou et al., 2012). NUA1 can also phosphorylate LATS1, leading to its degradation. Degradation of LATS1 promotes increases in cell size, aneuploidy and senescence (Humbert et al., 2011). Furthermore, NUA1 can interact with myosin phosphatase targeting subunit 1 (MYPT1) to trigger cell detachment and regulation of the mitotic checkpoint kinase

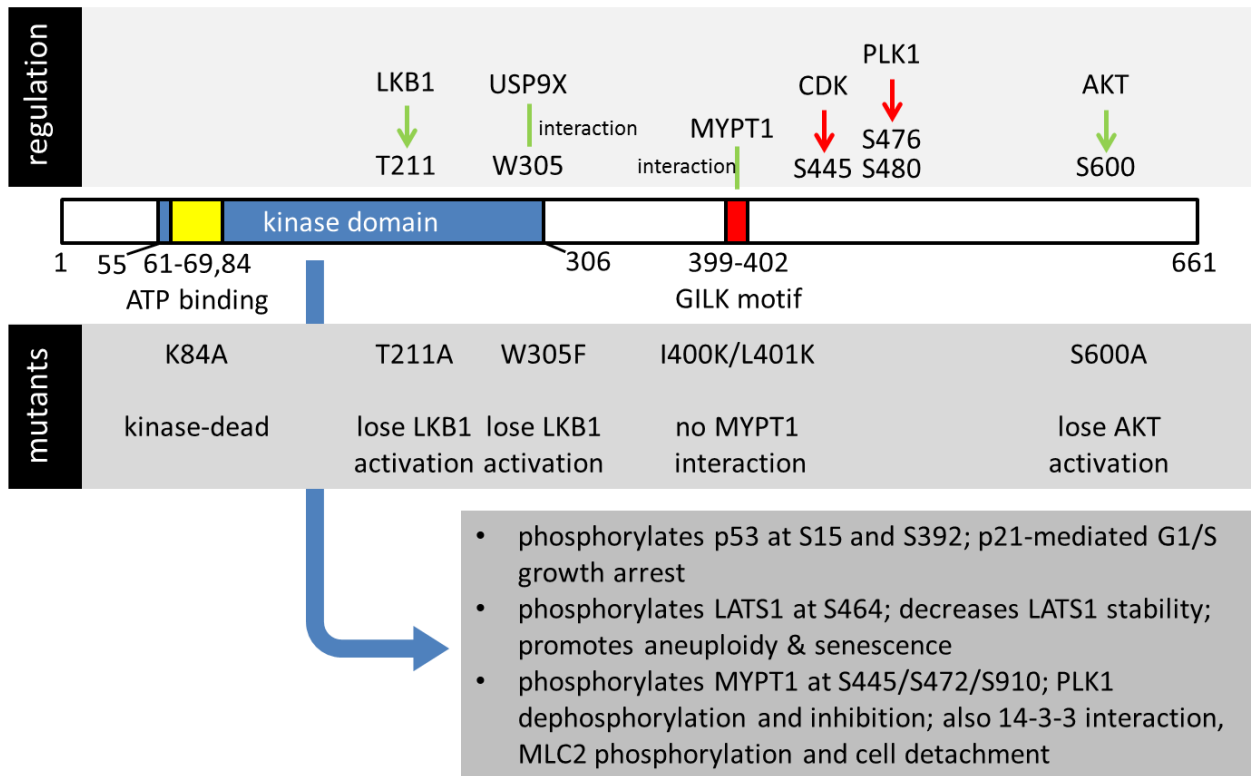


Figure 1.3. NUAK1 regulation and function. (*upper panel*) NUAK1 is regulated by LKB1 at Thr211 within its kinase domain to activate kinase activity. It is also positively regulated by AKT at S600. NUAK1 is negatively regulated by CDKs and PLK1 to trigger ubiquitination and degradation. Interaction with USP9X triggers de-ubiquitination. NUAK1 can interact with and phosphorylate MYPT1 to mediate changes with actomyosin signaling. (*middle panel*) NUAK1 mutants. Mutation at T211 and W305 prevent activation by LKB1. (*inset*) NUAK1 functions to phosphorylate several downstream substrates implicated in cell cycle and actomyosin dynamics. (Hou et al., 2011, Humbert et al., 2010, Banerjee et al., 2014) *Figure generated by Dr. Trevor Shepherd.*

PLK1, affecting cell cycle transition (Zagórska et al., 2010). In 2014, Banerjee and colleagues demonstrated that NUAK1 is reciprocally regulated with PLK1, in that NUAK1 expression during G1→S phase acts to inactivate PLK1 and PLK1 expression during G2→M phase acts to induce degradation of NUAK1. NUAK1 has also been implicated as an upstream regulator of AMPK and can cause decreased protein synthesis through mTORC1 inhibition (Liu et al., 2011). NUAK1 suppresses Fas induced apoptosis, through phosphorylation of caspase 6 (Suzuki et al., 2004). This anti-apoptotic response may be important for cancer cell survival.

The most well-characterized downstream target of NUAK1 is MYPT1. Encoded by the *PPP1R12A* gene, MYPT1 is a member of the PP1β phosphatase complex. MYPT1 is important to regulation of cell motility and control of cell cycle. In regard to cell motility, MYPT1 acts as a negative regulator of myosin light chain 2 (MLC2) and acts to dephosphorylate MLC2 to trigger cell adhesion. Phosphorylation of MYPT1 by NUAK1 at Ser445, Ser472, or Ser909 promote MYPT1 interaction with 14-3-3, thus preventing MYPT1 from inactivating MLC2 (Zagórska et al., 2010). In terms of cell cycle, NUAK1 can phosphorylate MYPT1, preventing MYPT1-mediated dephosphorylation and inactivation of PLK1, thus causing G2→M transition (Banerjee et al., 2014).

Using MYPT1 phosphorylation as a readout of NUAK1 activity, Banerjee and colleagues (2014) classified two novel NUAK1 inhibitors. WZ4003 was originally developed as a structurally inactive inhibitor of EGFR signalling, but was found to specifically inhibit NUAK activity (Zhou et al., 2009). WZ4003 can inhibit both NUAK species. HTH-01-015 is a NUAK1-selective inhibitor which is relatively ineffective for inhibition of NUAK2. Upon EDTA-induced detachment of HEK293 cells, Banerjee and colleagues noted that treatment with WZ4003 or HTH01-015 led to dose-dependent decreases in MYPT1 phosphorylation. To this end, the authors also noted that NUAK inhibition using both compounds led to decreased cell migration in MEF cells. Lastly in both U2OS and MEF cell lines, the authors noted that treatment with both inhibitors led to decreased proliferation. Banerjee and colleagues propose that both compounds act as ATP mimetic inhibitors, according to their structures (Banerjee et al., 2014). Their results identify the potency of both inhibitors and warrant the use of these compounds *in vitro*.

To date, there have been many interesting functions of NUA1 brought to light in cancer, both as an oncogene and tumor suppressor. However, NUA1 has not been studied in the context of cancer dormancy and more specifically, in dormant ovarian cancer spheroids. Previously identified mechanisms of NUA1 signalling may be relevant to the context of EOC spheroids. Furthermore, the discovery of reagents for NUA1 inhibition allow for optimal study of NUA1 function *in vitro*. Therefore, it may be worthwhile to study the role of NUA1 in EOC spheroids to see if it may be contributing to dormancy and viability maintenance in this unique metastatic model.

1.7 Research Goal, Hypothesis and Experimental Objectives

LKB1-mediated regulation of NUA1 has not previously been studied in EOC spheroids. Our lab has previously identified LKB1 as an important master kinase in ovarian cancer, particularly in spheroids. The next step would be to understand how one of its downstream kinases, NUA1, is involved in EOC signal transduction. In particular, it would be critical to address if NUA1 is involved with maintenance of dormancy and chemoresistance in ovarian cancer spheroids.

I hypothesize that NUA1 is activated by LKB1 and maintains dormancy and viability in EOC spheroids. To investigate this hypothesis, I first aimed to characterize NUA1 expression across a wide array of cell lines and determined how NUA1 was regulated by LKB1 in EOC spheroids. Secondly, I investigated if NUA1 was important to viability in EOC spheroids and characterized a possible mechanism by which NUA1 was affecting EOC cell and spheroid viability. This project has allowed me to delve into the important role of NUA1 in EOC dormancy and viability, and has opened new potential avenues to high risk, high reward therapy in the treatment of ovarian cancer.

Chapter 2

2 Materials and Methods

2.1 Cell Culture

OVCAR8 (ATCC), HEYA8, HEY (gift from G.Mills, MD Anderson), OVCAR8*STK11*KO (CRISPR-Cas9 performed by Dr. Trevor Shepherd), and HEYA8*STK11*KO (CRISPR-Cas9 performed by Dr. Trevor Shepherd) cells were cultured using RPMI-1640 (Wisent), supplemented with 5% fetal bovine serum (FBS, Wisent). CAOV3, TOV21G, TOV112D, SKOV3, OVCAR3, OVCAR4, and OVCAR5 (ATCC) were cultured in DMEM-F12 (Gibco), supplemented with 10% FBS. FT190 and FT237 (gift from R. Drapkin, UPenn) were cultured in DMEM-F12, supplemented with 10% FBS. COV318 and COV362 (gift from Z. Khan, UWO) were cultured in RPMI-1640, supplemented with 5% FBS. Early passage ascites-derived cell lines (iOvCa) were established by Dr. Gabriel DiMattia and cultured in DMEM-F12, supplemented with 10% FBS. Ascites-derived cell lines (Table 2.1) were established according to protocol previously described by Shepherd and colleagues (2006). All work with patient materials has been approved by The University of Western Ontario Health Sciences Research Ethics Board (protocol number 12668E).

Cells were kept in culture using 10cm dishes (Sarstedt). For protein isolation in adherent culture, cells were seeded at a density of 1×10^5 cells/well in a 6-well dish (Sarstedt) and lysate was extracted 3 days post-seeding. For protein isolation in spheroid culture, cells were seeded at a density of 3×10^5 cells/well in 6-well ultra-low attachment dishes (ULA, Corning) and lysate was extracted 3 days post-seeding. Most experiments involved plating cells in parallel in adherent and spheroid culture using various formats. For 24-well format, cells were seeded at a density of 5×10^4 cells/well in adherent (Sarstedt) and ULA (Corning) plates. For 96-well format, cells were seeded at a density of 2×10^3 cells/well in adherent (Sarstedt) and ULA (Corning) plates. For drug treatments, spheroids were treated with indicated drug concentrations at time of seeding. Cells in adherent culture were treated with indicated concentrations one day post-seeding.

Table 2.1. Summary of low-passage, ascites-derived cell lines.

Cell Line	Tumor Histotype	Patient Stage	Chemonaïve	Known mutations
iOvCa97	grade III serous adenocarcinoma	IIIC	x	NA
iOvCa105	HGSOC	NA		<i>TP53</i>
iOvCa112	Grade II HGSOC	III		<i>TP53</i>
iOvCa129	HGSOC	IIIC	x	<i>TP53</i> <i>BRCA2</i>
iOvCa130	HGSOC	IIIC	x	<i>PIK3CA</i>
iOvCa131	HGSOC	NA		<i>TP53</i>
iOvCa142	HGSOC	NA		<i>TP53</i>
iOvCa147	HGSOC	NA		<i>TP53</i>
iOvCa168	HGSOC	IIIC		<i>TP53</i>
iOvCa170	HGSOC	IIIC		<i>TP53</i>
iOvCa185	Clear cell carcinoma	NA		<i>TP53</i>
iOvCa195	HGSOC	NA		<i>TP53</i> <i>BRCA1</i>
iOvCa198	HGSOC	NA		NA
iOvCa233	HGSOC	NA		NA
iOvCa241	LGSOC	NA		<i>KRAS</i>
iOvCa246	HGSOC	NA		<i>TP53</i>
iOvCa247	LGSOC	IIIC		<i>TP53</i> <i>PIK3CA</i>
iOvCa256	HGSOC	IV		<i>TP53</i>
iOvCa270	HGSOC	NA		<i>TP53</i>
iOvCa291	NA	NA		NA
iOvCa304	HGSOC	NA		<i>TP53</i>
iOvCa313	HGSOC	NA		<i>TP53</i>

HGSOC = High-grade serous ovarian cancer

LGSOC = Low-grade serous ovarian cancer

NA = not available

2.2 Generation of OVCAR-STK11KO Cells

The 20-nucleotide guide sequence targeting the *STK11* gene 5'-AGCTT GGCCC GCTTG CGGCG-3' was selected using the online *in silico* CRISPR Design Tool at <http://tools.genome-engineering.org>. Complementary oligonucleotides 5'-CACCG AGCTT GGCCC GCTTG CGGCG-3' and 5'-AAACC GCCGC AAGCG GGCCA AGCTC-3' (synthesized by Sigma-Genosys) were annealed and ligated into the *Bbs*I-digested restriction endonuclease site of pSpCas9(BB)-2A-Puro plasmid (gift from Dr. Fred Dick, Western University) as per the protocol described in Ran *et al.* (2014) to generate the pSpCas9-sg*STK11* plasmid. OVCAR8 cells were seeded at 2×10^5 cells/well into 6-well plates and transfected with 1 μ g of pSpCas9-sg*STK11* plasmid into each well using LipofectAMINE 2000 (Invitrogen) according to manufacturer's instructions. The next day, media was replaced with complete growth media containing 1 μ g/mL puromycin. Puromycin selection was performed for only one day, then cells were allowed to expand in complete growth media within each original well of the 6-well plate. Cells were trypsinized, counted, and seeded into 96-well plates at ~ 1 cell/well to perform limiting dilution subcloning of potential *STK11*-knockout OVCAR8 cells. Wells containing single colonies were expanded into 24-well plates then 6-well plates for protein isolation and confirmation of *STK11* knockout by western blotting for LKB1 expression. Five clones lacking LKB1 protein expression were positively identified and subsequently mixed in equal ratios to generate the OVCAR8-*STK11*KO cell line population. This OVCAR8-*STK11*KO cell line is routinely verified to have sustained loss of LKB1 expression.

2.3 Western Blot

RIPA buffer was prepared for lysis using 50mM HEPES (pH 7.4), 150mM NaCl, 10% Glycerol, 1.5mM MgCl₂, 1mM EGTA, 1% Triton X-100, and 0.1% SDS, and stored at 4°C. Lysis buffer was prepared using RIPA buffer, 1mM sodium orthovanadate, 250mM β -glycerophosphate, 10mM sodium pyrophosphate, 10mM NaF, 1% sodium deoxycholate, 1mM PMSF, and 1X protease inhibitor cocktail (Roche). For adherent cultures, cells were washed twice with PBS prior to addition of lysis buffer and scraped.

Spheroids were collected and centrifuged at 2000rpm for 5 minutes. Media was aspirated from spheroid pellet, and the pellet was resuspended in PBS and centrifuged at 2000rpm for 5 minutes. Lysis buffer was added to spheroid pellet, after PBS was aspirated.

Adherent and spheroid lysates were incubated in lysis buffer on ice for 30 minutes, with vortexing every 5 minutes. After 30 minutes, both adherent and spheroid lysates were centrifuged at 14 800 rpm for 20 minutes. Supernatant was isolated post-centrifugation and lysates were stored at -80°C. Protein concentration was quantified using Bradford assay, with Biorad protein assay reagent (Bradford, 1976).

Protein samples were prepared using 50µg of protein, determined according to Bradford assay, and 4x protein loading buffer. Protein loading dye was prepared using 62.5 mM Tris-HCl pH 6.8, 2.5 % SDS, 0.002 % Bromophenol Blue, 0.7135 M (5%) β-mercaptoethanol, and 10 % glycerol. Samples were boiled for 5 minutes prior to electrophoresis on 8% acrylamide gels. Electrophoresis was run for ~2 hours, followed by a 1 hour wet-transfer onto a PVDF membrane (Immobilon-P). Membranes were blocked for 1 hour with 5% milk (NUAK1) or 5% BSA (LKB1, MYPT1). Primary antibody was left on membranes overnight at 4°C. Antibodies used included NUAK1 (1:1000 dilution in 5% milk, Cell Signaling #4448), LKB1 (1:1000 dilution in 5% BSA, Cell Signaling #3050). pMYPT1 Ser472, pMYPT1 Ser445, pMYPT1 ser909 and GST-MYPT1 were purchased from MRC Protein Phosphorylation and Ubiquitination Unit (University of Dundee, Scotland) and prepared 1:1000 in 5% BSA. Anti-tubulin antibody was purchased from Sigma and applied for 1 hour at 1:1000 dilution in 5% BSA. Following overnight incubation, membranes were washed 3x with TBST for a total of 30 minutes and incubated for 1 hour with secondary antibody (1:10 000 dilution) using HRP horseradish peroxidase-conjugated anti-rabbit and anti-mouse (GE healthcare) and anti-sheep (Sigma) secondaries. Membranes were washed 3x with with TBST for a total of 30 minutes and imaged using Luminata Forte substrate (Millipore) on Biorad Gel-doc. Images were taken from 20 – 900 seconds, and all western blots shown and quantified are from 300 second exposure, except tubulin which is shown and quantified at a 35 second exposure.

2.4 Phostag™ Western Blot

Phostag™ lysis buffer was prepared similar to above, however EGTA, sodium pyrophosphate and β -glycerophosphate were excluded from preparation. Protein lysates were prepared in the same way as described above.

Phostag™ gels were prepared using Phostag™ solution (Wako Chem) and 10mM MnCl₂, as 8% acrylamide gels, according to manufacturer's protocol. Electrophoresis was run for ~3 hours, after which gels were washed for 10 minutes with 1x transfer buffer with 1mM EDTA, followed by 10 minutes with 1x transfer buffer without EDTA. Wet transfer was run for 1 hour on PVDF membranes (Immobilon-P). Membranes were incubated in primary antibody for 2 days, and imaging was performed as described above. Images were taken from 20 – 900 seconds. Images shown and quantified are from 900 second exposure.

2.5 siRNA-mediated knockdown

Transfections were performed as previously described by Peart and colleagues (2015), using 2 μ L of siRNA for each well. Cells were seeded at a density of 1 x 10⁵ cells/well in a 6-well dish and transfected with siRNA the following day. siRNA transfections were performed using DharmaFECT-1, according to manufacturer's protocol, in 2mL media (GE Life Sciences). Media was supplemented with an additional 2mL of growth media 24 hours after transfection. Cells were trypsinized and counted (TC10 cell counter, Biorad) and seeded for experimental conditions after 72 hours (6-well, 24-well, 96-well). Plates were extracted 3 days post-seeding for cell viability readings (see below). Western blot knockdown analysis was performed on lysates extracted from 6-well adherent culture, 3 days post-seeding.

Double knockdown experiments were done using the same volume of DharmaFECT-1 as single knockdown conditions, to prevent toxicity. siRNA amounts for each individual siRNA were halved in double knockdown conditions.

2.6 Reattachment Assays

Day 3 transfected spheroids, from 24-well ULA plates, were plated on to 6-well plates. Cells were left in culture for 48 hours, after which point cells were fixed and stained using Hema3 staining (Protocol). Fixed and stained colonies were counted.

2.7 Clonogenic Assays

OVCAR8 and TOV21G cells were seeded at 500 cells/well in a 6-well dish. OVCAR4 and HEYA8 cells were seeded at 1000 cells/well in a 6-well dish. The following day, cells were treated with DMSO, WZ4003 (Tocris), or HTH-01-015 (Tocris) at indicated concentrations. Cells were left in culture for 10 days, after which point colonies were fixed and stained using Hema3 staining (Protocol). Fixed and stained colonies were counted.

2.8 CellTiter-Glo® Viability Assay

For adherent and spheroid cells in 96-well format, all media was aspirated off each well after 72 hours in culture. Aspiration was carefully performed to ensure spheroids remained intact. A 1:1 mixture of CellTiter-Glo® reagent (Promega) and media was prepared. 200µL of prepared mixture was added to each well. Cells were triturated, approximately 20 times/well, to lyse cells and spheroids. Plates were left overnight at -80°C to ensure lysis. The following day, 100µL was transferred from each well into a new white-walled 96-well plate. Readings were measured on Wallac 1420 Victor 2 spectrophotometer plate reader, measuring luminescence.

For adherent cells in 24-well format, all media was aspirated off after 72 hours in culture. A 1:1 mixture was prepared as described above. 200µL of prepared mixture was added to each well. Cells were triturated, approximately 20 times/well, to lyse cells. Plates were left overnight at -80°C to ensure lysis. The following day, 100µL was transferred from each well into a new white-walled 96-well plate. Luminescence was measured on Wallac 1420 victor 2 spectrophotometer. For cells in spheroid culture in 24-well format, spheroids were collected in 1.5mL Eppendorf tubes and centrifuged at 4000rpm for 5 minutes. Media was aspirated from cell pellets until 100µL of media was remaining. An

additional 100 μ L of CellTiter-Glo[®] reagent was added directly to each tube. Spheroid pellets were lysed by trituration, approximately 40 times/sample. Spheroid pellets were left overnight at -80 $^{\circ}$ C to ensure lysis. The following day, 100 μ L was transferred from each sample into a new white-walled 96-well plate. Readings were measured on Wallac 1420 Victor 2 spectrophotometer plate reader using luminescence setting (Kangas et al., 1984).

2.9 CyQUANT[®] Viability Assay

Spheroids from 24-well ULA plates were transferred to 1.5mL Eppendorf tubes and centrifuged at 4000rpm for 5 minutes. Media was completely aspirated from tubes, without disturbing spheroid pellet. Samples were left overnight at -80 $^{\circ}$ C. The following day, CyQUANT[®] (Life Technologies) reagent was prepared according to manufacturer's protocol. 100 μ L of mixture was added to each sample. Spheroid pellets were mixed with CyQUANT[®] reagent and triturated, approximately 40 times/sample. Samples were transferred from tubes into white-walled 96-well plates and incubated in dark for 60 minutes. Viability readings were measured on Wallac 1420 Victor 2 spectrophotometer plate using fluorescence setting, with an excitation wavelength of 480nm and an emission wavelength of 520nm (Jones et al., 2001).

2.10 Trypan Blue Exclusion Viability Assay

Spheroids from 24-well ULA plates were transferred to 1.5mL Eppendorf tubes and centrifuged at 4000rpm for 5 minutes. Media was completely aspirated from tubes, without disturbing spheroid pellet. Pellets were washed twice with 1mL of PBS, and centrifuged at 4000rpm for 5 minutes between each wash. A volume of 250 μ L of trypsin-EDTA (0.25%) was added to each sample and pellet was resuspended in trypsin-EDTA. Samples were left in 37 $^{\circ}$ C water bath for 30 minutes, and were vortexed every 10 minutes during this time. After incubation, 250 μ L of FBS was added to each sample to inactivate trypsin. Pellet was resuspended in mixture and completely dissociated using trituration. 50 μ L of each sample was aliquoted into new Eppendorf tubes. An additional 50 μ L of Trypan Blue dye (ThermoFischer Scientific) was added to each tube and vortexed. 15 μ L of mixture was pipetted on to cell counter slide and viability readings were taken using

TC10 cell counter (Biorad). Total cell number and live cell number were recorded, indicating Trypan Blue excluded cells (Strober, 2001).

2.11 IC50 Determination

Cells were seeded in 96-well adherent culture at a density of 2000 cells/well. The following day, cells were treated with DMSO, 10-fold serial dilutions of WZ4003 or 10-fold serial dilutions of HTH01-015 (as indicated in experiment). For IC50 in spheroid culture, cells were seeded in 96-well adherent culture at a density of 2000 cells/well and immediately treated with DMSO or 1-100 μ M (as indicated in experiment) of carboplatin (Bicaku et al., 2012).

AlamarBlue (ThermoFischer) and CellTiter-Glo® viability readings were used for WZ4003 IC50 determination. For AlamarBlue assay, 11% v:v dye was added to cells 72 hours post-treatment. Viability readings were taken each hour after addition of dye, up until 5 hours after dye addition, on Synergy H4 plate reader (Biotek) by measuring fluorescence using an excitation wavelength of 560nm and an emission wavelength of 590nm (Nakayama et al., 1997). Dose-response curves shown are from 3-hour viability readings. For CellTiter-Glo® viability, assay was performed as described above for CellTiter-Glo® in 96-well adherent culture.

Incucyte ZOOM (Essen Bioscience) growth curves were used for HTH01-015 IC50 determination. Cells were treated with inhibitor, one day post-seeding, and left in the Incucyte ZOOM for 72 hours, with images being captured every 3 hours. 4 images were captured for each well, and percent confluence was calculated for each time point by the Incucyte system by taking the average of 6 wells. Growth curves were graphed using Graphpad PRISM (version 6). Doubling times were calculated using Graphpad PRISM, using non-linear regression.

Carboplatin IC50 in spheroids was determined using CellTiter-Glo®, as described above for CellTiter-Glo® in 96-well spheroid culture.

2.12 Incucyte ZOOM Growth Curves

Cells were seeded in 96-well adherent culture at a density of 2000 cells/well. The following day, cells were treated with DMSO or WZ4003 at 0.1 μ M, 0.5 μ M, or 2.5 μ M. Cells were left in the Incucyte ZOOM for 72 hours after treatment, with image capture every 3 hours. Percent confluence was calculated by Incucyte for each time point, by taking the average from 4 images. Data was plotted on Graphpad PRISM to generate growth curves. Doubling times were calculated using Graphpad PRISM, using non-linear regression analysis.

2.13 Quantitative Real-time PCR

Cells from single and double siRNA-mediated knockdown experiments were trypsinized, counted and seeded for viability experiments 72 hours after transfection. The remainder of the cell suspension was centrifuged at 2000rpm for 5 minutes and the media was aspirated. Cell pellets were frozen at -80°C to begin lysis. Cell pellets were thawed and RNA isolation was performed using RNA extraction kit (Qiagen) per manufacturer's protocol. Optional DNase step was performed to prevent genomic contamination. RNA was eluted into 40 μ L of RNase-free water. RNA concentration was quantified by measuring RNA on UV-VIS spectrophotometer (Nanodrop).

For cDNA preparation, two tubes were prepared for each sample. One of the two tubes was used to ensure that RNA was not contaminated with genomic DNA (no RT sample). cDNA was prepared using 2 μ g of RNA, and was calculated according to concentration indicated by UV-VIS spectrophotometer. Random primer (300ng/ μ L), dNTP (10mM), and RNase-free water were added to reaction mixture. Mixtures were vortexed, denatured at 65°C for 5 minutes and promptly placed on ice. 5x first strand buffer (Invitrogen) and 0.1M DTT (Invitrogen) were added to each sample, and samples were briefly centrifuged using quickspin setting. Samples were incubated at room temperature for 2 minutes. To one set of tubes only, Superscript™ II RT (Invitrogen) was added, and mixed in by swirling with pipette tip. cDNA synthesis was performed in iCycler (Biorad) by incubating for 10 minutes at 25°C, followed by 50 minutes at 42°C. Reaction inactivation was performed at 70°C for 15 minutes.

For the next step, PCR was performed for *GAPDH* to assess RNA quality. Master mix was prepared containing 10x PCR Buffer (Invitrogen), 50mM MgCl₂, 10mM dNTP, 10μM *GAPDH* forward primer, 10μM *GAPDH* reverse primer (Table 2.2), and Taq DNA polymerase (5U/μL, Invitrogen). Master mix was added to each cDNA sample in a separate tube. PCR was performed in iCycler (Biorad), beginning with a 4-minute denaturation at 95°C. 29 repetitive cycles of denaturing, annealing and extending were performed with 30 seconds at 95°C, 30 seconds at 60°C and 30 seconds at 72°C respectively. Reaction inactivation was performed at 72°C for 10 minutes. Samples were cooled to 4°C and maintained at this temperature until removal.

PCR samples were run on an agarose gel to assess cDNA quality and rule out genomic contamination. DNA gels were made as 1% agarose DI-LE in 1x TBE. Redsafe™ dye (InTRON Biotechnology) was added into DNA gels as a substitute for ethidium bromide. Samples were run in DNA gel for 30 minutes at 110V. Gels were imaged on Biorad Gel-doc using Ethidium-Bromide setting.

Samples for quantitative PCR was prepared using a master mix. Master mix was prepared using Cyber green master mix (Invitrogen), 1:1000 Rox reference dye (Invitrogen), 1:50 forward primer, 1:50 reverse primer, and RNase-free water. Master mix was added to each cDNA sample in a separate tube. Primers used were *GAPDH* forward, *GAPDH* reverse, *NUAK1* forward, *NUAK1* reverse, *NUAK2* forward and *NUAK2* reverse (Table 2.2). Quantitative PCR was performed using Quantstudios 3 (Applied Biosystems) starting with 50°C for 2 minutes. This was followed by a denaturing step of 95°C for 10 minutes, followed by 40 repetitive cycles of 95°C for 15 seconds and 60°C for 15 seconds. deltaCt values were used to determine relative mRNA levels for genes of interest, to verify siRNA knockdown (Livek and Scmittigen, 2001).

Table 2.2. qPCR primer sequences^a

Gene	Forward Primer (5'→3')	Reverse Primer (5'→3')
GAPDH	5'CATGAGAAGTATGACAACAGCCCT	5'AGTCCTTCCACGATACCAAAGT
NUAK1	5'ATGCTAAGTACCCTCTGAATG	5'GCAACAAGCAGTCAGTCGATC
NUAK2	5'GTCAATCCGGAAGGACAAAA	5'TCACGATCTTGCTCTTC

^a Primers purchased from Sigma Aldrich

2.14 Tritiated Thymidine Incorporation Assay

Cells were seeded in adherent and spheroid culture in 24-well format, at a density of 50 000 cells/well. Spheroids were immediately treated with 0.5 μ M WZ4003 at time of seeding. Adherent cells were treated with 0.5 μ M WZ4003 the following day. Cells were exposed to tritiated thymidine 24 hours after treatment.

Tritiated thymidine was added (1 μ Ci/ μ L) to each well and incubated for either 24 hours for spheroids or 2 hours for adherent cells. For spheroids, media was collected and cells were pelleted. Cell pellets were washed twice in cold 1x PBS followed by cold 10% TCA (trichloroacetic acid, Sigma). Cells were lysed by adding 500 μ L of lysis buffer (1N NaOH/0.1% SDS) to the pellet and resuspending. For adherent cells, wells were washed twice in cold 1x PBS followed by a wash with cold 10% TCA. Cells were lysed in the wells by adding 500 μ L of lysis buffer. For spheroids and adherent cells, 400 μ L of cell lysate was then added to 400 μ L of 1N HCl and mixed with 5 mL of scintillation fluid (ScintiVerse BD Cocktail, Fisher Chemical) in scintillation vials. Counts per minute (cpm) was measured using a liquid scintillation counter (MacDonald et al., 2017). Assay was performed in collaboration with Piru Perampalam and Dr. Fred Dick.

2.15 Spheroid size determination

Phase contrast images of spheroids were captured using 10x setting on Leica DMI 4000B inverted microscope. Horizontal and vertical diameters were measured using ImageJ (NIH). Spheroid area (πr^2) was determined using average of horizontal and vertical diameters.

2.16 Graphing and Statistical Analysis

Waterfall plot of NUA1 expression was generated using Microsoft Excel 2016, all other graphs were generated using Graphpad PRISM 6 (Graphpad Software, version 6).

Analyses were performed using Student's *t*-tests, one-way ANOVA and two-way ANOVA tests followed by Tukey's *post-hoc* test. Significance was set to $p < 0.05$ (*, $p < 0.05$, **, $p < 0.01$, ***, $p < 0.005$, ****, $p < 0.0001$)

Chapter 3

3 Results

3.1 NUAK1 has limited profile in EOC

To begin, a survey of NUAK1 expression was conducted in a variety of EOC cell lines in adherent culture. This was an important first step to determine which cell lines would be good candidates to work with in subsequent experiments.

Well-established EOC cell lines were screened first for NUAK1 expression to compare with previously published literature. Results indicated that NUAK1 had a limited expression profile in EOC cell lines, with few cell lines having high expression levels of NUAK1. NUAK1 is highly expressed in OVCAR8, TOV21G and COV362 cells, but has low to undetectable expression in all other lines (Fig. 3.1B, Fig 3.2). These results differed from a previous survey of NUAK1 expression in well-established cell lines, which suggested that NUAK1 was evenly expressed in EOC (Zhang et al., 2015).

Our lab has access to patient-derived ascites samples, from which spheroids in suspension can be used to create cell lines. NUAK1 expression was screened, using these early passage cell lines (generated by Dr. Gabriel DiMattia). Out of the 22 cell lines screened, NUAK1 was only expressed in 6, with high expression in the iOvCa198, iOvCa168 and iOvCa256 cell lines (Fig. 3.1C, Fig. 3.2). Interestingly, the iOvCa198 and iOvCa247 cell lines were derived from the same patient at different times during treatment. iOvCa198, which highly expresses NUAK1, was isolated after the patient had undergone 6 cycles of carboplatin and paclitaxel, and had stage IIIB disease. The latter cell line, iOvCa247 was derived a year later when the patient had developed carboplatin-resistant disease and was treated with 13 cycles of paclitaxel; this latter cell line lacks NUAK1 expression.

The fallopian tube epithelial cell lines can be used to study the importance of various proteins and kinases at the site of origin of high-grade serous ovarian cancers (Fotheringham et al., 2011). To compare NUAK1 expression in cancer cell lines to

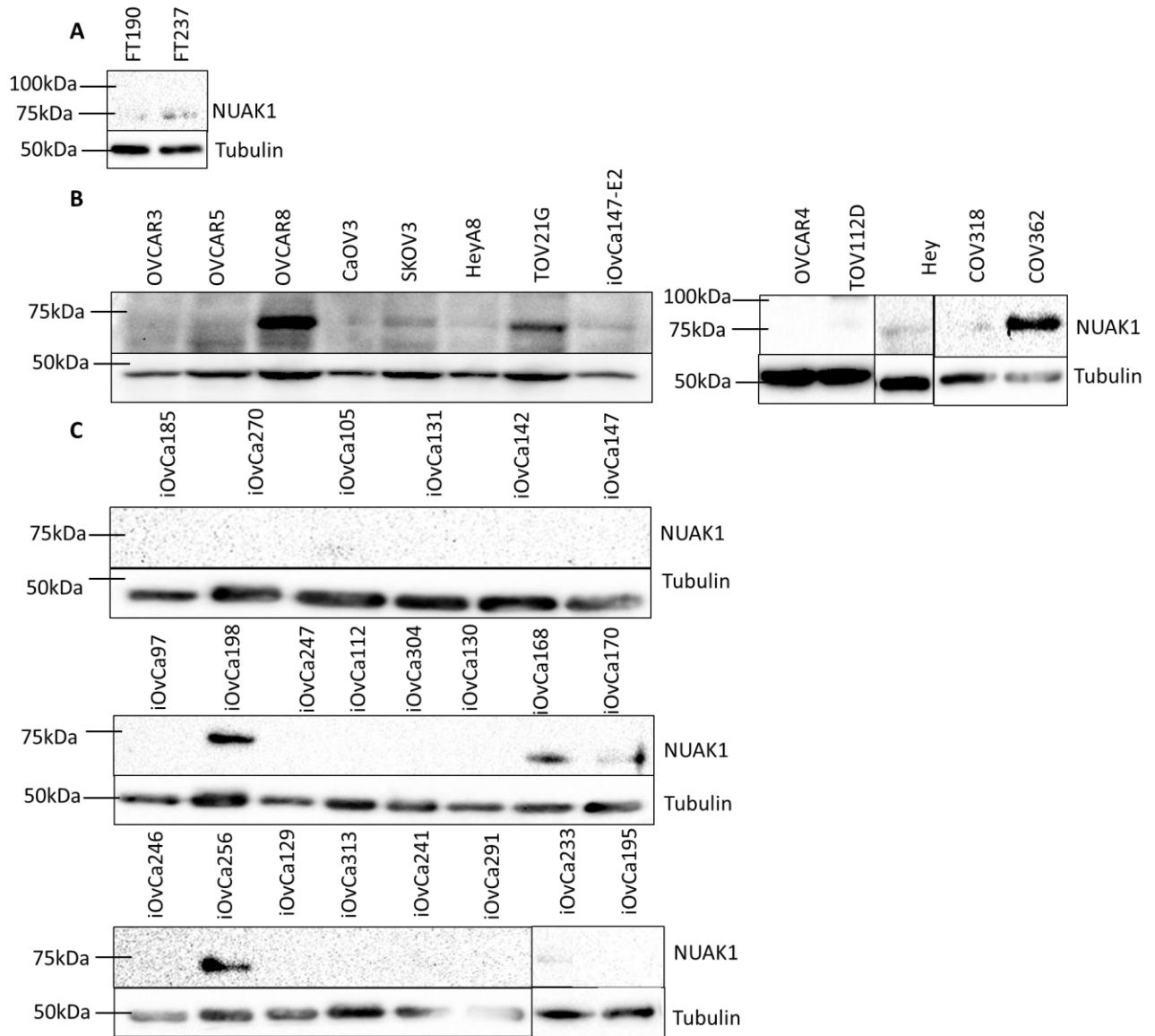


Figure 3.1. Representative western blots of NUA1 expression in EOC. Western blot conducted using day 3 adherent culture lysates. (A) NUA1 is expressed in fallopian tube epithelial cell lines (Gift from R. Drapkin, UPenn) (n=3) (B) NUA1 is expressed in well-established EOC cell lines (n=3) (C) NUA1 is expressed few in newly-established, low-passage, human EOC ascites derived cell lines, established by Dr. Gabriel DiMattia (Translational Ovarian Cancer Research Program, UWO). (n=3)

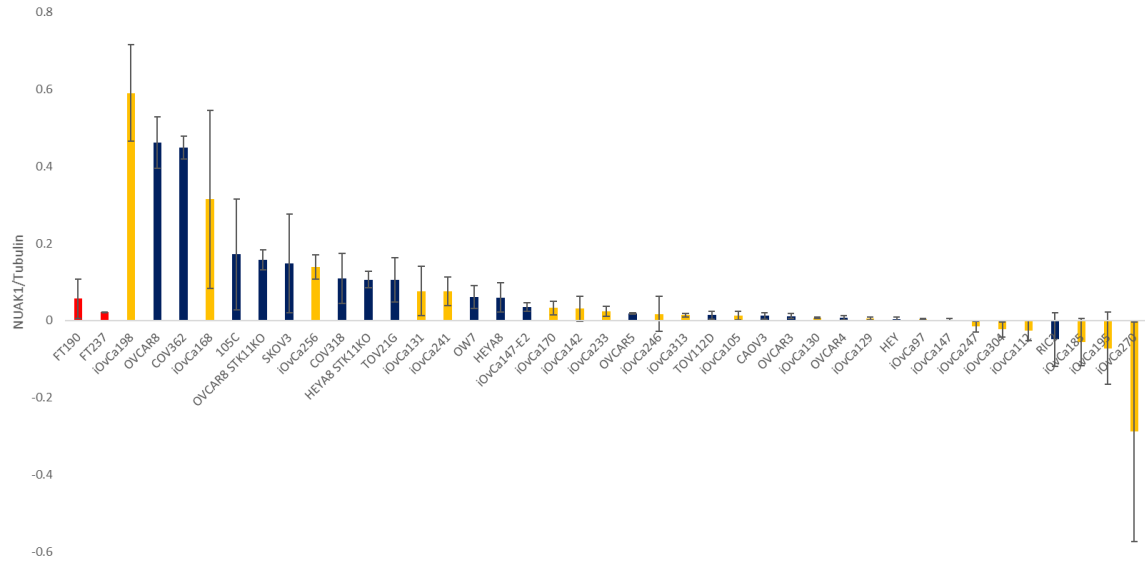


Figure 3.2. Quantification of NUAK1 expression across 38 cell lines. Y-axis represents ratio of NUAK1/Tubulin adjusted volumes, measured using Imagelab. Well-established cell lines are shown in navy (n=14), low-passage ascites derived cell lines are shown in yellow (n=24), and immortalized fallopian tube epithelial lines are shown in red (n=2).

normal tissue, the immortalized fallopian tube epithelial cells were used. The data suggests that NUA1 is expressed in these cell lines, but at a low level (Fig. 3.1A, Fig. 3.2).

This screen of NUA1 expression enabled us to identify ideal cell lines to use for expression knockdown and kinase inhibitor experiments.

3.2 NUA1 expression decreases in spheroid culture

To understand the importance of NUA1 in EOC metastatic behavior, NUA1 expression was assessed in spheroids established over 3 days and compared to expression in adherent culture. Trends suggest that NUA1 expression decreases from adherent to day 3 spheroid culture in most the well-established lines, possibly implicating that NUA1 levels may remain low during dormancy in EOC spheroids (Fig 3.3).

3.3 NUA1 is regulated by LKB1

After noting that NUA1 is expressed in some EOC cell lines, I proceeded to assess if NUA1 is regulated by LKB1 (Peart et al., 2015). In these experiments, NUA1 expression and phosphorylation was assessed to determine if LKB1 mediated changes in NUA1 regulation. For these experiments, OVCAR8 *STK11*KO cells were utilized, which were engineered using CRISPR-Cas9 to ablate LKB1 expression, (Buensuceso and Shepherd, unpublished data) and were compared to expression in OVCAR8 cells, which have high NUA1 expression levels.

To understand how NUA1 was regulated by LKB1, western blot was performed to see how total NUA1 protein levels were impacted by loss of LKB1. Results indicated that NUA1 levels decreased in *STK11*KO cells relative to OVCAR8 LKB1-wildtype cells in both adherent and day 3 spheroid culture conditions (Fig. 3.4A). This suggests that NUA1 expression is regulated by LKB1.

To examine this further, and assess how NUA1 was regulated by LKB1, western blot was performed to analyze NUA1 phosphorylation by LKB1. Currently, there are no commercially available antibodies that can detect NUA1 phosphorylation at threonine

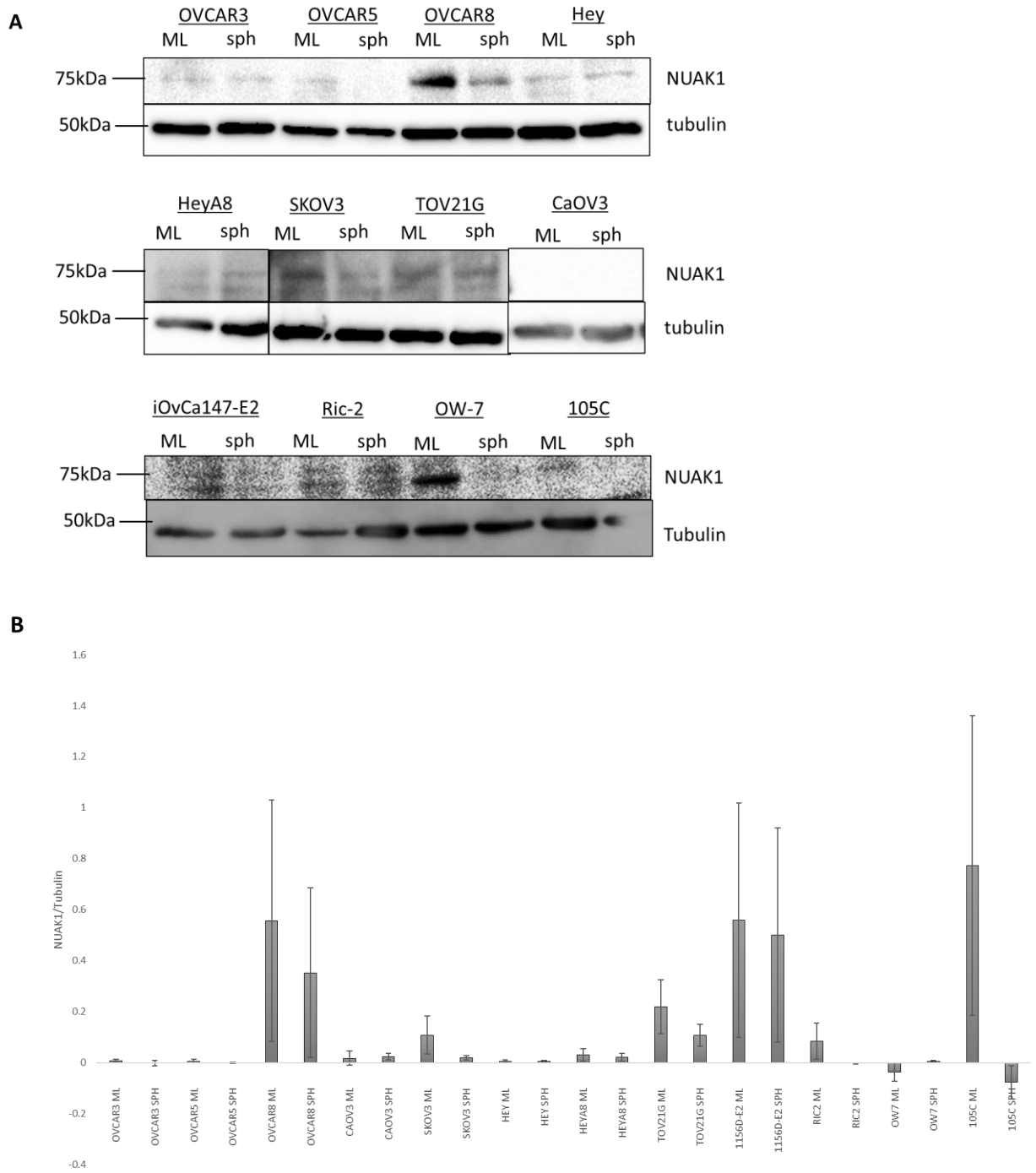


Figure 3.3. NUAK1 expression decreases in spheroid culture of some well-established cell lines. Western blot performed on day 3 adherent and spheroid lysates. **(A)** Representative western blots showing that NUAK1 expression decreases in adherent (ML) to day 3 spheroid (sph) culture. **(B)** Quantification of NUAK1/Tubulin (n=3)

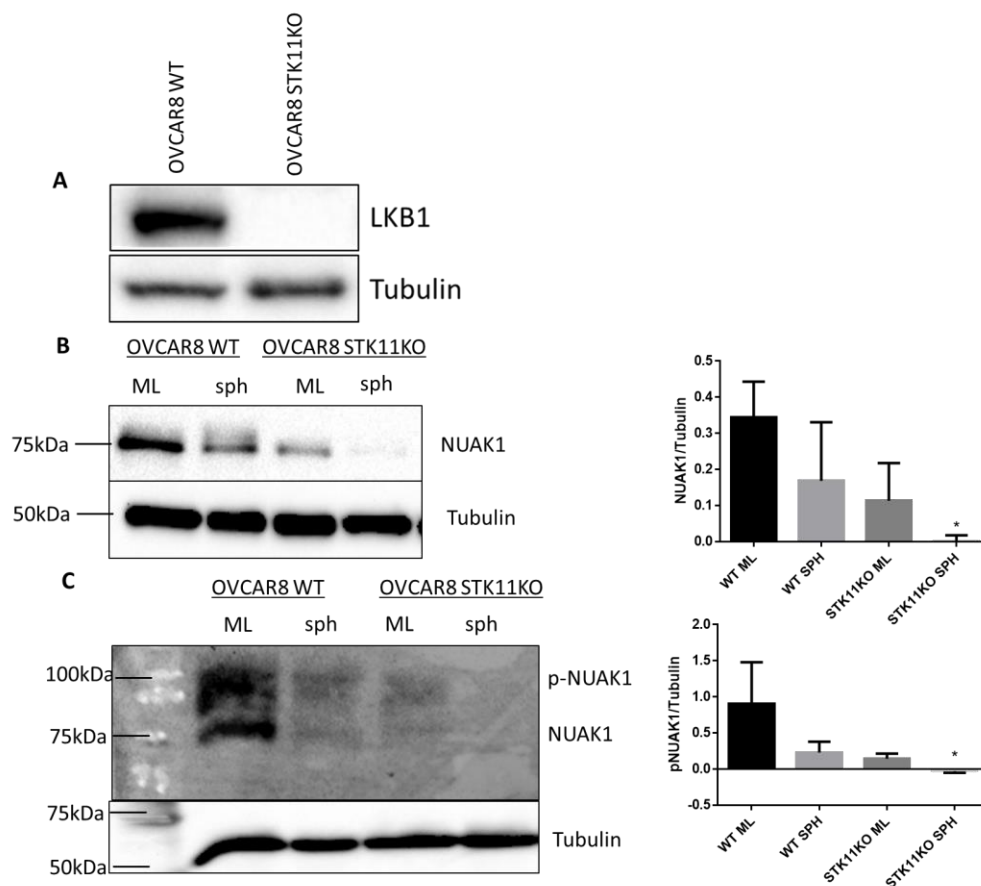


Figure 3.4. NUAK1 is regulated by LKB1. (A) Representative western blot showing LKB1 knockout. *STK11*KO cells lack expression of LKB1 and were created by CRISPR-Cas9 technology. (B) Representative western blot showing NUAK1 expression in OVCAR8 parental and *STK11*KO cells using monolayer (ML) and day 3 spheroid (sph) lysates. In OVCAR8 cells, NUAK1 levels decrease from wildtype (WT) to *STK11*KO cells. (n=3) Quantification on right using 3 replicates. There is a significant decrease in NUAK1 expression between OVCAR8 WT cells in monolayer and *STK11*KO cells in spheroid culture. Data is plotted as mean \pm SD, analysis using one-way ANOVA and Tukey's *post-hoc* test (*, $p < 0.05$) (C) Representative western blot showing p-NUAK1 expression in OVCAR8 parental and *STK11*KO cells using monolayer (ML) and day 3 spheroid (sph) lysate on Phostag™ acrylamide gels. p-NUAK1 decreases upon loss of LKB1. Quantification on right using 3 replicates. There is a significant decrease in p-NUAK1 upon loss of LKB1 in sph. Data is plotted as mean \pm SD, analysis using one-way ANOVA and Tukey's *post hoc* test (*, $p < 0.05$)

211 (LKB1-mediated phosphorylation site). To overcome this, Phostag™ acrylamide gels were used. Phostag™ gels work by labeling phosphorylated protein residues using the Phostag™ substrate such that phosphorylated proteins become higher in molecular weight and resolve independently from their non-phosphorylated counterparts (Kosako, 2009). Any antibody that recognizes total protein can be used on these gels to resolve phosphorylated proteins. Phostag™ reagent was used on western blot of lysates from OVCAR8 WT and *STK11*KO cells and results indicated that phosphorylation of NUAK1 decreases upon loss of LKB1 in OVCAR8 cells (Fig. 3.4B). These results are consistent with total NUAK1 western blot findings, suggesting that LKB1 is likely required to phosphorylate NUAK1 and perhaps stabilize its expression.

3.4 NUAK1 knockdown increases EOC spheroid cell viability

LKB1 is a critical regulator of EOC spheroid viability and chemoresistance, therefore it was important to investigate if its downstream substrate, NUAK1, was implicated in spheroid viability. To interrogate NUAK1 function in spheroids, siRNA-mediated knockdown of NUAK1 was conducted in OVCAR8 and HeyA8 cells, which have high and low levels of NUAK1 respectively (Fig. 3.2). Initial experiments entailed use of the CyQUANT viability assay, which measures viability based on DNA content within a sample. Surprisingly, results showed that si*NUAK1* day 3 spheroids were more viable than the siNT control spheroids by 40-60% (Fig. 3.5B), with significantly higher viability in OVCAR8 spheroids ($p=0.046$). To further understand this phenotype, a spheroid reattachment assay was conducted. This assay involves plating day 3 spheroids in 6-well plates to assess how many spheroids are able to reattach, indirectly indicating the metastatic potential of spheroids. si*NUAK1* spheroids exhibited a significantly higher reattachment potential (OVCAR8, 150% increase \pm 37% SEM; HeyA8, 120% increase \pm 26% SEM) than siNT spheroids in both cell lines (OVCAR8 $p=0.009$, HeyA8 $p=0.007$) (Fig. 3.7C, D). To interrogate the effects of NUAK1 knockdown in primary cells, siRNA-mediated knockdown of NUAK1 was performed in the iOvCa198 cell line which has high expression of NUAK1 (Fig. 3.2). For this experiment, siRNA-mediated knockdown of NUAK1 was performed in adherent and day 3 spheroid culture and the metabolic

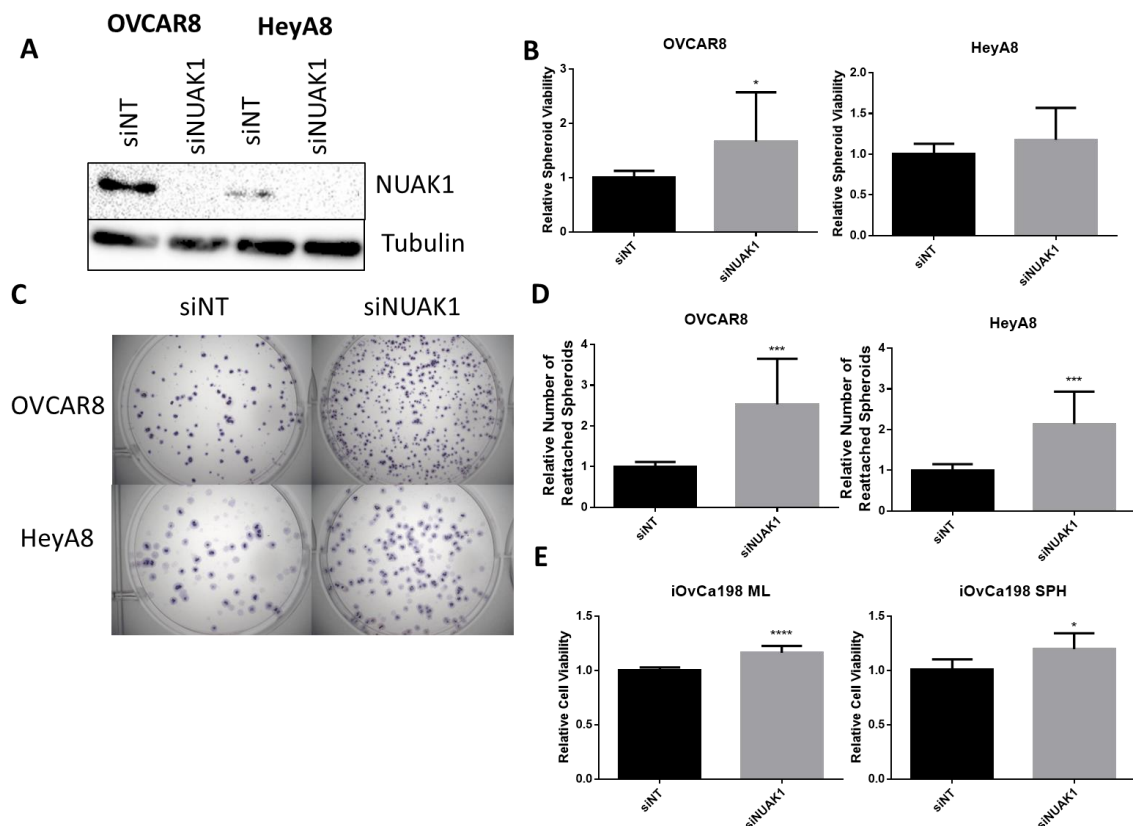


Figure 3.5. NUAK1 knockdown increases spheroid viability and reattachment. **(A)** Western blot confirming NUAK1 knockdown. **(B)** CyQUANT spheroid viability. siNUAK1 spheroids appear to be more viable than siNT spheroids in both cell lines (n=3). Data is plotted as mean \pm SD, analysis performed using Student's *t*-test (*, $p < 0.05$) **(C)** Spheroid reattachment images taken using Zeiss Axiozoom Stereo microscope at 4x. Plates were fixed and stained with Hema3 to count spheroids. **(D)** Spheroid reattachment quantification. siNUAK1 had higher reattachment counts than control (n=3) Data is plotted as mean \pm SD, analysis performed using Student's *t*-test (***, $p < 0.005$) **(E)** CellTiter-Glo® viability for day 3 monolayer (ML) and spheroid (SPH) samples from iOvCa198 cell line. siNUAK1 cells and spheroids are more viable than siNT treated cells. Data is plotted as mean \pm SD, analysis performed using Student's *t*-test (*, $p < 0.05$) (n=3)

based CellTiter-Glo® assay was used to assess cell viability. Loss of NUAK1 significantly increased both adherent (16% increase \pm 2.2% SEM, $p < 0.001$) and day 3 spheroid (20% increase \pm 5.4% SEM, $p=0.0162$) viability (Fig. 3.2E). These initial experiments suggest that loss of NUAK1 confers increased spheroid cell viability, with the subsequent higher capacity to reattach.

To ensure that the increase in viability upon loss of NUAK1 was not a result of the CyQUANT and CellTiter-Glo® viability assays, knockdown of NUAK1 was performed and viability was analyzed using the Trypan Blue exclusion assay. The Trypan Blue assay used for this experiment involves the use of a diazo blue dye that accumulates within dead cells, which are unable to pump the dye out (Stober, 2001). As a result, using this dye allows one to measure the proportion of both viable cells and dead cells and thus offers a direct measure of cell viability. In this experiment, I also determined whether loss of NUAK2, the most closely related family member to NUAK1, had similar effects on day 3 spheroid viability. Results indicated that loss of NUAK1 caused a significant increase (OVCAR8, 110% increase \pm 27% SEM, $p=0.004$, HeyA8, 220% increase \pm 19% SEM, $p<0.0001$) in viable cell number in spheroids, in both lines (Fig. 3.6). However, reduction of NUAK2 had no effect on viable spheroid number. Once again, this suggests that specific loss of NUAK1 confers more viable spheroids, as seen by the increase in viable cell number within spheroids.

3.5 NUAK1 and NUAK2 are unable to functionally compensate for each other

To study the effects of NUAK compensation, and to understand the importance that both NUAKs hold in EOC cell viability, single and double knockdowns of *NUAK1* and *NUAK2* were conducted. This experiment was performed in 96-well format to identify the significance of NUAK1/2 knockdown on single spheroids. Single and double NUAK1/2 knockdown was conducted using siRNA against NUAK1 and NUAK2, independently and together. This experiment was originally done in 7 well-established cell lines. However, after qRT-PCR knockdown analysis, only cell lines which had >50% knockdown of NUAK species were chosen for further analysis (Fig. 3.7).

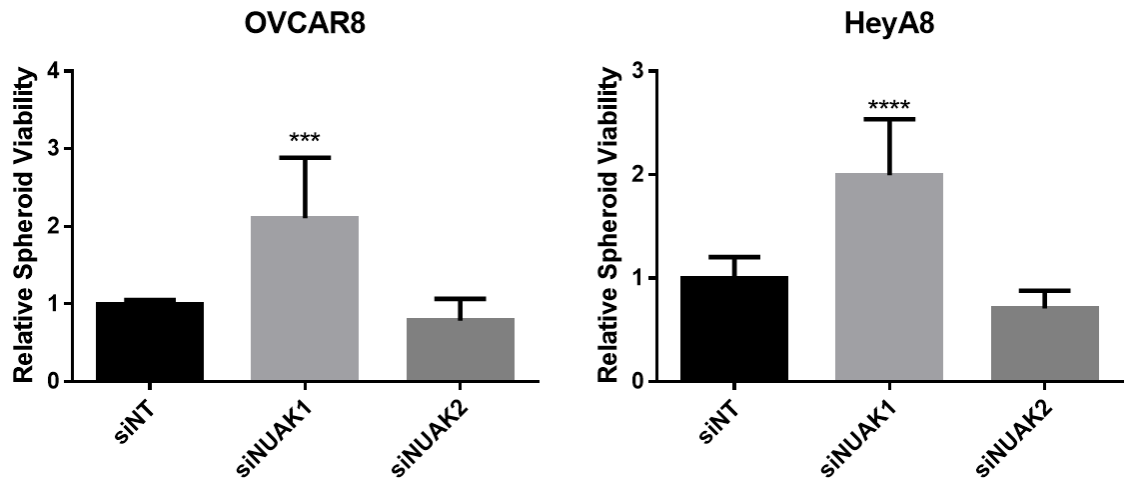


Figure 3.6.NUAK1 knockdown increases viable cell number in spheroids. Viability readings from Trypan Blue exclusion assay, demonstrating in both cell lines that loss of NUAK1 confers significantly increased viable cell number (n=3). Data is plotted as mean \pm SD, analysis using one-way ANOVA and Tukey's *post hoc* test (***, $p < 0.005$) (for viable cells)

Data illustrates that loss of NUA1 alone increases spheroid size and significantly increases spheroid viability in OVCAR4 and HeyA8 cells (Figs. 3.8, 3.9). Where spheroid viability is increased, adherent cell viability is also significantly increased to roughly the same extent, and is significant in OVCAR4 and HeyA8 cells (Fig. 3.9). Loss of NUA2 significantly increases spheroid size, spheroid viability and adherent viability in OVCAR4 cells, but decreases viability in HEYA8, OVCAR8 and TOV21G cells (Figs. 3.8, 3.9). Loss of NUA1 and NUA2 together significantly increases adherent and spheroid cell viability in and OVCAR4 and HeyA8 cell lines, but decreases viability in TOV21G and OVCAR8 cells (Fig. 3.9). TOV21G cells had a significant decrease in adherent and spheroid viability in all loss of NUA scenarios (Fig. 3.9). This may be because TOV21G cells lack expression of LKB1 (TCGA, 2011), the direct activator of NUAs, therefore loss of LKB1 may be affecting NUA1/2 functionality in these cells. Effective knockdown was confirmed in all cell lines using qRT-PCR (Fig. 3.7). In terms of compensation at the mRNA level, NUA1 mRNA increases in response to NUA2 loss in OVCAR4, OVCAR8 and TOV21G cells (Fig. 3.8). However, NUA2 is unable to compensate for loss of NUA1.

Overall these results suggest that loss of NUA1 has a significant effect on adherent and spheroid viability, and can compensate for loss of NUA2 at the mRNA level in most cell lines screened. Double knockdown results more closely mirror NUA1 knockdown alone in OVCAR4 and HeyA8 cells, possibly indicating that NUA1 is the more important of the two species. Functional compensation may be occurring in OVCAR8 cells, which decrease in spheroid viability upon loss of both NUA species. This data may indicate that functional compensation may be a cell line specific effect which is not uniform across all EOC cell lines. Thus, inhibitor studies may be important to understand the behavior which both NUA species have in EOC.

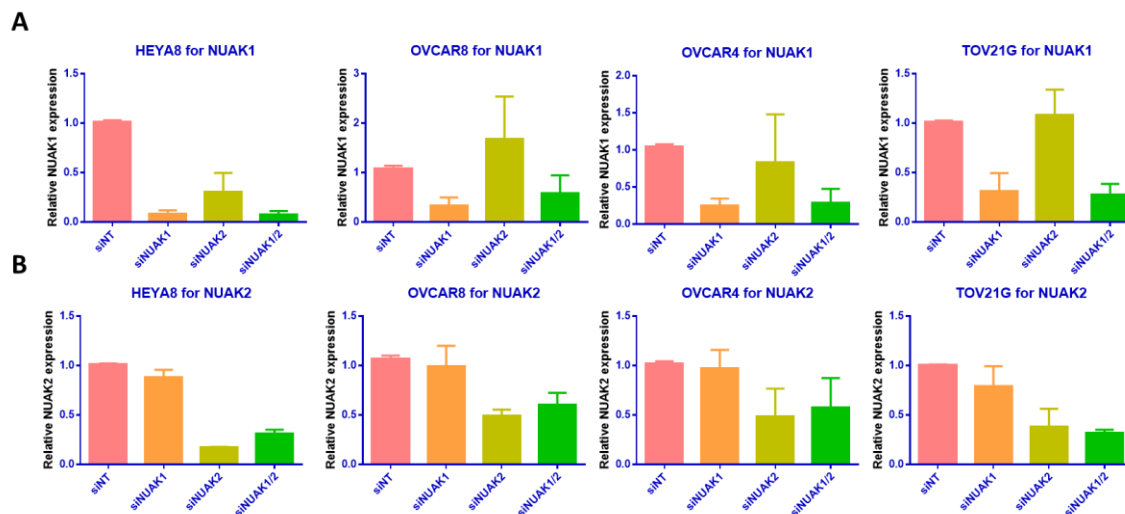


Figure 3.7. Validation of knockdown from single and double NUA1/2 knockdown experiments. (A) *NUAK1* mRNA expression, relative to *GAPDH*, in siNT, si*NUAK1* and si*NUAK1/2* treatments. Data is plotted as mean \pm SD. (B) *NUAK2* mRNA expression, relative to *GAPDH*, in siNT, si*NUAK2* and si*NUAK1/2* treatments. Data is plotted as mean \pm SD. (n=3)

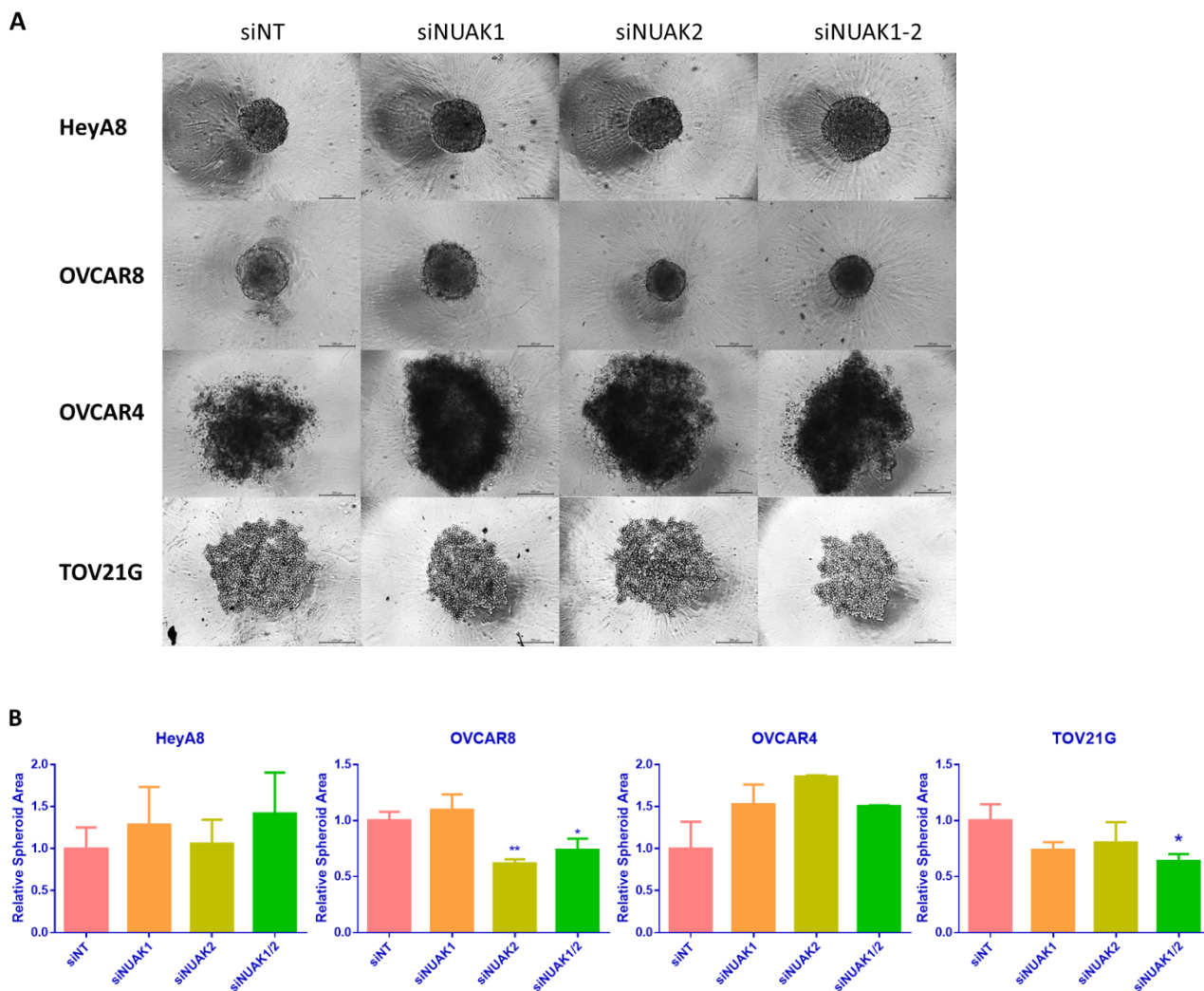


Figure 3.8. Assessment of single and double NUAk knockdown on EOC spheroids. (A) Representative spheroid images taken at 10x magnification (250 μ M scalebar). (B) Quantification of spheroid area. Spheroids were quantified by taking the horizontal and vertical diameter using ImageJ, and averaging diameters to calculate area. Data is plotted as mean \pm SD, analysis performed using one-way ANOVA and Tukey's *post hoc* test (*, $p < 0.05$, **, $p < 0.01$) (n=3)

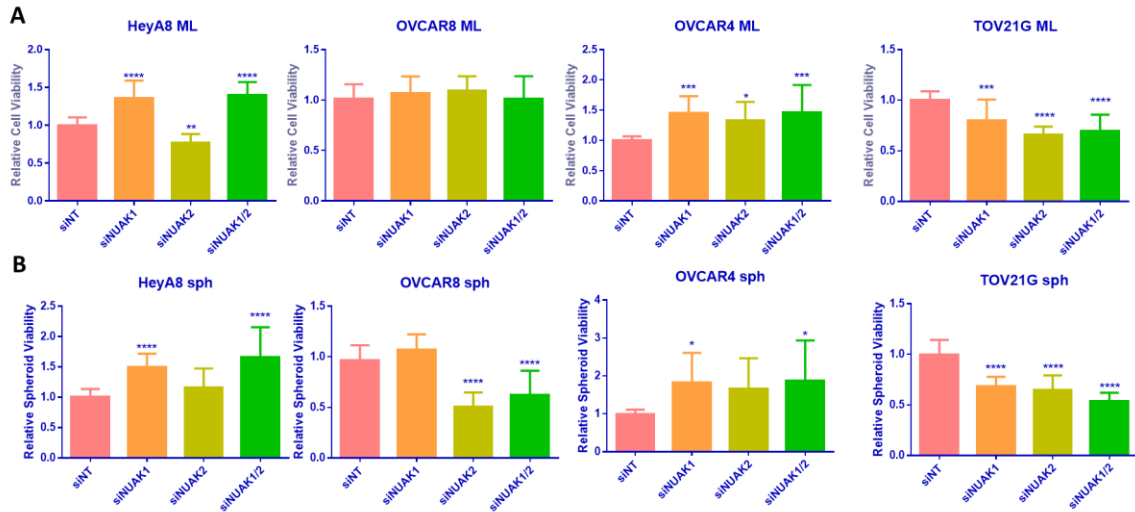


Figure 3.9. Viability from single and double NUAK knockdowns. (A) CellTiter-Glo® based viability in adherent culture in 4 cell lines. Data is plotted as mean \pm SD, analysis performed using one-way ANOVA and Tukey's *post hoc* test (*, $p < 0.05$, **, $p < 0.01$, ***, $p < 0.005$, ****, $p < 0.0001$). (B) CellTiter-Glo® based viability in spheroid culture in 4 cell lines. Data is plotted as mean \pm SD, analysis performed using one-way ANOVA and Tukey's *post hoc* test (*, $p < 0.05$, ****, $p < 0.0001$). (n=3)

3.6 NUAK1 inhibition increases EOC cell growth and clonogenicity

After noting that NUAK1 knockdown increased EOC cell and spheroid viability, I wanted to explore the effects of NUAK1/2 inhibition using other assays in adherent culture. To begin studying this we obtained the WZ4003 dual NUAK inhibitor (Banerjee et al., 2014). Prior to testing the inhibitor using various assays, dose response curves were generated for the compound using OVCAR8 and HEYA8 cells. To generate dose-response curves alamarBlue, a metabolism-based viability assay which indirectly measures mitochondrial activity, and CellTiter-Glo® were used as two different measures of cell viability. Interestingly, complete dose response curves were not formed with the chosen concentrations, as the initial concentrations of WZ4003 used seemed to increase adherent cell viability, producing a biphasic response (Fig. 3.10). Only at 100µM was there significant cell death in both cell lines. Upon consideration of published drug concentrations known to affect NUAK1/2 activity (Banerjee et., al, 2014), and the increased cell viability observed at lower concentrations, 0.1µM, 0.5µM, and 2.5µM concentrations were chosen for treatment in various assays.

To explore NUAK inhibition, the WZ4003 NUAK1/2 inhibitor was used to investigate growth kinetics. To do this the Incucyte ZOOM live cell imaging system was used. This system monitors cell growth over time by capturing images at frequent intervals (every 3 hours in this study) and calculating percent confluence. For these growth curve experiments, OVCAR4, OVCAR8, HeyA8 and TOV21G cell lines were used. The effects of NUAK inhibition on the FT190, immortalized fallopian tube epithelial cell line, were also tested to assess if NUAK inhibition altered growth kinetics of non-transformed cells. In addition to growth curve analysis, Graphpad PRISM was used to calculate doubling time in the presence of WZ4003. Data indicated that NUAK inhibition significantly increased growth in OVCAR4 and HEYA8 cell lines at later time points, but does not significantly impact the growth curve in OVCAR8 and TOV21G cells (Fig. 3.11). FT190 cells did not show increased confluence in response to WZ4003, but did see a significant decrease in growth at the highest concentration used, suggesting toxicity (Fig 3.11A). In regards to doubling time, all cell lines tested exhibited a shortening of

doubling time at the 0.5 μ M dose (Table 3.1). The doubling time decreases suggested that NUAK inhibition may increase the proliferative potential of cells.

The clonogenic assay was also used to test the effects of NUAK inhibition. The clonogenic assay involves plating cells at a low density in 6-well adherent culture plates and assessing the ability of those cells to form colonies under an extended period of time. In this study, the clonogenic assay was used to assess the effects of NUAK1/2 inhibition on colony forming potential. This assay was done in the same four EOC cell lines used to generate growth curves. Results from OVCAR8 and HeyA8 cells indicate that there is a significant dose-dependent increase in clonogenicity with use of the WZ4003 NUAK inhibitor (Fig. 3.12, 3.13). Results from OVCAR4 and TOV21G cells suggest a trend towards a similar dose-dependent increase in clonogenicity, however this was not found to be statistically significant (Fig 3.13). These results suggest that NUAK inhibition is increasing clonogenicity, which may be due to increased proliferation or decreased apoptosis.

3.7 Specific NUAK1 inhibition increases EOC cell growth

WZ4003 is a dual NUAK inhibitor and can thus target NUAK2 in addition to NUAK1; however, my siRNA-mediated knockdown experiments indicated a more important role of NUAK1 in EOC. To further this, we acquired the HTH-01-015 inhibitor which is known to specifically inhibit NUAK1 (Banerjee et al., 2014). To begin, the appropriate dose of HTH-01-015 was calculated. A range of HTH-01-015 doses was assessed by measuring cell growth using the confluence function in the Incucyte ZOOM. Similar to WZ4003 results, HTH-01-015 was able to increase cell growth at low doses, as seen by the shift in the growth curves for both OVCAR8 and HEYA8 cell lines (Fig. 3.14). Concurrently with this growth curve shift, a decrease in doubling time was observed at the low dose treatments (Table 3.2). However, the decreased doubling time observed at the low doses was not as dramatic as the change in doubling time observed with WZ4003. Upon evaluating dose-response, concentrations of 0.5 μ M and 2.5Mm were chosen as optimal concentrations for future experiments. These concentrations increased EOC cell growth, a phenotype that was examined further.

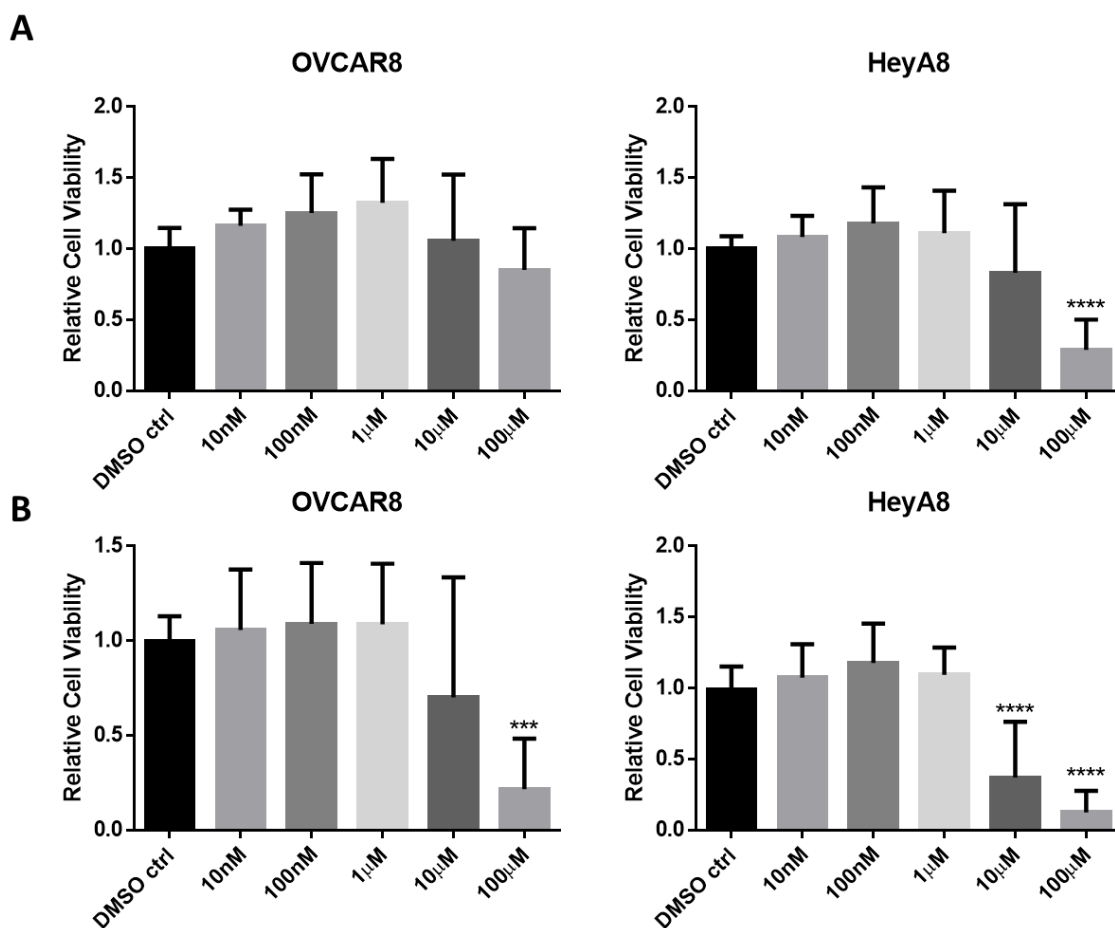


Figure 3.10. Dose-response curves using WZ4003 NUAKE inhibitor, treated with concentrations as indicated. (A) alamarBlue based cell viability readings. Data is plotted as mean \pm SD, analysis performed using one-way ANOVA and Tukey's *post hoc* test (****, $p < 0.001$). (n=3) (B) CellTiter-Glo® based cell viability readings. Data is plotted as mean \pm SD, analysis performed using one-way ANOVA and Tukey's *post hoc* test (***, $p < 0.005$, ****, $p < 0.001$) (n=3).

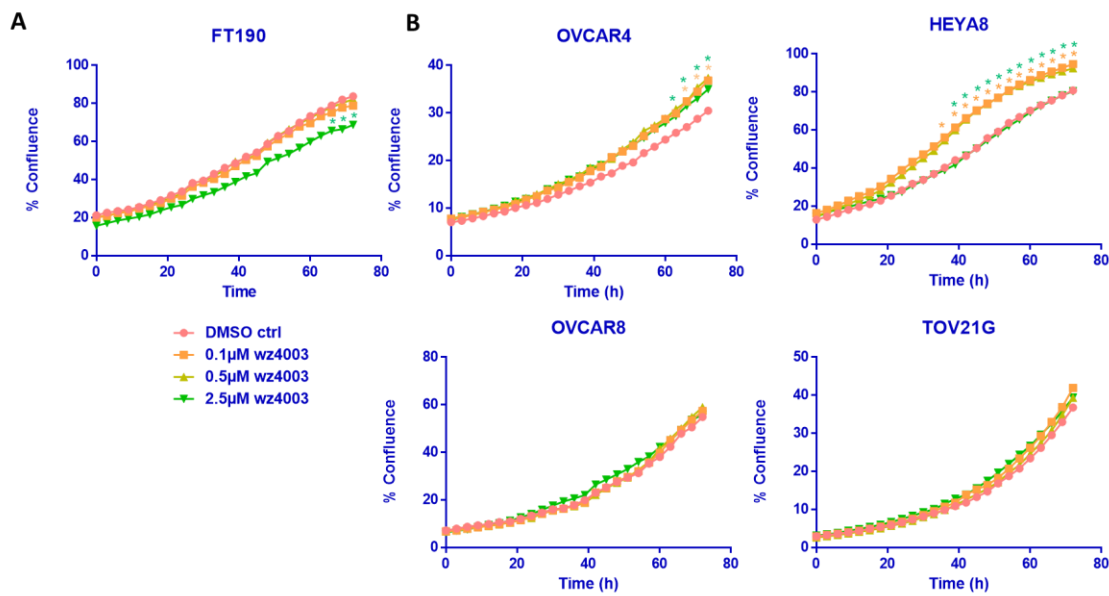


Figure 3.11. Treatment with WZ4003 influences growth kinetics of EOC cell lines. **(A)** FT190, immortalized fallopian tube epithelial cells, treated with 3 concentrations of WZ4003. Cells were seeded at 2000cells/well in 96 well format in 150μL and treated with the listed treatments the following day. Cells were monitored in the Incucyte ZOOM system for 72h. Confluence was calculated using the Incucyte ZOOM software. Confluence was plotted on Graphpad PRISM to create growth curves, analysis was conducted using two-way ANOVA to identify timepoints where treatments became significant, followed by Tukey's *post hoc* test, (*, $p < 0.05$). **(B)** OVCAR4, HEYA8, OVCAR8 and TOV21G cells treated with various concentrations of WZ4003. Cells were seeded at 2000cells/well in 96 well format in 150μL and treated with the listed treatments the following day. Cells were monitored in the Incucyte ZOOM system for 72h. Confluence was calculated using the Incucyte ZOOM software. Confluence was plotted on Graphpad PRISM to create growth curves, analysis was conducted using two-way ANOVA, followed by Tukey's *post hoc* test, (*, $p < 0.05$). (n=3)

Table 3.1. Doubling times^a for WZ4003 treatment.

Cell Line	Treatment	Doubling Time (h)
FT190	DMSO	32.76 ± 0.28
	0.1µM WZ4003	32.36 ± 1.24
	0.5µM WZ4003	30.99 ± 2.03
	2.5µM WZ4003	33.55 ± 2.22
OVCAR4	DMSO	35.27 ± 3.09
	0.1µM WZ4003	31.61 ± 1.84
	0.5µM WZ4003	31.37 ± 1.97
	2.5µM WZ4003	33.54 ± 3.14
OVCAR8	DMSO	24.93 ± 1.57
	0.1µM WZ4003	23.12 ± 0.39
	0.5µM WZ4003	22.91 ± 0.77
	2.5µM WZ4003	25.23 ± 1.64
HeyA8	DMSO	23.71 ± 0.88
	0.1µM WZ4003	22.13 ± 0.82
	0.5µM WZ4003	21.10 ± 0.22
	2.5µM WZ4003	25.12 ± 1.28
TOV21G	DMSO	20.69 ± 0.37
	0.1µM WZ4003	20.61 ± 0.52
	0.5µM WZ4003	19.69 ± 0.65
	2.5µM WZ4003	22.43 ± 1.31

^aDoubling time calculated using non-linear regression, exponential fit curves, in Graphpad PRISM. The doubling time shown is the average ±SD from 3 experiments, using the mean of means. (N=3)

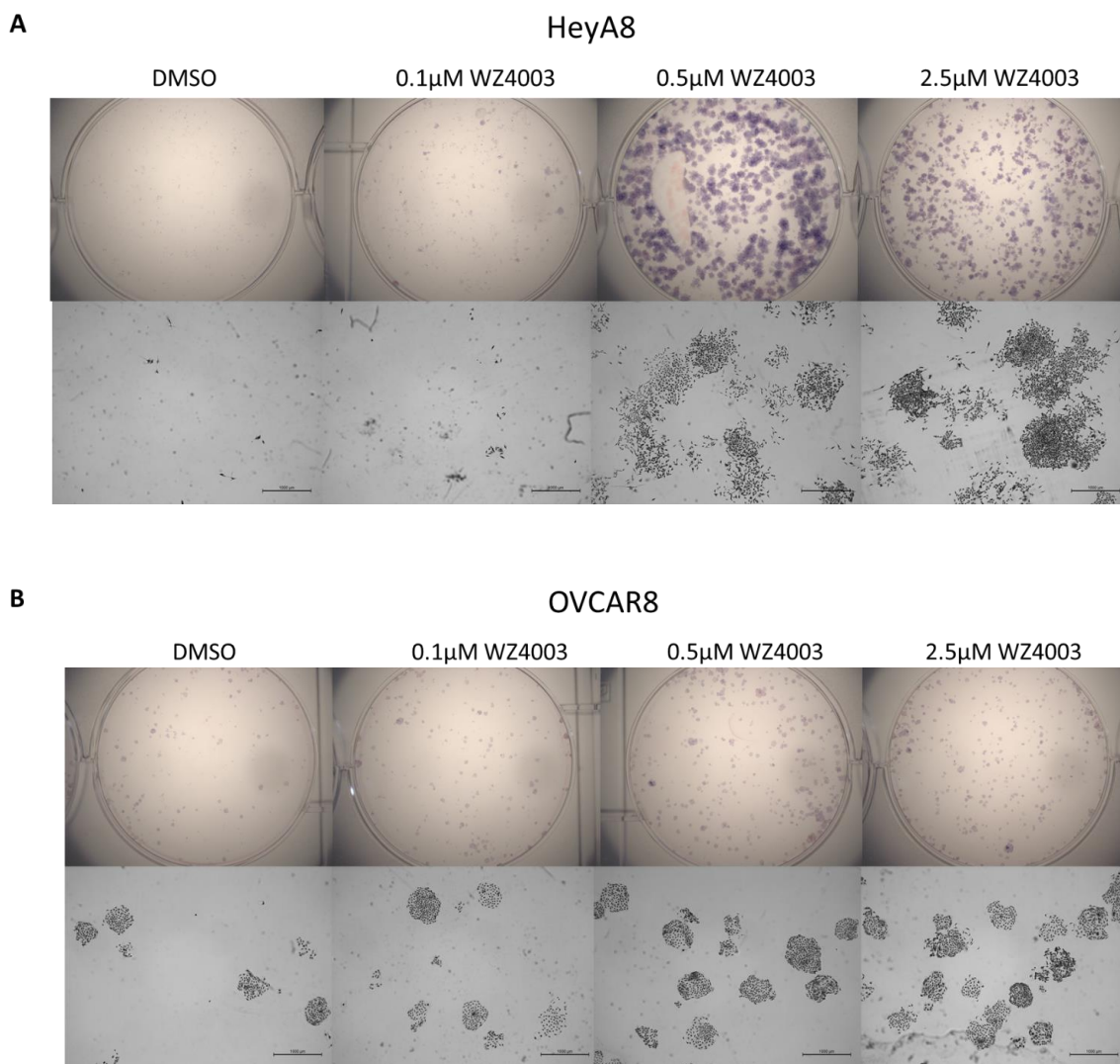


Figure 3.12. Treatment with WZ4003 produces a dose-dependent increase in clonogenicity. (A) HeyA8 cells treated with WZ4003. Cells were seeded at a density of 1000cells/well, treated the day after seeding, and fixed and stained 7 days after treatment. Top images show whole-well taken using Zeiss Axiozoom stereomicroscope at 4x. Bottom images show 100x magnification views of wells using Leica light microscope (100 μ M scalebar). (n=3). (B) OVCAR8 cells treated with WZ4003. Cells were seeded at a density of 500cells/well, treated the day after seeding, and were fixed and stained 7 days after treatment. Top images show whole-well taken using Zeiss Axiozoom stereomicroscope at 4x. Bottom images show 100x magnification views of wells using Leica light microscope (100 μ M scalebar).

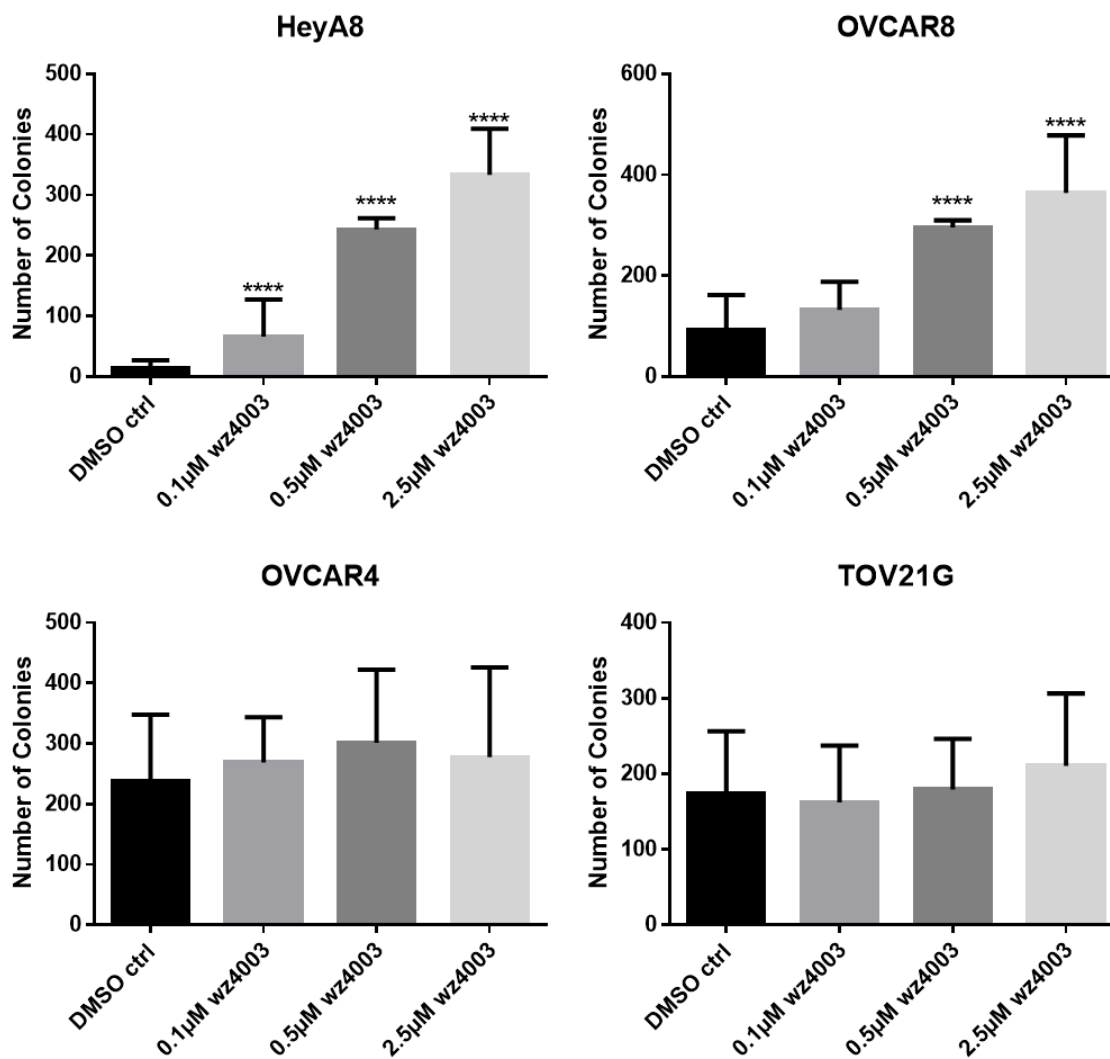


Figure 3.13. WZ4003 clonogenic assay colony quantification. Data is plotted as mean \pm SD, analysis performed using one-way ANOVA and Tukey's *post hoc* test (****, $p < 0.001$) ($n=3$)

To test the effects of HTH-01-015 on EOC cells, the clonogenic assay was performed using OVCAR8 and HEYA8 cells. Treatment with HTH-01-015 had no significant effect on clonogenic capacity in both EOC cell lines (Fig. 3.15). This may suggest that NUAK1 and NUAK2 loss both contribute to colony forming ability in EOC cells.

3.8 NUAK1 inhibition is insufficient to induce platinum sensitivity

NUAK1 knockdown and WZ4003 treatment produces increases in EOC cell viability, which may be attributed to increased proliferation. If this increased cell viability caused by NUAK1 inhibition was due to increased proliferation, then this may sensitize spheroids to platinum based chemotherapy. To test this, a combination therapy experiment was employed to see if WZ4003 and carboplatin together could decrease spheroid viability and promote platinum sensitivity. However, prior to doing this experiment it was necessary to determine the appropriate concentration of carboplatin to use for treating EOC spheroids with. In 96-well format, OVCAR4, OVCAR8 and HEYA8 were dosed with concentrations of carboplatin between 1-100 μ M (Fig. 3.16). A dose of 50 μ M was selected since it was sufficient to modestly affect spheroid viability, but not cause complete cell killing.

After determining the appropriate dose of carboplatin, the combination therapy experiment was performed in both adherent and spheroid culture in 96-well format, using the CellTiterGlo® assay. Results indicated that treatment with carboplatin alone and in combination with WZ4003 resulted in a significant decrease in adherent and spheroid viability. However, there was no significant difference in viability between the carboplatin treatment and the combination therapy treatment (Fig 3.17). These results suggest that NUAK inhibition is not sufficient to further sensitize spheroids to platinum-based chemotherapy.

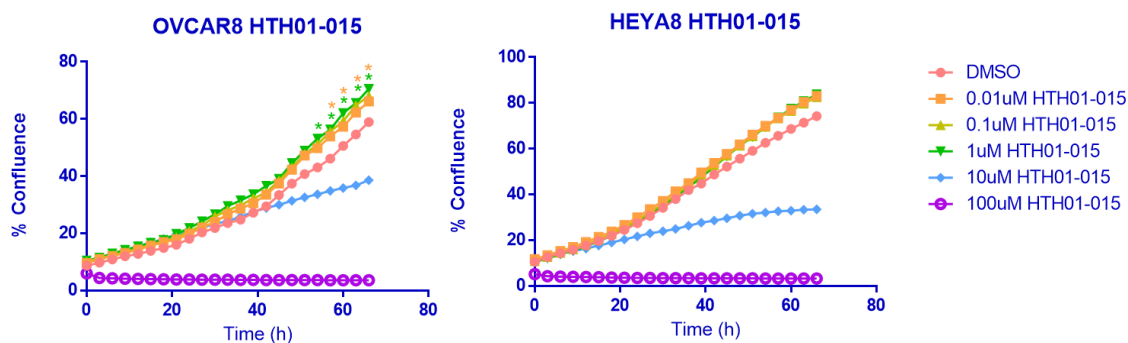


Figure 3.14. Dose response of HTH01-015 on EOC cell growth. OVCAR8 and HEYA8 cells were seeded at 2000cells/well in 150 μ L. The following day, cells were treated with DMSO or various concentrations of HTH01-015 listed above, in an additional 50 μ L. Cells were left in the Incucyte ZOOM for 72h after which confluence was calculated. Growth curves were formed on Graphpad PRISM and data was analyzed using two-way ANOVA and Tukey's *post hoc* test, (*, $p < 0.05$) (n=3)

Table 3.2. Doubling times^a for HTH01-015 treatment.

Cell Line	Treatment	Doubling Time (h)
OVCAR8	DMSO	23.78h ± 0.179h
	0.01µM HTH01-015	23.07h ± 0.62h
	0.1µM HTH01-015	23h ± 0.226h
	1µM HTH01-015	23.54h ± 0.158h
	10µM HTH01-015	42.15h ± 1.94h
	100µM HTH01015	-193.15h ± 20.93h
HEYA8	DMSO	21.99h ± 0.627h
	0.01µM HTH01-015	21.80h ± 0.78h
	0.1µM HTH01-015	21.03h ± 0.87h
	1µM HTH01-015	20.61h ± 0.92h
	10µM HTH01-015	40.87h ± 5.95h
	100µM HTH01015	-118.15h ± 16.78h

^aDoubling time calculated using non-linear regression, exponential fit curves, in Graphpad PRISM. The doubling time shown is the average ±SD from 3 experiments, using the mean of means. (n=3)

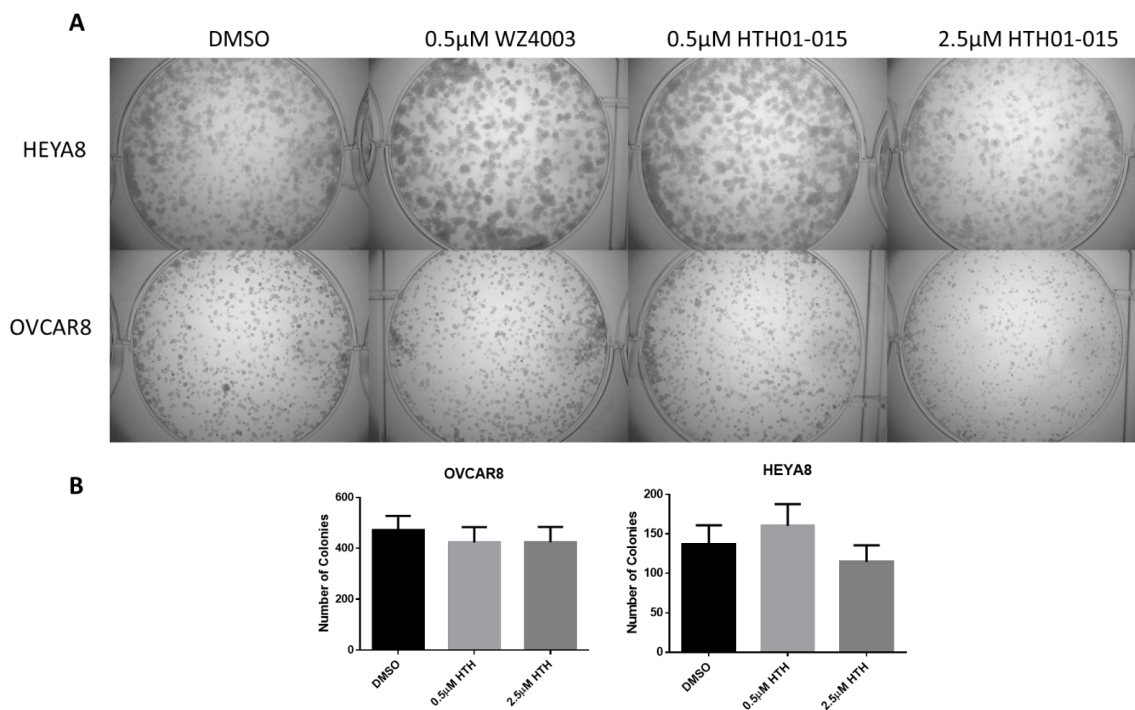


Figure 3.15. Treatment with HTH01-015 has no effect on clonogenicity. (A) Cells treated with HTH01-015, or WZ4003, as indicated. Cells were seeded at a density of 1000cells/well, treated the day after seeding, and fixed and stained 7 days after treatment. Top images show whole-well taken using Zeiss Axiozoom stereomicroscope at 4x. (B) Quantification of colony formation. Data is plotted as mean \pm SD, analysis performed using one-way ANOVA and Tukey's *post hoc* test (n=3)

3.9 NUAK1 inhibition does not affect thymidine incorporation

To investigate why the combination therapy experiment did not work as predicted, and to determine if in fact NUAK inhibition is directly affecting proliferation, tritiated thymidine incorporation assays were performed. The tritiated thymidine incorporation assay involves incorporation of radioactively labeled thymidine into cells that are actively synthesizing new DNA. Higher radioactivity readings are indicative of higher DNA content in S-phase, which is reflective of increased proliferation (Gieni et al., 1995). For this assay, cells were treated in adherent and spheroid culture with 0.5 μ M WZ4003 and pulsed with thymidine 24 hours after treatment. Results from OVCAR4, OVCAR8 and HEYA8 cells suggested that there was no difference between thymidine incorporation in DMSO and WZ4003-treated cells, in adherent and spheroid culture (Fig. 3.18). This suggests that NUAK inhibition does not influence proliferation, and may instead influence other processes. This supports our results in which WZ4003 treatment had no further carboplatin sensitization effect on spheroids.

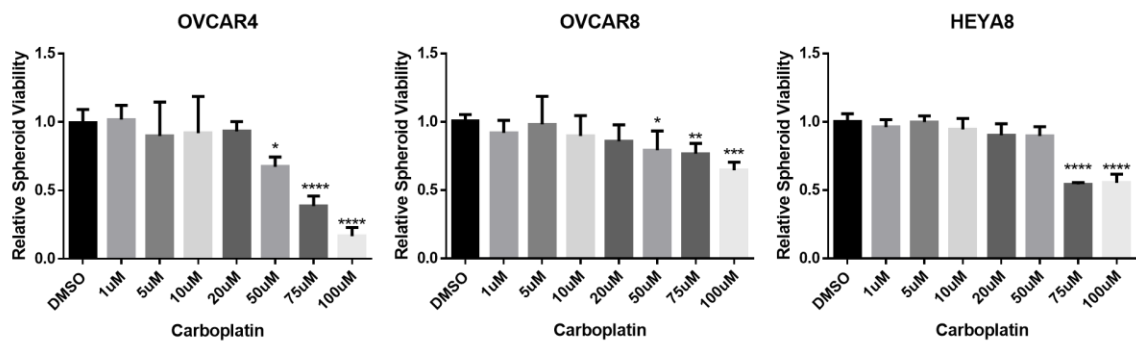


Figure 3.16. Carboplatin dose-response curves in spheroids. OVCAR4, OVCAR8 and HEYA8 cells were seeded at 2000cells/well in 96 well ULA plates, in 150µL. Immediately after seeding, cells were treated with concentrations of carboplatin between 1-100µM, as indicated. Cells were extracted after 72h for CellTiterGlo® based viability readings. Data is plotted as mean±SD for 6 replicates, analysis performed using one-way ANOVA and Tukey's *post hoc* test. (*, $p < 0.05$, **, $p < 0.01$, ****, $p < 0.001$). (n=2)

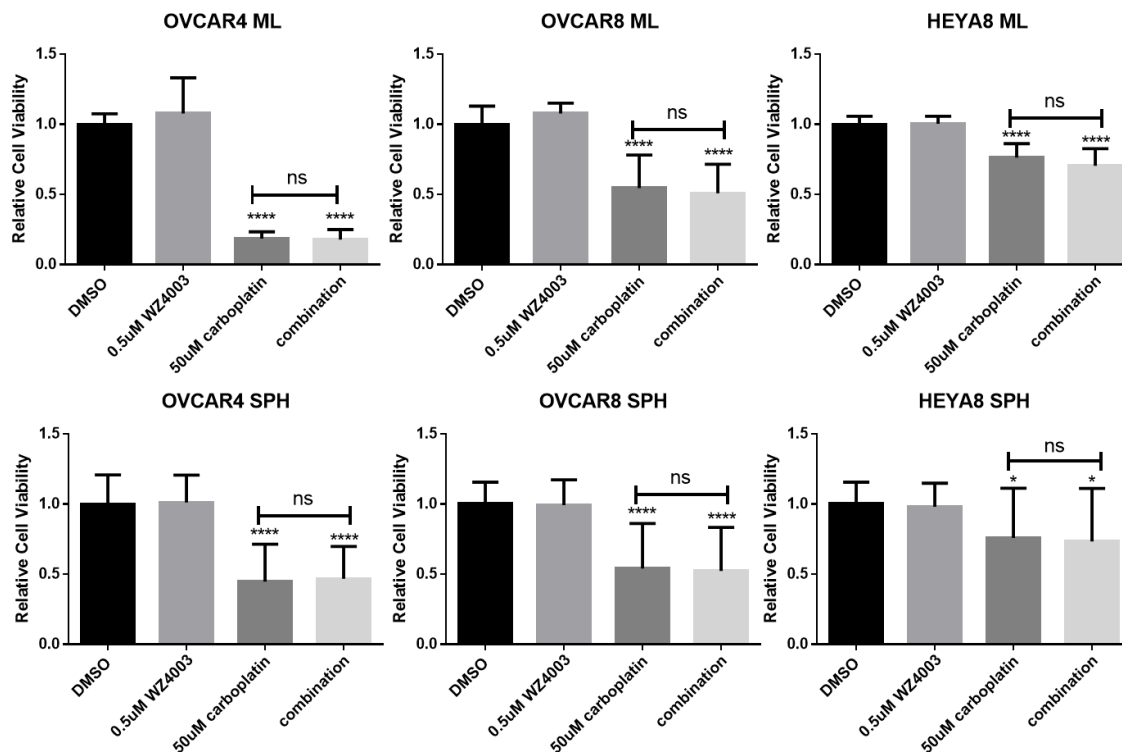


Figure 3.17. WZ4003 does not further sensitize EOC cells to carboplatin. CellTiterGlo® data suggests that NUAk inhibition does not sensitize cells and spheroids to carboplatin based therapy. (monolayer) Cells were seeded in 96-well format, with 2000cells/well, in 150µL, and treated with either DMSO, 0.5µM WZ4003, 0.5µM carboplatin or a combination of both treatments the following day. Cells were extracted after 72h and CellTiterGlo® was added to measure viability. Relative cell viability, as mean±SD, was plotted using Graphpad PRISM, analysis was performed using one-way ANOVA and Tukey's *post hoc* test, (****, $p < 0.001$). (spheroid) Cells were seeded in 96-well format with 2000cells/well, in 150µL, and treated immediately after seeding with treatments listed above. Cells were extracted after 72h and CellTiterGlo® was added to measure viability. Relative cell viability, as mean±SD, was plotted using Graphpad PRISM, analysis was performed using one-way ANOVA and Tukey's *post hoc* test, (****, $p < 0.001$). (n=3)

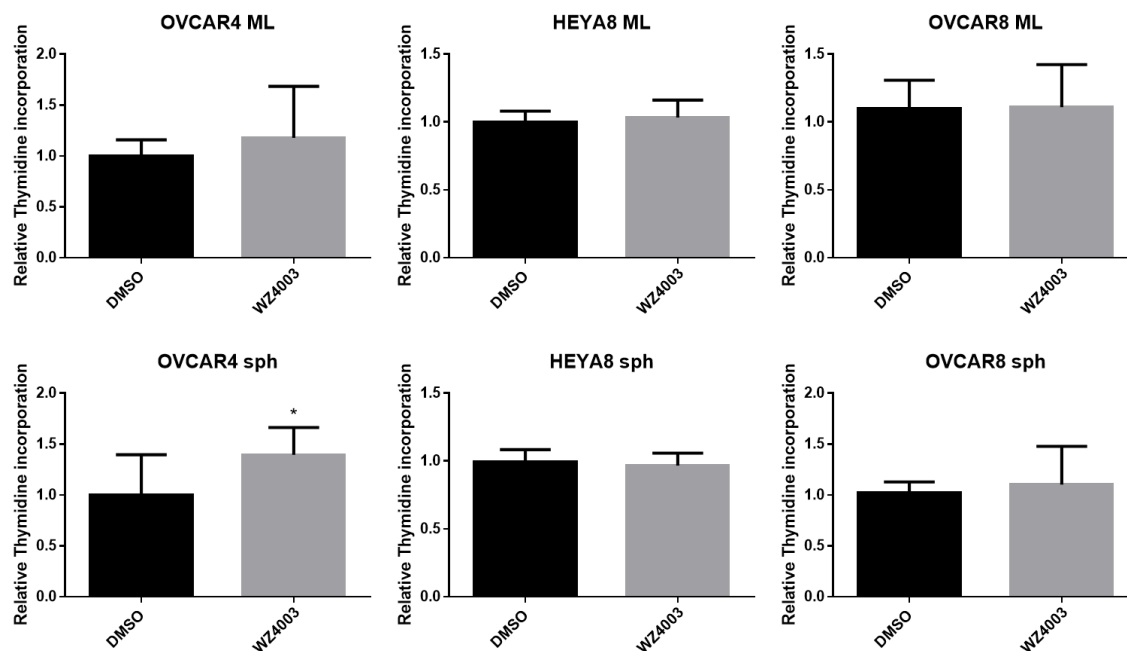


Figure 3.18. NUAK inhibition does not affect thymidine incorporation. Cells were seeded in 6- well format at 100 000cells/well in adherent culture and 200 000 cells/well in spheroid culture. Cells were treated with DMSO and 0.5 μ M WZ4003 at time of seeding for spheroids and 1-day post-seeding for adherent culture. Spheroids were pulsed with tritiated thymidine for 24 hours, 1 day post-treatment. Adherent cells were pulsed with tritiated thymidine for 2 hours, 1 day post-treatment. Data is plotted as mean \pm SD for 3 replicates, analysis performed using Student's *t*-test. (*, $p < 0.05$) (n=3) *Experiment conducted in collaboration with Piru Perampalam and Dr. Fred Dick*

Chapter 4

4 Discussion

4.1 Summary of findings

Results presented in this thesis offer new insight into the previously unknown role of NUA1 in EOC. To begin, the array of NUA1 expression was demonstrated in well-established EOC cell lines, newly-established early-passage EOC cell lines, and immortalized fallopian tube epithelial lines. This screen of NUA1 protein expression indicated that NUA1 has limited expression in EOC. This differs from previously published literature on NUA1 in EOC, which suggested that NUA1 is evenly expressed in EOC cell lines (Zhang et al., 2015). It was also noted that NUA1 levels decrease from adherent to spheroid culture, which may permit increased survival in spheroids. Results indicated that NUA1 is regulated by LKB1 in EOC cells, and that its expression and phosphorylation are dependent upon intact LKB1. Transient knockdown data indicated a unique and unexpected phenotype, whereby NUA1 knockdown increases viable cell number within spheroids derived from EOC cell lines. Alongside increased viable cell number, data suggested that NUA1 knockdown drastically increases reattachment potential, which may be an indirect indication of the metastatic potential of spheroids. Single and double knockdown experiments outlined the more important role of NUA1 in EOC cell and spheroid viability. These experiments suggested that NUA2, the most closely related family member to NUA1, is not as important to EOC cell and spheroid viability, yet functional compensation may be a cell line specific event. To further explore the roles of NUAs in EOC, the WZ4003 dual NUA inhibitor was used. Inhibitor studies indicated that NUA1/2 inhibition results in increased cell growth and increased clonogenicity. Studies using the HTH-01-015, NUA1 specific inhibitor, indicated that NUA1 inhibition alone increased EOC cell growth, however this was not followed by increased clonogenicity. Lastly, results suggested that the increased viability phenotype that is seen upon NUA inhibition could not be exploited to further sensitize spheroids to platinum-based chemotherapy. This may be because NUA1 does not affect cell cycle, as indicated by the tritiated thymidine incorporation assay, and NUA inhibition is affecting processes which are independent

of proliferation. Data presented in this study has indicated the unique role of NUA1 in EOC and has identified a unique survival mechanism which spheroids may use to increase viability.

Data presented here showing NUA1 regulation by LKB1 is in line with data that has been recently observed by our laboratory. Our lab has recently conducted a Kinobead assay, a technique used to analyze changes in kinase activity. The assay involves the use of multiplexed inhibitor beads combined with tandem mass spectrometry, to capture and analyze active kinases within lysates (Cooper et al., 2013). Results from this assay, using the OVCAR8 and OVCAR8 *STK11*KO cell lines, suggested that NUA1 was the only ARK species regulated by LKB1, and that NUA1 activity decreases upon loss of LKB1 in both adherent and spheroid culture (Buensuceso and Shepherd, unpublished data). This assay validated my pursuit of NUA1 as our ARK of interest, and suggests that NUA1 activity is regulated by LKB1 in EOC cells.

4.2 Potential growth suppressive of NUA1 in EOC

Findings presented in this study indicate that NUA1 may have growth suppressive, and potential tumor suppressive, activity in EOC cells and spheroids. Firstly, it was noted that NUA1 is expressed at the protein level in a very limited subset of EOC cell lines. These results are supported by the publicly available Human Protein Atlas dataset, which suggests that NUA1 has low-undetectable staining in EOC tissue samples (Uhlen et al., 2015). This may be an indication that NUA1 expression is not beneficial for growth and viability in EOC cells. For example, NUA1 was lost in the latter of two cancer cell lines which were derived from the same patient during different times in her treatment. Perhaps it may even be advantageous for EOC cells to decrease NUA1 expression to enhance chemoresistance. Furthermore, transient knockdown experiments suggested that NUA1 knockdown releases spheroids into a more viable state, with higher viable cell number in *siNUA1* spheroids and NUA1 knockdown increases spheroid reattachment potential. This data suggests that NUA1 expression may be restricting spheroid potential and that NUA1 loss may in fact enhance spheroid integrity and ability to further metastasize through reattachment. Inhibitor data supplements knockdown findings, as NUA1 inhibition increases cell growth and clonogenicity. These findings

suggest that NUAKE1 expression may be restricting EOC cell growth or adhesion. Overall, results indicate that NUAKE1 may be maintaining tumor suppressive activity and that loss of NUAKE1 may drive EOC cells and spheroids into a more viable and metastatic state. Therefore, it may be possible to exploit this potential tumor suppressive role of NUAKE1 and create NUAKE1 agonist therapies to reactivate NUAKE1 and reduce metastatic disease burden.

Results presented in this study differ from previously published literature regarding NUAKE1 function in EOC. In 2015, Zhang and colleagues gathered evidence to suggest that NUAKE1 promotes epithelial-to- mesenchymal transition (EMT) by inhibiting a promoter of mesenchymal-to-epithelial transition (MET), miR-1181. They show that miR-1181 acts to induce degradation of HOXA10, a target that triggers EMT in ovarian cancer cell lines. Furthermore, the authors suggest that NUAKE1 is evenly expressed in EOC cell lines, but our results in the same cell lines (OVCAR8, OVCAR3, Hey, SKOV3) show that NUAKE1 has a limited expression profile and is not expressed at the protein level in many of these lines. Zhang and colleagues suggest that NUAKE1 has an oncogenic role, since its expression acts to induce a metastatic phenotype; yet our results suggest that NUAKE1 has potential tumor suppressive activity in EOC cell lines. In support of the hypothesis proposed by Zhang and colleagues, Phippen and colleagues (2016) suggest that NUAKE1 is associated with poor prognosis in HGSOC. The authors conducted analysis of NUAKE1 transcript expression in 34 HGSOC patient samples and monitored progression free survival. They noted that NUAKE1 expression is correlated with lower progression free survival in patient samples. Furthermore, they knocked down NUAKE1 using RNAi in 2 cell lines and found that NUAKE1 knockdown decreased cell motility *in vitro*. While this study offers additional insight into NUAKE1 in EOC, it has only considered NUAKE1 expression at the RNA level. For this reason, my work with NUAKE1 at the protein level may offer better insight into NUAKE1 function in HGSOC.

My results suggest that NUAKE1 has tumor suppressive activity in EOC, and can be supported by previously published studies in other cancer sites suggesting that NUAKE1 has tumor suppressive function. Hou and colleagues (2011) describe a tumor suppressive role of NUAKE1 by which NUAKE1 activates p53. Using various cancer cell lines from

different sites, the authors show that LKB1-mediated activation of NUA1 triggers p53 phosphorylation, causing p21 transcription and cell cycle arrest at the G1 border. This may be a mechanism by which NUA1 is exerting tumor suppressive activity in EOC, but only in tumors or cell lines with intact p53, such as the HeyA8 cell line (Domcke et al., 2013). Most HGSOE tumors and cell lines lack functional p53 (Ahmed et al., 2010), therefore this mechanism may not be applicable to all cell lines in which I have conducted this study. In 2014, Banerjee and colleagues described a mechanism by which LKB1-activated NUA1 controls cell cycle through indirect regulation of PLK1 via interaction with the MYPT1-PP1 β complex. To this end, Werle and colleagues (2014) demonstrated that LKB1 activates NUA1 to enhance the binding of PP1 γ with MYPT1-PLK1-NUA1. This interaction results in inactivation of PLK1, preventing G2 \rightarrow M transition and mitotic progression. This tumor suppressive function of NUA1 may be applicable to my results and the observed phenotype in EOC cells. Although results from the tritiated thymidine incorporation assay indicated that that NUA1 inhibition did not significantly alter proliferation, the assay is limited to evaluating proliferation based on the S-phase. Perhaps NUA1 is still affecting proliferation through PLK1 inhibition, and is instead affecting G2 \rightarrow M. Additionally in support of NUA1 having tumor suppressive activity, Humbert and colleagues (2010) observed that NUA1 expression induces gross aneuploidies and premature senescence, using WI-38 human diploid fibroblasts. The authors noted that NUA1 knockdown increased cell growth and colony formation, while decreasing senescence, which mirrors my data from EOC cell lines. LATS1 acts as a regulator of genomic stability and senescence, and decreased LATS1 expression is associated with increased senescence (Takahashi et al., 2006). Humbert and colleagues demonstrated that NUA1 phosphorylates LATS1 at S464, enabling LATS1 degradation to induce senescence. Current theories suggest that cellular senescence can act as a tumor suppressive mechanism to prevent pre-malignant cells from undergoing malignant transformation upon oncogenic expression (Lowe et al., 2004). It may be possible that EOC cells are downregulating NUA1 to attain a more viable state, and preventing NUA1-mediated senescence in certain cell populations. The mechanisms of NUA1-mediated tumor suppression proposed by these 3 studies may be applicable to my findings.

4.3 Therapeutic implications of results

Initially, I believed that the increased spheroid cell viability seen upon loss of NUA1 may have been due to increased cell proliferation, which could render the cells more sensitive to chemotherapy. However, combination therapy results indicated that I was mistaken, and that NUA1 inhibition is insufficient to further induce platinum sensitization. Along with the increased clonogenicity and lack of sensitization with carboplatin, inhibition of NUA1 is unlikely to be an effective therapeutic strategy in EOC.

Results presented in this study imply the tumor suppressive nature of NUA1 in EOC, therefore it may be useful to develop NUA1 agonists and evaluate their potential therapeutic use. If we consider our knockdown and inhibitor results, then we could, in theory, activate NUA1 signalling to reduce spheroid viability and reattachment. NUA1 agonists could be used to reduce microscopic metastatic disease burden in late-stage EOC, and help minimize this clinically significant problem in EOC treatment. However, this will need to be evaluated further by first overexpressing NUA1 or using constitutively-active NUA1 mutants in EOC cells, as a complementary set of experiments to those proposed in this thesis.

4.4 NUA1 and LKB1

Results gathered by Peart and colleagues (2015) suggested that LKB1 functions as a key mediator of spheroid viability in EOC. In this study, results suggested that NUA1 acts as the direct downstream substrate of LKB1, yet the phenotype observed upon NUA1 knockdown is the opposite of LKB1. To explain this discrepancy, we must consider that LKB1 is a master kinase involved with stress metabolism, while NUA1 is one of the 13 direct downstream effectors of LKB1 (Hardie and Alessi, 2013). LKB1 signalling regulates a multitude of processes, and only a subset of these processes may be affected by NUA1.

Despite this discrepancy in knockdown phenotypes, targeting of NUA1 through the use of NUA1 agonists may still be beneficial to EOC treatment. We cannot directly target

LKB1 since loss of LKB1 activity may affect stress metabolism in normal cells in many other critical tissues. Furthermore, LKB1 has been widely implicated as a tumor suppressor and systemic administration of LKB1 inhibitors may cause neoplastic transformation within other epithelial sites (Zhao and Xu, 2014). If we could instead independently target NUA1 intraperitoneally without affecting LKB1 signaling, we would avoid risks associated with LKB1 inactivation in normal cells. Therefore, it may be worth further exploring the development and use of NUA1 agonists for EOC treatment.

4.5 Limitations of current study

My study helped to uncover a novel role of NUA1 in EOC, however there are aspects of the study which have limitations that could be addressed through further experimentation.

Firstly, analysis of NUA1 phosphorylation was only done using Phostag™ acrylamide gels. We were fortunate enough to obtain these gels to confirm results from the Kinobead assay (Buensusceso and Shepherd, unpublished data), where we discovered that NUA1 activity is regulated by LKB1. However, this system is limited because the phosphorylation residues cannot be identified, thus I cannot confirm that we are seeing phosphorylation of NUA1 at the Thr211 residue. To combat this limitation, we would need to synthesize our own antibody to detect NUA1 phosphorylation at the Thr211 residue and conduct site-specific mutagenesis to ensure we are seeing phosphorylation of NUA1.

Additionally, use of the WZ4003 NUA1 inhibitor may be potentially problematic since I was unable to detect whether the inhibitor is functioning in these cell lines at the chosen doses. Previous studies using the WZ4003 compound have been conducted in U2OS, HeLa, HEK293, and MEF cell lines using concentrations between 1-10µM, and have verified the efficacy of the inhibitor using MYPT1 phosphorylation as a readout (Banerjee et al., 2014; Zagorska et al., 2010). Despite my best efforts, I was unable to detect decreases in MYPT1 phosphorylation upon treatment with the WZ4003 compound. It is possible that this experiment may require further optimization in EOC

cells, or that NUAKE1 is acting independently of MYPT1 in EOC cells. To combat this, we could also consider looking at LATS1 phosphorylation at the S464 residue to see if NUAKE inhibition is affecting LATS1, instead of MYPT1, in EOC cells (Humbert et al., 2010).

My choice of the tritiated thymidine incorporation assay to measure proliferation may have resulted in us missing critical information regarding NUAKE1 function. The tritiated thymidine incorporation assay, like other thymidine analogue assays, is a measure of DNA synthesis which occurs during S-phase (Cavanagh et al., 2011). By choosing an assay which is biased towards S-phase, I may have missed the potential impact of NUAKE inhibition on other phases of cell cycle. Perhaps NUAKE1 functions to elicit cell cycle arrest at the G2→M phase by inhibiting PLK1 (Werle et al., 2013). To combat this, in the future we should consider conducting flow cytometry to assess if NUAKE1 inhibition alters the relative amount of cells present in G2→M phase.

4.6 Future Work

While I have discovered an interesting and unique role of NUAKE1 in EOC, there of course remain several experiments to conduct to potentially translate this discovery to the clinic. However, I would encourage prioritizing two categories of experiments. First, it would be critical to mechanistically understand the increased viability phenotype seen upon loss of NUAKE1. Following this classification, it would be important to further interrogate the potential tumor suppressive function of NUAKE1 in EOC cells.

Loss-of-function experiments for NUAKE1 produced an increase in cell and spheroid viability and metastatic potential. In an attempt to determine the mechanism behind this increased viability, the tritiated thymidine incorporation assay was used and data indicated that NUAKE1 inhibition did not affect cell cycle; at least this was not observable through DNA replication in S-phase. While we cannot entirely rule out cell cycle as a mechanism, it may suggest that NUAKE1 affects viability independent of proliferation. This increased viability phenotype may instead be attributed to a block of apoptosis. Perhaps loss or inhibition of NUAKE1 is resulting in decreased apoptosis, and thereby leads to increased viability. There are multiple methods that can be used to detect

changes in apoptosis, and there are three methods that could be directly employed in both EOC cells and spheroids: the cleaved caspase 3 assay, the Caspase-Glo® assay and flow cytometry using Annexin V. To conduct these experiments, I recommend first establishing CRISPR-Cas9 engineered cells which lack NUA1 expression. Ablation of NUA1 in cells will allow for more consistency when classifying cellular processes regulated by NUA1. The cleaved caspase 3 assay is based on extrinsic cell death signals. In extrinsic death, caspase 8 is activated by binding of the FADD ligand to the death receptor on the cell membrane. This results in cleavage of the executioner caspases (3, 6, and 7) to mediate apoptosis. Pro-caspase 3 (32kDa) is cleaved into 17 and 12 kDa subunits which are detectable using western blot (McIlwain et al., 2013). I recommend using NUA1 WT and *NUA1*KO cells in both adherent and spheroid culture, to see if caspase 3 cleavage decreases upon loss of NUA1. The Caspase-Glo® assay follows the same principle of tracking caspase-3 cleavage as the cleaved caspase western blot. The assay involves the use of a luciferin substrate which can bind to cleaved caspase 3, and can be quantified using luminescence (Riss et al., 2013). Like the cleaved caspase 3 western blot, I recommend quantifying apoptosis using the Caspase-Glo® assay in both adherent and spheroid culture. The advantage of this assay is that it can be conducted in 96-well or 24-well format, to look at the effects of apoptosis in single spheroids or a small population of spheroids. Lastly, Annexin V staining can be used to assess if apoptosis is affected by NUA1 function. During apoptosis phosphatidylserine, which is normally localized cytoplasmically, becomes exposed to the outer leaflet of the cytoplasmic membrane. Annexin V binds to phosphatidylserine to allow for detection of apoptosis using flow cytometry (Wlodkowic et al., 2009). While use of *NUA1*KO cells may be useful for experimental consistency in the experiments described above, it would also be worth treating cells with WZ4003 to assess the effects of NUA1 inhibition on apoptosis. I predict that NUA1 loss or inhibition would decrease the proportion of apoptotic cells, resulting in increased cell viability.

My experiments have identified the potential tumor suppressive nature of NUA1 in EOC. This remains to be further confirmed to evaluate if NUA1 agonists may be potentially beneficial as therapeutic agents. There are several assays that can be conducted to evaluate the tumor suppressive role of NUA1, some of which have been

already completed in this study. We have recently established stable NUAK1 overexpression clones in OVCAR3 and HeyA8 cells (Collins and Shepherd, unpublished data), which under normal circumstances have little NUAK1 expression (Fig. 3.2). The next step with these overexpression clones would be to test the effect of NUAK1 overexpression on proliferation and viability. I predict that NUAK1 overexpression will decrease cell viability and potential proliferative potential in EOC cells. To better understand the true tumor suppressor nature of NUAK1, we could also make use of immortalized fallopian tube epithelial cells (Karst and Drapkin, 2012). I have determined that FT190 and FT237 cells have low, but detectable, levels of NUAK1. If we were to ablate NUAK1 expression and activity using CRISPR-Cas9 in fallopian tube cells we could test, using *in vitro* models, to see if loss of NUAK1 induces a more malignant phenotype. I recommend using fallopian tube epithelial *NUAK1KO* cells to test changes in growth kinetics, clonogenicity, spheroid formation potential and reattachment. I predict that loss of NUAK1 in these immortalized “normal” cells will result in a more malignant phenotype. In fact, I currently have evidence to support our prediction, as FT190 cells treated with WZ4003 had a shortened doubling time (Table 3.1).

Mouse models can also be used to assess the tumor suppressive activity of NUAK1. Possibly one of the first steps in evaluating the tumor suppressive activity of NUAK1 *in vivo* would be using EOC cancer cell lines, with ablated NUAK1, and assessing tumor formation. I recommend using CRISPR-Cas9 to knock out NUAK1 in OVCAR8 cells and orthotopically inject these cells into immunocompromised mice. I predict that mice injected with OVCAR8 *NUAK1KO* cells will have a higher tumor burden and decreased survival. To truly test if NUAK1 is tumor suppressive in EOC, we should consider generating inducible *Nuak1*-ko mice. *NUAK1* must be deleted using an inducible method because *Nuak1* null mice are embryonic lethal, since NUAK1 loss prevents closure of the ventral body wall (Hirano et al., 2006). I recommend deleting *Nuak1* in an inducible and site-specific manner, by targeting the fallopian tube epithelium in female mice after puberty (Perets et al., 2013). This may lead to spontaneous tumor development. However, I realize that loss of NUAK1 on its own may be insufficient to induce neoplastic transformation. Therefore, we may also consider inducible knockout of *Trp53* and *Nuak1* to see if loss of NUAK1, alongside p53, furthers disease progression.

If we are successful in characterizing the tumor suppressive ability of NUA1 *in vitro* and *in vivo*, we should then consider designing NUA1 agonists. This process may possibly require determination of the protein structure of NUA1, using X-ray crystallography; as this has not yet been done for NUA1. We may then have to determine the correct domain of NUA1 to target using a small molecule, and design a structure accordingly. However, discovery of X-ray structures are usually required for design of peptide-based agonists (Hruby, 2012), and may not be applicable to NUA1 activation. We may also consider conducting a random chemical screen to test the efficacy of non-peptide compounds on NUA1 activation. Like the NUA1 antagonist screen conducted by Banerjee and colleagues (2014), we could conduct a similar screen of drug compounds and assess for increased NUA1 kinase activity using an *in vitro* kinase activity assay. Furthermore, compounds must be tested *in vitro* and *in vivo* using mouse models to identify potential adverse effects. While conducting these studies, we must also consider disease heterogeneity and realize that not all patients may respond to NUA1 agonist therapies. We should conduct studies to investigate which subset of patients will respond best to NUA1 agonist therapies, and classify this based on NUA1 expression and possibly LKB1 status.

4.7 Overall Conclusion

Overall, I have contributed to growing ARK literature and have identified a novel and unique role of NUA1 in EOC. I have shown that NUA1 is regulated by LKB1 in EOC cells and have demonstrated its tumor suppressive potential. My results support the tumor suppressive role of NUA1 to help address the ongoing debate of NUA1 as an oncogene and a tumor suppressor (Sun et al., 2013). From this study, we have gained further insight into context dependence in cancer. Many previous studies have implicated NUA1 as an oncogene, through various mechanisms (Sun et al., 2013). Yet our study has identified the potential tumor suppressive nature of NUA1 in a model of EOC metastasis. This suggests that NUA1, like its upstream regulator LKB1, can have opposing functions in different tissue sites (Peart et al., 2015). This study has helped us appreciate context dependence and the role which NUA1 may be playing in the normal fallopian tube and EOC.

My studies began with an investigation of the downstream substrates of LKB1, which has metastatic promoting properties in EOC, to identify which substrate was critical for EOC spheroid viability (Peart et al., 2015). My initial hope with this project was to determine which ARK, downstream of LKB1, could be used as a therapeutic target to reduce spheroid viability and permit chemosensitivity. My results led me on a unique path, where I discovered that NUA1 is regulated by LKB1 in these cells, but that intact NUA1 is not critical for spheroid viability and chemosensitization. Instead I found the opposite effect of LKB1, whereby loss of NUA1 promoted spheroid viability. Although I ended on a different path than where I had planned, I have gained new insight into mechanisms of tumor suppression in EOC and future studies could uncover a potential alternate route of reducing metastatic burden by activating NUA1. If we can identify ways to block spheroid growth, survival, and reattachment, then this could be a worthwhile strategy for reducing disease burden in late-stage ovarian cancer patients.

Chapter 5

5 Appendices

5.1 Appendix A: ARK mutations and mRNA expression

Prior to the discovery of NUAKE1 as our ARK of interest, we conducted wide scale analyses on all ARKs to see which was the most relevant in EOC.

These studies began by using publicly available datasets, to see if the ARKs were mutated, or potentially important, in high grade serous tumor samples. We analyzed cBioportal data using The Cancer Genome Atlas (TCGA, 2011) provisional data, and found that several of the ARKs are mutated in ovarian tumor samples (Fig. 5.1A). Data indicated that NUAKE2 was the most mutated ARK species, with 7% of tumors having NUAKE2 amplification. However, NUAKE1 was not highly mutated in EOC tumor samples. We then analyzed ARK expression, at the mRNA level in 47 EOC cell lines, using Cancer Cell Line Encyclopedia (CCLE), and found that several ARKs are expressed at the mRNA level (Fig. 5.1B). NUAKE1 had the highest, yet most variable, expression profile in EOC and was followed closely by NUAKE2. To analyze NUAKE data more closely, we looked exclusively at the mRNA expression profiles of NUAKE1 and NUAKE2 (Fig. 5.2). We noticed that NUAKE1 and NUAKE2 mRNA expression was directly proportional in most cell lines, other than the OVCAR8 cell line which has amplified NUAKE1 levels. We compared the CCLE mRNA data to our own NUAKE1 protein expression data (Fig. 3.2) and noticed that it did not correlate well. CCLE data indicated that OVCAR4 cells have high NUAKE1 expression, while COV362 cells have low NUAKE1 expression. Our protein data indicates the opposite trend, where OVCAR4 cells have low NUAKE1 levels, and COV362 cells have high NUAKE1 levels. Perhaps this indicates a discrepancy between NUAKE1 mRNA and protein levels, since NUAKE1 can be tagged for ubiquitination (Banerjee et al., 2014).

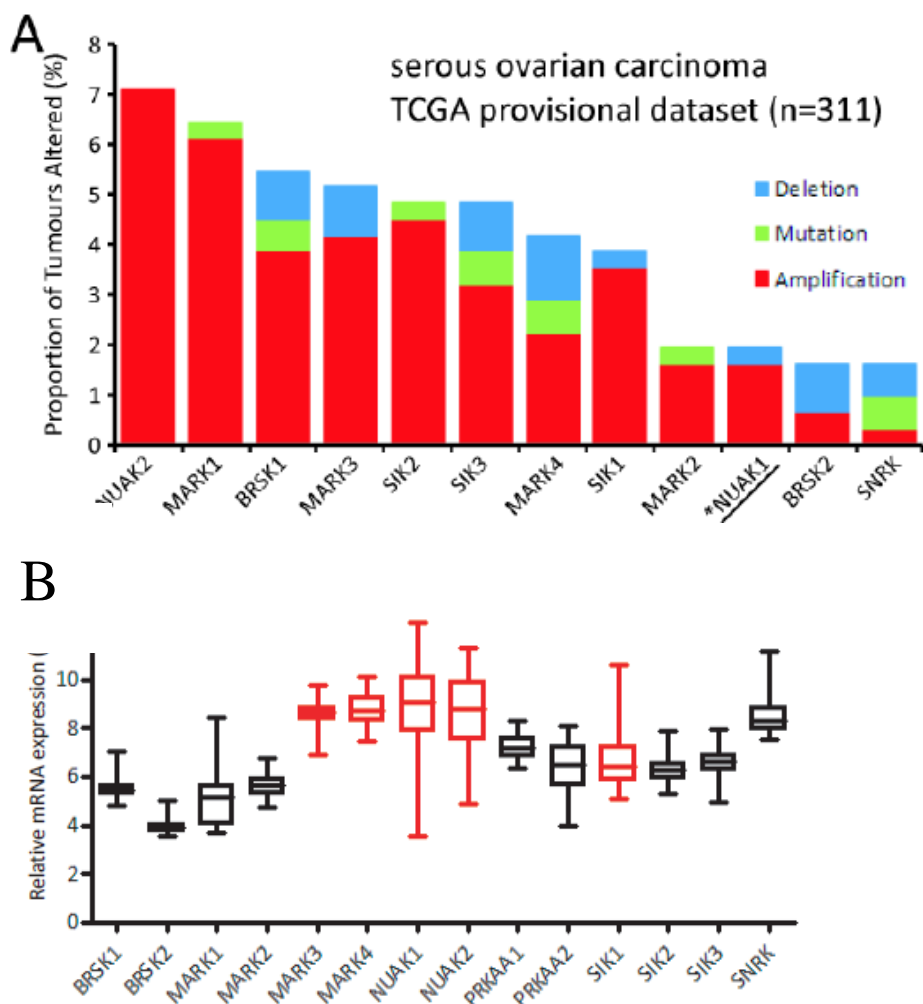


Figure 5.1.(A) Copy number and mutational status of ARK genes in serous ovarian cancer (TCGA provisional dataset, Gao et al., 2013). NUAK1 is not highly genomically altered in EOC, yet NUAK2 is the most amplified ARK in EOC. *Figure generated by Dr. Trevor Shepherd.* (B) mRNA expression levels of ARKs and PRKAAs across 47 ovarian cancer cell lines. Shown in red is ARKs we conducted preliminary siRNA knockdown screen on. (Cancer cell line encyclopedia) (TCGA, 2011; Gao et al., 2013)

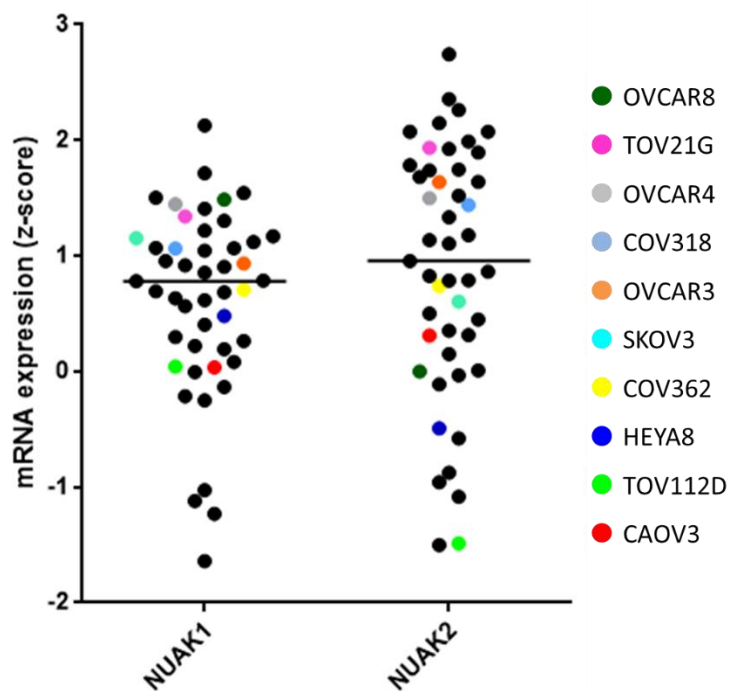


Figure 5.2.NUAK1 and NUAK2 mRNA expression from 47 EOC cell lines (CCLE, cBioportal). Data is plotted as mean (solid lines) and z-scores. Coloured dots indicate cell lines available in our program. NUAK1 and NUAK2 are expressed at similar levels in EOC cell lines. *Figure generated by Dr. Trevor Shepherd.*

To assess ARK mRNA expression further in EOC, we conducted an Affimetrix microarray in 5 ascites derived patient samples (Peart and Shepherd, unpublished data) (Fig. 5.3A). We noted that our data from patient samples correlated with CCLE cell line data, and that NUAK1 had the highest expression profile amongst patient samples. However, we noted that there was less variability between NUAK1 expression in patient samples than in cell lines, as indicated by CCLE data.

Using qPCR on our set of well-established ovarian cancer cell lines, we explored to see if ARKs are expressed at the mRNA level (Kobylecky and Shepherd, unpublished data) (Fig. 5.3B). We confirmed that many of the ARKs are expressed at the mRNA level in ovarian cancer cell lines and that our data diverged slightly from CCLE data. Out of the 10 cell lines we screened, we noted that MARK species had the highest expression levels of all the ARKs in EOC. This divergence between datasets may be due to our limited sample size.

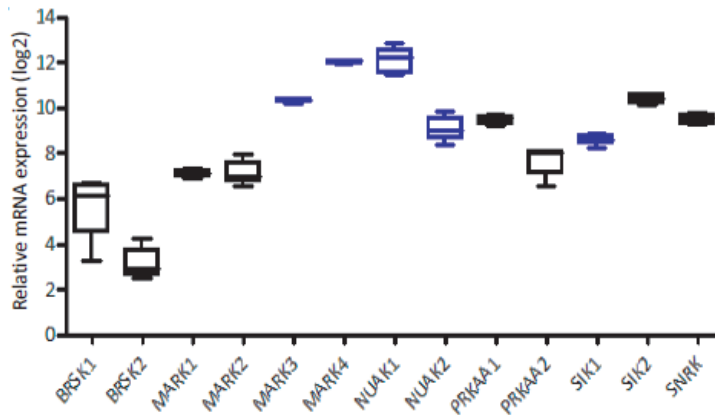
Our analysis of publicly available datasets alongside our own experiments helped us to understand ARK expression in EOC. Particularly, we determined that NUAK1 is one of the least mutated and most-variably expressed ARK species in EOC.

5.2 siARK Screen

The siARK screen is a project that we carried out to determine which ARKs are functionally relevant to EOC spheroid viability (Ramos-Valdes and Shepherd, unpublished data). This project involved siRNA mediated knockdown of all ARK species, LKB1, and AMPK subunits in 11 EOC cell lines, consisting of both well-established and early-passage ascites-derived cell lines. CellTiterGlo® was used to assess day 3 adherent and spheroid viability in transfected cells (Fig 5.4).

Results suggested that knockdown of NUAK species improved viability in many of the cell lines screened (Fig. 5.4B). Knockdown of SIK species and SNRK decreased cell viability in a few of the cell lines (Fig. 5.4B). Despite some promising results with NUAK species, SIK species, and SNRK, there was no consistent target that was critical

A



B

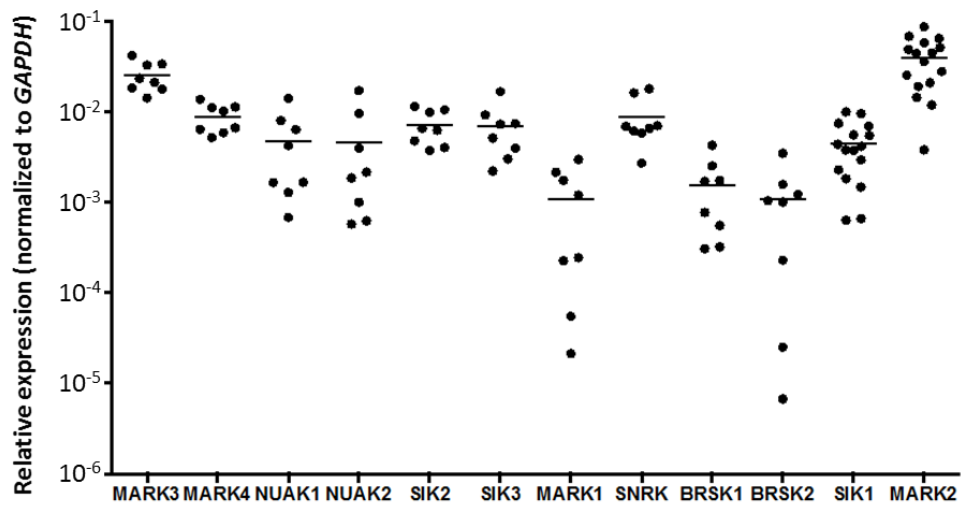


Figure 5.3. (A) Affimetrix microarray analysis of ARK expression levels in 5 primary ascites samples. *Experiment conducted by Teresa Peart* (B) Relative mRNA expression level of ARKs among 10 ovarian cancer cell lines using qRT PCR. (n=3) *Experiment conducted by Elizabeth Kobylecky*

for viability in all cell lines screened. However, our data from the siARK screen further supported our inclination to pursue NUA1 as a target in EOC.

5.3 MARK3 studies in EOC

Prior to pursuing NUA1 as a target in EOC, I investigated the potential role of MARK3 in EOC cell and spheroid viability. To begin, I surveyed MARK3 expression in EOC cell lines and found that MARK3 has an even expression profile across all EOC cell lines (Fig. 5.5). This may be because MARK3 is ubiquitously expressed in many tissue sites. I also investigated MARK3 expression in adherent and spheroid culture, using well-established EOC cell lines. I noted that MARK3 expression decreased from adherent to spheroid culture in OVCAR3, OVCAR5, SKOV3 and TOV21G cells (Fig. 5.6). To examine potential changes in MARK3 phosphorylation between adherent and spheroid culture I used a pan-phospho MARK antibody. I found that pMARK expression decreased from adherent to spheroid culture in all cell lines tested (Fig 5.6A). However, this may not be necessarily indicative of MARK3 phosphorylation decreasing, and may be attributed to one of the other 3 MARK species instead.

I then examined the potential link between MARK3 and LKB1, using our CRISPR-Cas9 engineered *STK11*KO cells. I assayed for MARK3 expression to assess changes in total levels upon loss of LKB1 (Fig. 5.6B). I noted that unlike NUA1, loss of LKB1 did not affect total MARK3 expression. In terms of pMARK expression, I saw opposite trends in OVCAR8 and HeyA8 cells. In OVCAR8 cells, pMARK expression increased in *STK11*KO cells relative to wildtype cells (Fig. 5.6B). In HeyA8 cells, pMARK expression decreased in *STK11*KO cells relative to wildtype cells (Fig. 5.6B). These opposing trends suggested that MARK3 expression and activity was not regulated by LKB1, which was further supported by our data from the Kinobead assay.

To understand if MARK3 was relevant to EOC spheroid viability or spheroid reattachment potential, I performed siRNA-mediated knockdown of MARK3 in spheroid experiments. I measured day 3 spheroid viability using Cyquant® and found that loss of MARK3 had no effect (Fig. 5.7B). To this end, I also noted that siMARK3 spheroids did not differ in reattachment potential, compared to siNT spheroids (Fig. 5.7C).



Figure 5.5. MARK3 is expressed in EOC cell lines. Protein expression detected using Western blot of EOC cell lysates. MARK3 is highly expressed in OVCAR3 and TOV21G cells and is moderately expressed among all other cell lines. (N=3)

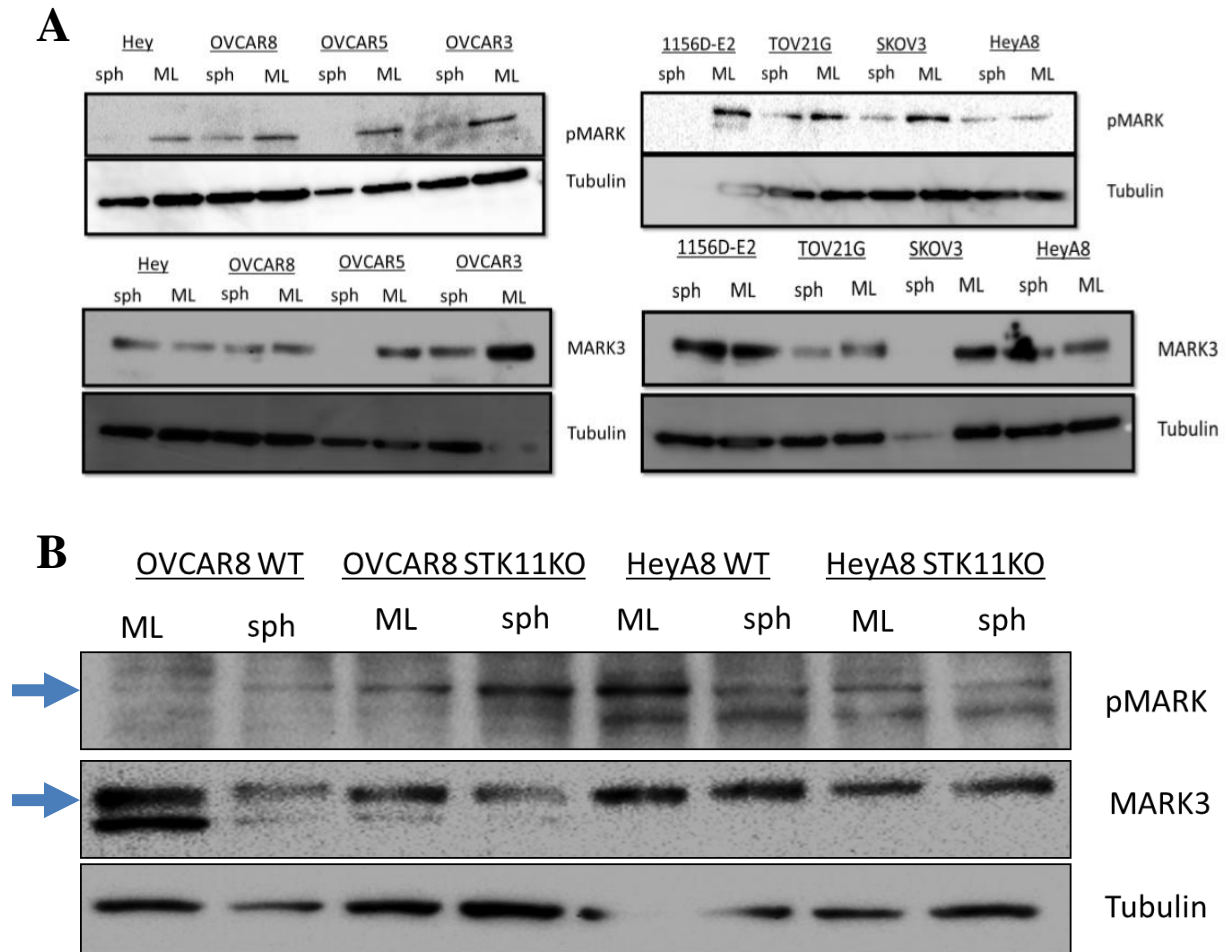


Figure 5.6. (A) pan phospho-MARK (p-MARK) expression in monolayer and day 3 spheroids in 8 cell lines (n=3). p-MARK expression decreases in spheroids in all cell lines (*bottom*) MARK3 expression in monolayer and spheroid in 8 cell lines (n=3). Total MARK3 expression decreases from adherent to spheroid culture in OVCAR3, OVCAR5, TOV21G and SKOV3 cells. Expression levels of MARK1,2, and 4 are unknown. **(B)** Evaluation of MARK expression levels in LKB1 intact and LKB1 knockout cell lines. pMARK and MARK3 expression in OVCAR8, HeyA8, OVCAR8 STK11KO and HeyA8 STK11KO cells using ML and day 3 sph lysates. STK11KO cells lack expression of LKB1 and were created by CRISPR-Cas9 technology. In OVCAR8 cells, pMARK expression increases from WT to STK11KO cells in both ML and sph, however, HeyA8 cells show the opposite trend where pMARK levels decrease from WT to STK11KO for both ML and sph. MARK3 levels appear to be relatively unchanged. (n=5)

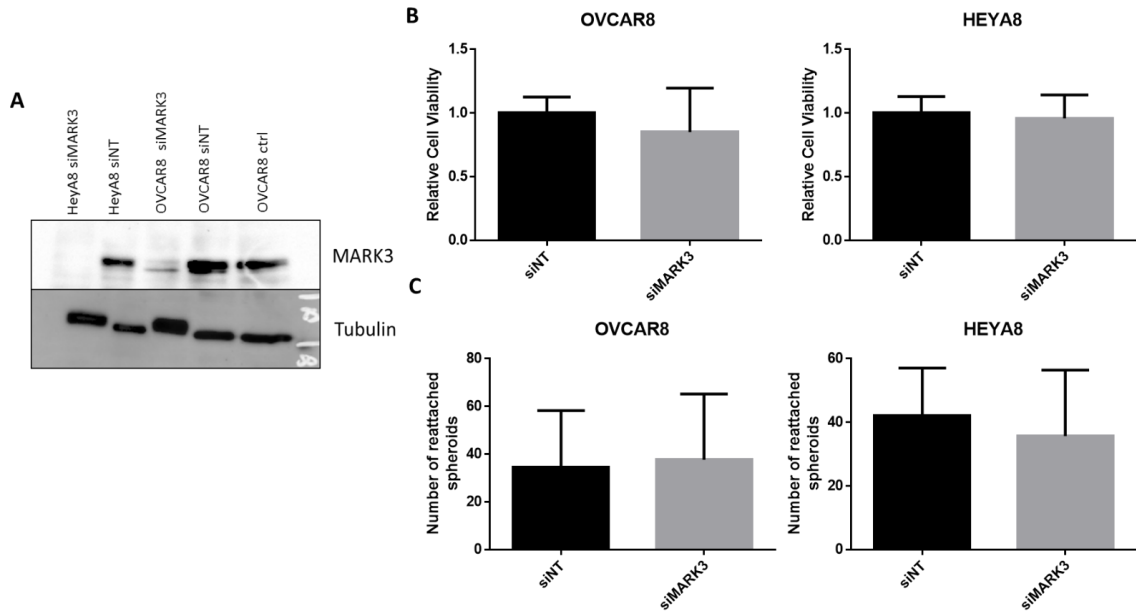


Figure 5.7. MARK3 does not affect spheroid viability or reattachment potential. **(A)** Western blot in day 3 adherent cells transfected with siNT and siMARK3, indicating successful siRNA mediated knockdown of MARK3. **(B)** Day 3 spheroid viability in OVCAR8 and HeyA8 cells transfected with siRNA against MARK3. There is no significant difference between siNT and siMARK3 spheroid viability. Data plotted as mean \pm SD, analysis performed on Graphpad PRISM using unpaired *t*-test ($N=3$). **(C)** Day 3 spheroid reattachment showing no difference between reattachment potential of siNT and siMARK3 spheroids. Data plotted as mean \pm SD, analysis performed on Graphpad PRISM using unpaired *t*-test ($n=3$).

Collectively, my data illustrates that MARK3 is likely not relevant to spheroid viability and dormancy, downstream of LKB1.

References

- Ahmed, A. A., Etemadmoghadam, D., Temple, J., Lynch, A. G., Riad, M., Sharma, R., ... Brenton, J. D. (2010). Driver mutations in TP53 are ubiquitous in high grade serous carcinoma of the ovary. *The Journal of Pathology*, 221(1), 49–56.
- Ahmed, A. A., Lu, Z., Jennings, N. B., Etemadmoghadam, D., Capalbo, L., Jacamo, R. O., ... Bast, R. C. (2010). SIK2 Is a Centrosome Kinase Required for Bipolar Mitotic Spindle Formation that Provides a Potential Target for Therapy in Ovarian Cancer. *Cancer Cell*, 18(2), 109–121.
- Alexander, A., & Walker, C. L. (2011). The role of LKB1 and AMPK in cellular responses to stress and damage. *FEBS letters*, 585(7), 952-957
- Auersperg, N., Siemens, C. H., & Myrdal, S. E. (1984). Human ovarian surface epithelium in primary culture. *In Vitro*, 20(10), 743–55.
- Bachmann, M., Hennemann, H., Pei, X. X., Hoffmann, I., & Möröy, T. (2004). The oncogenic serine/threonine kinase Pim-1 phosphorylates and inhibits the activity of Cdc25C-associated kinase 1 (C-TAK1): A Novel role for Pim-1 at the G2M cell cycle checkpoint. *Journal of Biological Chemistry*, 279(46), 48319–48328.
- Banerjee, S., Buhrlage, S. J., Huang, H.-T., Deng, X., Zhou, W., Wang, J., ... Gray, N. S. (2014). Characterization of WZ4003 and HTH-01-015 as selective inhibitors of the LKB1-tumour-suppressor-activated NUA1 kinases. *The Biochemical Journal*, 457(1), 215–25.
- Banerjee, S., Zagorska, A., Deak, M., Campbell, D. G., Prescott, A., & Alessi, D. R. (2014). Interplay between Polo kinase, LKB1-activated NUA1 kinase, PP1 β MYPT1 phosphatase complex and the SCF β TrCP E3 ubiquitin ligase. *The Biochemical Journal*, 245, 233–245.
- Bicaku, E., Xiong, Y., Marchion, D. C., Chon, H. S., Stickles, X. B., Chen, N., ... Lancaster, J. M. (2012). In vitro analysis of ovarian cancer response to cisplatin, carboplatin, and paclitaxel identifies common pathways that are also associated with overall patient survival. *British Journal of Cancer*, 106(12), 1967–1975
- Bosetti, C., Negri, E., Trichopoulos, D., Franceschi, S., Beral, V., Tzonou, A., ... Vecchia, C. La. (2002). Long-term effects of oral contraceptives on ovarian cancer risk. *International Journal of Cancer*, 102(3), 262–265.
- Bradford, M. M. (1976). A rapid and sensitive method for the quantitation of microgram quantities of protein utilizing the principle of protein-dye binding. *Analytical Biochemistry*, 72(1–2), 248–254.
- Bright, N. J., Carling, D., & Thornton, C. (2008). Investigating the regulation of brain-specific kinases 1 and 2 by phosphorylation. *Journal of Biological Chemistry*, 283(22), 14946–14954.

- Brown, J., & Frumovitz, M. (2014). Mucinous tumors of the ovary: Current thoughts on diagnosis and management. *Current Oncology Reports*, *16*(6).
- Carlson, J. W., Miron, A., Jarboe, E. A., Parast, M. M., Hirsch, M. S., Lee, Y., ... Crum, C. P. (2008). Serous Tubal Intraepithelial Carcinoma: Its Potential Role in Primary Peritoneal Serous Carcinoma and Serous Cancer Prevention. *Journal of Clinical Oncology*, *26*(25), 4160–4165.
- Cavanagh, B. L., Walker, T., Norazit, A., & Meedeniya, A. C. B. (2011). Thymidine analogues for tracking DNA synthesis. *Molecules*.
- Chan, K. T., Asokan, S. B., King, S. J., Bo, T., Dubose, E. S., Liu, W., ... Bear, J. E. (2014). LKB1 loss in melanoma disrupts directional migration toward extracellular matrix cues. *Journal of Cell Biology*, *207*(2), 299–315.
- Charoenfuprasert, S., Yang, Y.-Y., Lee, Y.-C., Chao, K.-C., Chu, P.-Y., Lai, C.-R., ... Shih, N.-Y. (2011). Identification of salt-inducible kinase 3 as a novel tumor antigen associated with tumorigenesis of ovarian cancer. *Oncogene*, *30*(33), 3570–3584.
- Chen, H., Huang, S., Han, X., Zhang, J., Shan, C., Tsang, Y. H., ... Poon, R. Y. C. (2014). Salt-inducible kinase 3 is a novel mitotic regulator and a target for enhancing antimitotic therapeutic-mediated cell death. *Cell Death & Disease*, *5*, e1177.
- Chen, P., Li, K., Liang, Y., Li, L., & Zhu, X. (2013). High NUA1 expression correlates with poor prognosis and involved in NSCLC cells migration and invasion. *Experimental Lung Research*, *39*(1), 9–17.
- Cheng, H., Liu, P., Wang, Z. C., Zou, L., Santiago, S., Garbitt, V., ... Zhao, J. J. (2009). SIK1 couples LKB1 to p53-dependent anoikis and suppresses metastasis. *Science Signaling*, *2*(80), ra35.
- Condello, S., Morgan, C. a, Nagdas, S., Cao, L., Turek, J., Hurley, T. D., & Matei, D. (2014). β -Catenin-regulated ALDH1A1 is a target in ovarian cancer spheroids. *Oncogene*, *34*(May), 1–12.
- Contreras, C. M., Gurumurthy, S., Haynie, J. M., Shirley, L. J., Akbay, E. A., Wingo, S. N., ... Castrillon, D. H. (2008). Loss of Lkb1 provokes highly invasive endometrial adenocarcinomas. *Cancer Research*, *68*(3), 759–766.
- Cooper, M. J., Cox, N. J., Zimmerman, E. I., Dewar, B. J., Duncan, J. S., Whittle, M. C., ... Graves, L. M. (2013). Application of Multiplexed Kinase Inhibitor Beads to Study Kinome Adaptations in Drug-Resistant Leukemia. *PLoS ONE*, *8*(6).
- Correa, R. J. M., Peart, T., Valdes, Y. R., Dimattia, G. E., & Shepherd, T. G. (2012). Modulation of AKT activity is associated with reversible dormancy in ascites-derived epithelial ovarian cancer spheroids. *Carcinogenesis*, *33*(1), 49–58.

- Domcke, S., Sinha, R., Levine, D. a, Sander, C., & Schultz, N. (2013). Evaluating cell lines as tumour models by comparison of genomic profiles. *Nature Communications*, 4, 2126.
- Dubeau, L. (2008). THE CELL OF ORIGIN OF OVARIAN EPITHELIAL TUMORS. *The Lancet. Oncology*, 9(12), 1191–1197.
- Eneling, K., Brion, L., Pinto, V., Pinho, M. J., Sznajder, J. I., Mochizuki, N., ... Bertorello, A. M. (2012). Salt-inducible kinase 1 regulates E-cadherin expression and intercellular junction stability. *The FASEB Journal*.
- Fathalla, M. F. (1971). INCESSANT OVULATION-A FACTOR IN OVARIAN NEOPLASIA ? *The Lancet*.
- Features, M. B., Vang, R., Shih, I.-M., & Kurman, R. J. (2009). Ovarian Low-grade and High-grade Serous Carcinoma. *Advances in Anatomic Pathology*, 16(5), 267–282.
- Forstner, R., Sala, E., Kinkel, K., & Spencer, J. A. (2010). ESUR guidelines: Ovarian cancer staging and follow-up. *European Radiology*, 20(12), 2773–2780.
- Fotheringham, S., Levanon, K., & Drapkin, R. (2011). Ex Vivo Culture of Primary Human Fallopian Tube Epithelial Cells. *Journal of Visualized Experiments*, (51), 3–7.
- Frumovitz, M., Schmeler, K. M., Malpica, A., Sood, A. K., & Gershenson, D. M. (2010). Unmasking the complexities of mucinous ovarian carcinoma. *Gynecologic Oncology*.
- Gao, J., Aksoy, B. A., Dogrusoz, U., Dresdner, G., Gross, B., Sumer, S. O., ... Schultz, N. (2013). Integrative analysis of complex cancer genomics and clinical profiles using the cBioPortal. *Sci Signal*, 6(269), p11.
- Gieni, R. S., Li, Y., & HayGlass, K. T. (1995). Comparison of [3H]thymidine incorporation with MTT- and MTS-based bioassays for human and murine IL-2 and IL-4 analysis. Tetrazolium assays provide markedly enhanced sensitivity. *Journal of Immunological Methods*, 187(95), 85–93.
- Godwin, A. K., Testa, J. R., Handel, L. M., Liu, Z., Vanderveer, L. A., Tracey, P. A., & Hamilton, T. C. (1992). Spontaneous transformation of rat ovarian surface epithelial cells: Association with cytogenetic changes and implications of repeated ovulation in the etiology of ovarian cancer. *Journal of the National Cancer Institute*, 84(8), 592–601.
- Goodwin, J. M., Svensson, R. U., Lou, H. J., Winslow, M. M., Turk, B. E., & Shaw, R. J. (2014). An AMPK-independent signaling pathway downstream of the LKB1 tumor suppressor controls snail1 and metastatic potential. *Molecular Cell*, 55(3), 436–450.
- Gurumurthy, S., Hezel, A. F., Berger, J. H., Bosenberg, M. W., & Bardeesy, N. (2008). LKB1 deficiency sensitizes mice to carcinogen-induced tumorigenesis. *Cancer Research*, 68(1), 55–63.

- Hardie, D. G., & Alessi, D. R. (2013). LKB1 and AMPK and the cancer-metabolism link - ten years after. *BMC Biology*, 11, 36.
- Hirano M., Kiyonari H., Inoue A., Furushima K., Murata T., Suda Y., Aizawa S. (2006) A new serine/threonine protein kinase, Omphk1, essential to ventral body wall formation. *Dev. Dyn.* 235, 2229–2237
- Hou, X., Liu, J.-E., Liu, W., Liu, C.-Y., Liu, Z.-Y., & Sun, Z.-Y. (2011). A new role of NUA1: directly phosphorylating p53 and regulating cell proliferation. *Oncogene*, 30(26), 2933–2942.
- Humbert, N., Navaratnam, N., Augert, A., Da Costa, M., Martien, S., Wang, J., ... Bernard, D. (2010). Regulation of ploidy and senescence by the AMPK-related kinase NUA1. *The EMBO Journal*, 29(2), 376–386.
- Jones, L. J., Gray, M., Yue, S. T., Haugland, R. P., & Singer, V. L. (2001). Sensitive determination of cell number using the CyQUANT cell proliferation assay. *Journal of Immunological Methods*, 254(1–2), 85–98.
- Kangas, L., Grönroos, M., & Nieminen, A. L. (1984). Bioluminescence of cellular ATP: a new method for evaluating cytotoxic agents in vitro. *Medical Biology*, 62(6), 338–43.
- Karst, A. M., & Drapkin, R. (2012). Primary culture and immortalization of human fallopian tube secretory epithelial cells. *Nature Protocols*, 7(9), 1755–1764.
- Kosako, H. (2009). Phos-tag Western blotting for detecting stoichiometric protein phosphorylation in cells. *Protocol Exchange*, 1–5.
- Kuo, K. T., Guan, B., Feng, Y., Mao, T. L., Chen, X., Jinawath, N., ... Wang, T. L. (2009). Analysis of DNA copy number alterations in ovarian serous tumors identifies new molecular genetic changes in low-grade and high-grade carcinomas. *Cancer Res*, 69, 4036–4042.
- Kurman, R. J., & Shih, I.-M. (2010). The Origin and Pathogenesis of Epithelial Ovarian Cancer- a Proposed Unifying Theory. *The American Journal of Surgical Pathology*, 34(3), 433–443.
- Kusakai, G., Suzuki, A., Ogura, T., Miyamoto, S., Ochiai, A., Kaminishi, M., & Esumi, H. (2004). ARK5 expression in colorectal cancer and its implications for tumor progression. *The American Journal of Pathology*, 164(3), 987–995.
- Kuwabara, Y., Yamada, T., Yamazaki, K. Du, W., Banno, K., Aoki, D., Sakamoto., M.(2008) Establishment of an ovarian metastasis model and possible involvement of E-cadherin down-regulation in the metastasis. *Cancer Sci*, 99(10), 1933-1939
- L'Espérance, S., Bachvarova, M., Tetu, B., Mes-Masson, A.-M., & Bachvarov, D. (2008). Global gene expression analysis of early response to chemotherapy treatment in ovarian cancer spheroids. *BMC Genomics*, 9, 99.

- Lacey Jr., J. V., Mink, P. J., Lubin, J. H., Sherman, M. E., Troisi, R., Hartge, P., ... Schairer, C. (2002). Menopausal hormone replacement therapy and risk of ovarian cancer. *JAMA*, 288(3), 334–341.
- Lengyel, E. (2010). Ovarian cancer development and metastasis. *The American Journal of Pathology*, 177(3), 1053–64.
- Lewandowski, K. T., & Piwnica-Worms, H. (2014). Phosphorylation of the E3 ubiquitin ligase RNF41 by the kinase Par-1b is required for epithelial cell polarity. *Journal of Cell Science*, 127(Pt 2), 315–27.
- Liu, L., Ulbrich, J., Müller, J., Wüstefeld, T., Aeberhard, L., Kress, T. R., ... Murphy, D. J. (2012). Deregulated MYC expression induces dependence upon AMPK-related kinase 5. *Nature*, 483(7391), 608–612.
- Livak, K. J., & Schmittgen, T. D. (2001). Analysis of relative gene expression data using real-time quantitative PCR and the $2^{-\Delta\Delta CT}$ Method. *Methods*, 25, 402–408.
- Lizcano, J. M., Göransson, O., Toth, R., Deak, M., Morrice, N. A., Boudeau, J., ... & Alessi, D. R. (2004). LKB1 is a master kinase that activates 13 kinases of the AMPK subfamily, including MARK/PAR- 1. *The EMBO journal*, 23(4), 833-843.
- Lowe, S. W., Cepero, E., & Evan, G. (2004). Intrinsic tumour suppression. *Nature*, 432(7015), 307–15.
- Lu, S., Niu, N., Guo, H., Tang, J., Guo, W., Liu, Z., ... Zhang, B. (2013). ARK5 promotes glioma cell invasion, and its elevated expression is correlated with poor clinical outcome. *European Journal of Cancer*, 49(3), 752–763.
- MacDonald, J., Ramos-Valdes, Y., Perampalam, P., Litovchick, L., DiMattia, G. E., & Dick, F. A. (2017). A Systematic Analysis of Negative Growth Control Implicates the DREAM Complex in Cancer Cell Dormancy. *Molecular Cancer Research*, 15(4), 371 LP-381
- Makhija, S., Taylor, D. D., Gibb, R. K., & Gerçel-Taylor, Ç. (1999). Taxol-induced Bcl-2 phosphorylation in ovarian cancer cell monolayer and spheroids. *International Journal of Oncology*, 14(3), 515–521.
- Marquez, R. T., Baggerly, K. A., Patterson, A. P., Liu, J., Broaddus, R., Frumovitz, M., ... Lu, K. H. (2005). Patterns of gene expression in different histotypes of epithelial ovarian cancer correlate with those in normal fallopian tube, endometrium, and colon. *Clinical Cancer Research*, 11(17), 6116–6126.
- McIlwain, D. R., Berger, T., & Mak, T. W. (2013). Caspase functions in cell death and disease. *Cold Spring Harbor Perspectives in Biology*.
- Mihaylova, M. M., & Shaw, R. J. (2011). The AMPK signalling pathway coordinates cell growth, autophagy and metabolism. *Nature Cell Biology*, 13(9), 1016–23.

- Miyoshi, H., Nakau, M., Ishikawa, T. O., Seldin, M. F., Oshima, M., & Taketo, M. M. (2002). Gastrointestinal hamartomatous polyposis in Lkb1 heterozygous knockout mice. *Cancer Research*, 62(8), 2261–2266.
- Nakayama, G. R., Caton, M. C., Nova, M. P., & Parandoosh, Z. (1997). Assessment of the Alamar Blue assay for cellular growth and viability in vitro. *Journal of Immunological Methods*.
- Namiki, T., Tanemura, A., Valencia, J. C., Coelho, S. G., Passeron, T., Kawaguchi, M., ... Hearing, V. J. (2011). AMP kinase-related kinase NUA2 affects tumor growth, migration, and clinical outcome of human melanoma. *Proceedings of the National Academy of Sciences of the United States of America*, 108(16), 6597–6602.
- Naora, H., & Montell, D. J. (2005). Ovarian cancer metastasis: integrating insights from disparate model organisms. *Nature Reviews. Cancer*, 5(5), 355–366.
- Peart, T., Ramos Valdes, Y., Correa, R. J. M., Fazio, E., Bertrand, M., McGee, J., ... Shepherd, T. G. (2015). Intact LKB1 activity is required for survival of dormant ovarian cancer spheroids. *Oncotarget*.
- Perets, R., Wyant, G. A., Muto, K. W., Bijron, J. G., Poole, B. B., Chin, K. T., ... Drapkin, R. (2013). Transformation of the Fallopian Tube Secretory Epithelium Leads to High-grade Serous Ovarian Cancer in Brca;Tp53;Pten Models. *Cancer Cell*, 24(6), 751–765.
- Phippen, N. T., Bateman, N. W., Wang, G., Hamilton, C. A., Maxwell, G. L., Darcy, K. M., & Conrads, T. P. (2015). Poor survival associated with NUA1 overexpression in serous ovarian cancer may be explained by chemotherapy resistance. *Front Oncol*, 6, 213.
- Piek, J. M., Verheijen, R. H., Kenemans, P., Massuger, L.F. Bulten, H., van Diest, P. J. (2003) BRCA1/2-related ovarian cancers are of tubal origin: a hypothesis. *Gynecol Oncol*, 90(2):491
- Quirk, J. T., & Natarajan, N. (2005). Ovarian cancer incidence in the United States, 1992-1999. *Gynecologic Oncology*, 97(2), 519–523.
- Ran, F. A., Hsu, P. D., Wright, J., Agarwala, V., Scott, D. A., & Zhang, F. (2013). Genome engineering using the CRISPR-Cas9 system. *Nat Protoc*, 8(11), 2281–2308.
- Rines, A. K., Burke, M. A., Fernandez, R. P., Volpert, O. V., & Ardehali, H. (2012). Snf1-related kinase inhibits colon cancer cell proliferation through calcyclin-binding protein-dependent reduction of β -catenin. *FASEB Journal*, 26(11), 4685–4695.
- Riss, T. L., Moravec, R. A., Niles, A. L., Duellman, S., Benink, H. A., Worzella, T. J., & Minor, L. (2013). Cell Viability Assays. In *Assay Guidance Manual* [Internet] (Vol. 114, pp. 785–796).

- Roby, K. F., Taylor, C. C., Sweetwood, J. P., Cheng, Y. Pace, J. L., Tawfik, O., Persons D. L., Smith, P. G., Terranova, P. F. (2000). Development of a syngeneic mouse model for events related to ovarian cancer. *Carcinogenesis*, *21*, 585-591.
- Rossing, M. A., Daling, J. R., Weiss, N. S., Moore, D. E., & Self, S. G. (1994). Ovarian tumors in a cohort of infertile women. *The New England Journal of Medicine*, *331*(12), 771-776.
- Scherer, S. E., Muzny, D. M., Buhay, C. J., Chen, R., Cree, A., Ding, Y., ... Gibbs, R. A. (2006). The finished DNA sequence of human chromosome 12. *Nature*, *440*(7082), 346-351.
- Schorge, J. O., McCann, C., & Del Carmen, M. G. (2010). Surgical debulking of ovarian cancer: what difference does it make? *Reviews in Obstetrics and Gynecology*, *3*(3), 111-117.
- Shackelford, D. B., & Shaw, R. J. (2009). The LKB1-AMPK pathway: metabolism and growth control in tumour suppression. *Nature Reviews. Cancer*, *9*(8), 563-75.
- Shaw, R. J., Bardeesy, N., Manning, B. D., Lopez, L., Kosmatka, M., DePinho, R. A., & Cantley, L. C. (2004). The LKB1 tumor suppressor negatively regulates mTOR signaling. *Cancer cell*, *6*(1), 91-99.
- Shepherd, T. G., Thériault, B. L., Campbell, E. J., & Nachtigal, M. W. (2007). Primary culture of ovarian surface epithelial cells and ascites-derived ovarian cancer cells from patients. *Nature Protocols*, *1*(6), 2643-2649
- Spicer, J., Rayter, S., Young, N., Elliott, R., Ashworth, A., & Smith, D. (2003). Regulation of the Wnt signalling component PAR1A by the Peutz-Jeghers syndrome kinase LKB1. *Oncogene*, *22*(30), 4752-4756.
- Strober, W. (2001). Trypan blue exclusion test of cell viability. *Current Protocols in Immunology* / Edited by John E. Coligan ... [et Al.], Appendix 3, Appendix 3B.
- Sun, X., Gao, L., Chien, H. Y., Li, W. C., & Zhao, J. (2013). The regulation and function of the NUAK family. *Journal of Molecular Endocrinology*, *51*(2)
- Sutherland, R. M., & Durand, R. E. (1976). Radiation response of multicell spheroids--an in vitro tumour model. *Current Topics in Radiation Research Quarterly*, *11*(1), 87-139.
- Suzuki, A., Kusakai, G. I., Kishimoto, A., Lu, J., Ogura, T., Lavin, M. F., & Esumi, H. (2003). Identification of a novel protein kinase mediating Akt survival signaling to the ATM protein. *Journal of Biological Chemistry*, *278*(1), 48-53.
- Suzuki, A., Kusakai, G.-I., Kishimoto, A., Shimojo, Y., Miyamoto, S., Ogura, T., ... Esumi, H. (2004). Regulation of caspase-6 and FLIP by the AMPK family member ARK5. *Oncogene*, *23*(42), 7067-75.

- Suzuki, A., Lu, J., Kusakai, G.-I., Kishimoto, A., Ogura, T., & Esumi, H. (2004). ARK5 is a tumor invasion-associated factor downstream of Akt signaling. *Molecular and Cellular Biology*, 24(8), 3526–3535.
- Takahashi, A., Ohtani, N., Yamakoshi, K., Iida, S., Tahara, H., Nakayama, K., ... Hara, E. (2006). Mitogenic signalling and the p16INK4a-Rb pathway cooperate to enforce irreversible cellular senescence. *Nature Cell Biology*, 8(11), 1291–1297.
- TCGA, R.N. (2011) Integrated genomic analyses of ovarian carcinoma. *Nature* 474 (7353): p. 609-15.
- Tiainen, M., Vaahtomeri, K., Ylikorkala, A., & Mäkelä, T. P. (2002). Growth arrest by the LKB1 tumor suppressor: induction of p21(WAF1/CIP1). *Human Molecular Genetics*, 11(13), 1497–504.
- Tomao, F., Lo Russo, G., Spinelli, G. P., Stati, V., Prete, A. A., Prinzi, N., ... Tomao, S. (2014). Fertility drugs, reproductive strategies and ovarian cancer risk. *Journal of Ovarian Research*, 7, 51.
- Tsuchihara, K., Ogura, T., Fujioka, R., Fujii, S., Kuga, W., Saito, M., ... Esumi, H. (2008). Susceptibility of Snark-deficient mice to azoxymethane-induced colorectal tumorigenesis and the formation of aberrant crypt foci. *Cancer Science*, 99(4), 677–682.
- Uhlén, M., Fagerberg, L., Hallström, B. M., Lindskog, C., Oksvold, P., Mardinoglu, A., ... Pontén, F. (2015). Tissue-based map of the human proteome. *Science*, 347(6220).
- van Veelen, W., Korsse, S. E., van de Laar, L., & Peppelenbosch, M. P. (2011). The long and winding road to rational treatment of cancer associated with LKB1/AMPK/TSC/mTORC1 signaling. *Oncogene*, 30(20), 2289-2303.
- Vanderhyden, B. C., Shaw, T. J., & Ethier, J.-F. (2003). Animal models of ovarian cancer. *Reproductive Biology and Endocrinology : RB&E*, 1, 67.
- Walkinshaw, D. R., Weist, R., Kim, G. W., You, L., Xiao, L., Nie, J., ... Yang, X. J. (2013). The tumor suppressor kinase LKB1 activates the downstream kinases SIK2 and SIK3 to stimulate nuclear export of class IIa histone deacetylases. *Journal of Biological Chemistry*, 288(13), 9345–9362.
- Whittle, D. O., Lee, M. G., & Hanchard, B. (2011). Peutz-Jeghers syndrome. *The West Indian Medical Journal*, 60(3), 340–3.
- Wlodkowic, D., Skommer, J., & Darzynkiewicz, Z. (2009). Flow cytometry-based apoptosis detection. *Methods in Molecular Biology (Clifton, N.J.)*, 559, 19–32.
- Yang, F. C., Tan, B. C. M., Chen, W. H., Lin, Y. H., Huang, J. Y., Chang, H. Y., ... Lee, S. C. (2013). Reversible acetylation regulates salt-inducible kinase (SIK2) and its function in autophagy. *Journal of Biological Chemistry*, 288(9), 6227–6237.

- Yang, Z., & Klionsky, D. J. (2010). Mammalian autophagy: core molecular machinery and signaling regulation. *Current opinion in cell biology*, 22(2), 124-131.
- Ye, X.-T., Guo, A.-J., Yin, P.-F., Cao, X.-D., & Chang, J.-C. (2014). Overexpression of NUA1 is associated with disease-free survival and overall survival in patients with gastric cancer. *Medical Oncology (Northwood, London, England)*, 31(7), 61.
- Yong Kim, S., Jeong, S., Chah, K.-H., Jung, E., Baek, K.-H., Kim, S.-T., ... Lee, K.-Y. (2013). Salt-inducible kinases 1 and 3 negatively regulate Toll-like receptor 4-mediated signal. *Molecular Endocrinology (Baltimore, Md.)*, 27(11), 1958–68.
- Zagórska, A., Deak, M., Campbell, D. G., Banerjee, S., Hirano, M., Aizawa, S., ... Alessi, D. R. (2010). New roles for the LKB1-NUAK pathway in controlling myosin phosphatase complexes and cell adhesion. *Science Signaling*, 3(115), ra25.
- Zhang, H. Y., Li, J. H., Li, G., & Wang, S. R. (2015). Activation of ARK5/miR-1181/HOXA10 axis promotes epithelial-mesenchymal transition in ovarian cancer. *Oncology Reports*, 34(3), 1193–1202.
- Zhao, R.-X., & Xu, Z.-X. (2014). Targeting the LKB1 tumor suppressor. *Current drug targets (Vol. 15)*.
- Zhou, W., Ercan, D., Chen, L., Yun, C. H., Li, D., Capelletti, M., ... Janne, P. A. (2009). Novel mutant-selective EGFR kinase inhibitors against EGFR T790M. *Nature*, 462(7276), 1070–1074.

Curriculum Vitae

PARIMA SAXENA

EDUCATION

The University of Western Ontario

MSc in Anatomy and Cell Biology

May 2015 - Present

The University of Western Ontario

H. BSc in Medical Science and Biology

September 2011 - April 2015

North Park Secondary School

International Business and Technology Program

September 2007 – June 2011

AWARDS AND ACHIEVEMENTS

Paul Harding Research Day – Poster Presentation Award

London Health Sciences Centre

May 2016

UWO Obstetrics and Gynecology Scholarship

2015 – 2016

Western Graduate Research Scholarship

2015-2017

Dean's List

The University of Western Ontario

January 2013 – January 2015

RELEVANT ACADEMIC CONTRIBUTIONS

MSc Candidate

2015 – Present

The role of LKB1-AMPK Related Kinase signaling in ovarian cancer spheroids

Dr. Trevor Shepherd

Department of Anatomy and Cell Biology

The University of Western Ontario

Undergraduate Research Student

May 2012 – September 2012

Patient profiling according to cell surface receptor expression in acute myeloid leukemia (AML)

Dr. Mark Minden

Department of Medical Biophysics

The University of Toronto

RELATED EXPERIENCE**Teaching Assistant for ACB4461**

January 2016 – May 2016

Translational Models of Cancer

Graded assignments, marked presentations, proctored exam.

Cancer Genetics Student

January 2015 – August 2015

London Health Sciences Centre

Pedigree design, risk assessment for patients with hereditary predispositions to cancer, patient consults

ABSTRACTS

Parima Saxena, Yudith Ramos Valdes, Ava Hosseini, Elizabeth Kobylecky, Gabriel DiMattia and Trevor G. Shepherd. (2016) Functional analysis of the AMPK Related Kinases in epithelial ovarian cancer. London Health Research Day, March 29, 2016, London, ON

Parima Saxena, Yudith Ramos Valdes, Ava Hosseini, Elizabeth Kobylecky, Gabriel DiMattia and Trevor G. Shepherd. (2016) Interrogation of AMPK Related Kinases in epithelial ovarian cancer. Paul Harding Research Day, May 11, 2016, London, ON

Parima Saxena, Yudith Ramos Valdes, Ava Hosseini, Elizabeth Kobylecky, Gabriel DiMattia and Trevor G. Shepherd. (2016) Interrogation of AMPK Related Kinases in epithelial ovarian cancer. Canadian Conference on Ovarian Cancer Research, May 14 – 17, 2016, Niagara Falls, ON

Parima Saxena, Yudith Ramos Valdes, Ava Hosseini, Elizabeth Kobylecky, Gabriel DiMattia and Trevor G. Shepherd. (2016) Interrogation of AMPK Related Kinases in epithelial ovarian cancer. Oncology Research Day, June 17, 2016, London, ON

Parima Saxena, Yudith Ramos Valdes, Adrian Buensuceco, Gabriel DiMattia and Trevor G. Shepherd. (2016) Functional analysis of NUA1 in epithelial ovarian cancer. ACB Research Day, October 21, 2016, London, ON

Parima Saxena, Yudith Ramos Valdes, Adrian Buensuceso, Kyle Francis, Kevin Brown, Karen Colwill, Anne-Claude Gingras, Robert Rottapel, Gabriel DiMattia and Trevor G. Shepherd. (2016) NUA1 has potential growth suppressive activity in metastatic epithelial ovarian cancer. Terry Fox Research Institute Research Day, December 5, 2016, Toronto, ON

Parima Saxena, Yudith Ramos Valdes, Adrian Buensuceso, Kyle Francis, Kevin Brown, Karen Colwill, Anne-Claude Gingras, Robert Rottapel, Gabriel DiMattia and Trevor G. Shepherd. (2017) NUA1 is a potential new tumor suppressor in epithelial ovarian cancer. Southern Ontario Reproductive Biology Conference, May 12, 2017, London, ON

Parima Saxena, Yudith Ramos Valdes, Adrian Buensuceso, Kyle Francis, Kevin Brown, Karen Colwill, Anne-Claude Gingras, Robert Rottapel, Gabriel DiMattia and Trevor G. Shepherd. (2017) NUA1 is a potential new tumor suppressor in epithelial ovarian cancer. Paul Harding Research Day, May 17, 2017, London, ON